Assessment of Seasonal Variation in Canopy Structure and Greenness in Tropical Wet Evergreen Forests of North East India

Thesis submitted to Andhra University, Visakhapatnam
in partial fulfillment of the requirement for the award of
Master of Technology in Remote Sensing and GIS

Submitted by

Dr. Kuldip Gosai

Supervised by

Dr. Subrata Nandy
Scientist/Engineer-SD
Forestry and Ecology Department
Indian Institute of Remote Sensing, ISRO
Dehradun

Dr. S.P.S. Kushwaha
Dean (Academics) & Group Director
Earth Resources & Systems Studies Group
Indian Institute of Remote Sensing, ISRO
Dehradun

Indian Institute of Remote Sensing
Indian Space Research Organisation
Department of Space, Govt. of India
Dehradun-248001, Uttarakhand
India

August 2015

DISCLAIMER

This document describes the work that has been carried out in partial fulfilment of Master of Technology program in Remote Sensing and Geographic Information System at Indian Institute of Remote Sensing (Indian Space Research Organisation, Department of Space, Government of India) Dehradun, India. All views and opinions expressed in this document remains the sole responsibility of the author and do not necessarily represent those of the Institute.

CERTIFICATE

This is to certify that the project entitled **"Assessment of Seasonal Variation in Canopy Structure and Greenness in Tropical Wet Evergreen Forests of North East India"** is a bonafide record of work carried out by **Dr. Kuldip Gosai** during 01 August 2014 to 14 August 2015. The report has been submitted in partial fulfilment of requirement for the award of **Master of Technology in Remote Sensing and GIS** with specialization in **Forestry and Ecology**, conducted at Indian Institute of Remote Sensing (IIRS), Indian Space Research Organisation (ISRO), Dehradun from 19 August 2013 to 14 August 2015. The work has been carried out under the supervision of Dr. Subrata Nandy, Scientist/Engineer-SD, Forestry and Ecology Department and Dr. S.P.S Kushwaha, Professor & Dean (Academics), IIRS, Dehradun. No part of this report is to be published without the prior permission/intimation from/to the undersigned.

Dr. Subrata Nandy
Project Supervisor
Scientist/Engineer-SD
Forestry and Ecology Department
Indian Institute of Remote Sensing, ISRO
Dehradun

Dr. S.P.S. Kushwaha
Project Co-supervisor
Dean (Academics) & Group Director
Earth Resources & Systems Studies
Group
Indian Institute of Remote Sensing, ISRO
Dehradun

Dr. Sarnam Singh
Scientist/Engineer-G
Head
Forestry and Ecology Department
Indian Institute of Remote Sensing, ISRO
Dehradun

Dr. S.P.S. Kushwaha
Dean (Academics) & Group Director
Earth Resources & Systems Studies
Group
Indian Institute of Remote Sensing, ISRO
Dehradun

ACKNOWLEDGEMENTS

DECLARATION

I, **Kuldip Gosai,** hereby declare that this dissertation entitled *"Assessment of Seasonal Variation in Canopy Structure and Greenness in Tropical Wet Evergreen Forests of North East India"* submitted to Andhra University, Visakhapatnam in partial fulfilment of the requirements for the award of **M.Tech. in Remote Sensing and GIS**, is my own work and that to the best of my knowledge and belief. It is a record of original research carried out be me under the guidance and supervision of Dr. Subrata Nandy, Scientist-SD, Forestry and Ecology Department and Dr. S.P.S. Kushwaha, Professor & Dean (Academics), Indian Institute of Remote Sensing, ISRO, Dehradun. It contains no material previously published or written by another person nor material which to a substantial extent nor material which to a substantial extent has been accepted for the award of any other degree or diploma of the university or other institute of higher learning, except where due acknowledgement has been made in the text.

Place: Dehradun   Kuldip Gosai
Date: 07.08.2015

ABSTRACT

Contrary to the rapid rate in its depletion at a global scale, tropical forests serve as one of the largest reservoir of carbon sinks. This intrinsic competence of the tropical forests puts them in a perplexed state wherein a slender change in any of its metrics *viz.*, structure, vegetation indices or Leaf Area Index forms a colossal concern. These metrics form a yardstick to denote its vigor and thus serve as a vital input both to forest managers as well as policy makers. The present study was carried out in a tropical wet evergreen forests of Arunachal Pradesh in North East India, the objectives of which were assessment of these uncorrected metrics and simulation of the same using Forest Light Interaction (FLIGHT) Radiative Transfer Model coupled with independent satellite observations from LiDAR and optical sensors. The study led to an improved bidirectional reflectance from MODIS BRDF products as compared to MODIS Data products for the vegetation canopies across all seasons. Vegetation Indices generated from MODIS BRDF product marked a significant improvement as compared to MODIS Vegetation Indices products at ICESat Footprint level. Waveform Centroid Relative Height, one of the key LiDAR metrics also showed consistency in retaining its structure on simulation of photon trajectories using FLIGHT. The novelty of the research was however the evenness maintained by the climax tropical forests of this part of the world in both its structure and greenness across all seasons. The study as a whole analyzed the estimation inaccuracies of both LiDAR and optical sensors and suggested ways for a better approximation.

Keywords: ICESat, GLAS, Footprint, MODIS Vegetation Indices Product, MODIS BRDF Adjusted Reflectance Product, Waveform Centroid Relative Height, FLIGHT Radiative Transfer Model

Table of Contents

LIST OF FIGURES

LIST OF TABLES

ABBREVIATIONS

AGB	Aboveground Biomass
ASCII	American Standard Code for Information Interchange
AMSL	Above Mean Sea Level
BRDF	Bidirectional Reflection Distribution Function
DBH	Diameter at Breast Height
DEM	Digital Elevation Model
EVI	Enhanced Vegetation Index
FLIGHT	Forest Light Interaction Model
GLAS	Geoscience Laser Altimeter System
GPS	Global Positioning System
GSD	Ground Sample Distance
ICESat	Ice, Cloud, and Land Elevation Satellite
IFOV	Instantaneous Field of View
IDLVM	Interactive Data Language Virtual Machine
LAI	Leaf Area Index
LASER	Light Amplification by Stimulated Emission of Radiation
LiDAR	Light Detection and Ranging
MODIS	Moderate Resolution Imaging Spectroradiometer
MEA	Millennium Ecosystem Assessment
NDVI	Normalized Difference Vegetation Index
NSIDC	National Snow and Ice Data Center
RMSE	Root Mean Square Error
RTM	Radiative Transfer Model
WCRH	Waveform Centroid Relative Height

Chapter 1

Introduction

_____

1.1   Background

Forests across all regions of the world have assumed larger implications in perspective of their capability to act as net carbon sinks (Hiratsuka *et al.,* 2003). FAO (Food and Agriculture Organization), therefore classifies all such lands into forests which bear vegetative association dominated by trees of any size, misused or not, proficient of producing wood or other forest produce, or wielding an influence upon the climate or water regime or providing shelter to livestock and wildlife (Anon., 2001). Tropical rainforests that stands in the equatorial zone (between the Tropic of Cancer and the Tropic of Capricorn) are found in Africa, Asia, Australia, Central America, Mexico, South America, besides Caribbean, Pacific and Indian Ocean islands (Olson *et al.*, 2001). They are known to possess high biodiversity and ca. 40 to 75% of all biotic species are native to it (Anon., 2009).

Tropical forests harbor half of the living animal and plant species on Earth (Anon., 2008) and two-thirds of all the known flowering plants. In tropical forests, the fundamental properties include height of the trees, whether they incline to have their crown in layers, and the presence of different types of climbers, lianas, and epiphytes. The physiognomic properties of tropical wet evergreen forests include tree buttresses, nature of the leaves (size, shape, margin, thickness), crown shape, whether the forest is evergreen and, if not, then how highly deciduous; and where on trees the flowers and fruits are borne. Amongst all forests, the tropical rainforest formations are the most structurally complex and diverse land ecosystems that have ever occurred on earth, with the greatest numbers of co-existing plant and animal species (Whitmore, 1975).

The canopy of tropical rainforest is often considered to be layered or stratified and different forest formations have different figures of strata. Strata (layers or storeys) are often easy to be viewed in the forest or in a profile diagram, and sometimes not (Whitmore, 1975). It comprises of lowland equatorial evergreen rainforests (found in the Amazon basin of south America, central Africa, Indonesia and New Guinea), montane rain forests, flooded forests as well as deciduous and evergreen forests found across India-China, central America, Caribbean islands, coastal west Africa, and parts of the Indian subcontinent (Bruijnzeel & Veneklaas, 1998).

1.2   Forests in India

India is sanctified with varied climatic conditions. A wide diversity of vegetation types, extending from tropical wet evergreen forests to alpine, and from desert to humid flourishes in India (Anon., 2007) covering an area of 697898 km^2 (Table 1.1). Out of ca. 200,000 known plants in the world, around 20,000 occur in India, which demonstrates the extravagance of its flora (Anon., 2007). Based on climate-rainfall and temperature as well as the phenology of the natural forest vegetation, forests in India have been categorized into 6 Groups and 16 Type Groups. Amongst the key forest types of India, the tropical wet evergreen forests are characterized as tall, dense and multi-layered forests (Champion & Seth, 1968) with rainfall of about 2500 mm (Upadhyay & Rai, 2013). Tropical rain forests (tropical wet evergreen forests) inhabit a narrow belt along the west coast, north east India and in Andaman and Nicobar Islands. Desert form of vegetation is found in

Rajasthan, Gujarat and in adjoining areas. Subtropical, temperate and alpine forms of vegetation are however found in Himalaya and other hill ranges (Anon., 2007).

Table 1-1 Geographic area, recorded forest area and forest cover of various States/UTs of India.

State/UT	Geographic area (km^2)	Forest Land		Forest Cover (FSI, 2013)	
		km^2	%	km^2	%
Andhra Pradesh	275,069	63,814	23.20	46,116	19.38
Arunachal Pradesh	83,743	51,541	61.55	67,321	81.18
Assam	78,438	26,832	34.21	27,671	37.29
Bihar	94,163	6,473	6.87	7,291	10.04
Chhattisgarh	135,191	59,772	44.21	55,621	43.70
Delhi	1,483	85	5.73	179.81	20.08
Goa	3,702	1,225	33.09	2,219	68.96
Gujarat	196,022	21,647	11.04	14,653	11.74
Haryana	44,212	1,559	3.53	1,586	6.49
Himachal Pradesh	55,673	37,033	63.60	14,683	27.63
Jammu & Kashmir	222,236	20,230	9.10	22,538	13.59
Jharkhand	79,714	23,605	29.61	23,473	32.74
Karnataka	191,791	38,384	19.96	36,132	21.93
Kerala	38,863	17,922	54.21	11,309	29.10
Madhya Pradesh	308,245	94,689	30.72	77,522	27.45
Maharashtra	307,713	61,357	19.94	50,632	19.43
Manipur	22,327	17,418	78.01	17,214	77.09
Meghalaya	22,429	9,496	42.34	17,288	80.05
Mizoram	21,081	16,717	79.30	19,054	91.44
Nagaland	16,579	9,222	55.62	13,044	80.92
Orissa	155,707	58,136	37.34	50,347	34.91
Punjab	50,362	3,084	6.12	1,772	6.49
Rajasthan	342,239	32,737	9.57	16,086	7.00
Sikkim	7,096	5,841	82.31	3,358	47.46
Tamilnadu	130,058	22,877	17.59	23,844	22.07
Tripura	10,486	6294	59.99	7,866	77.01
Uttar Pradesh	240,928	16,583	6.88	14,349	8.82
Uttarakhand	53,483	34,651	64.79	24,508	47.14
West Bengal	88,752	11,879	13.38	16,805	21.35
A & N Islands	8,249	7,171	86.93	6,711	81.85
Chandigarh	114	35	30.70	17.26	23.91
Dadra & Nagar Haveli	491	204	41.55	213	49.29
Daman & Diu	112	8.27	7.38	9.27	16.31
Lakshdweep	32	NA	NA	27.06	97.06
Pondicherry	480	13	2.71	50.06	16.47
Total	**3287263**	**778534.27**	**23.68**	**697,898**	**21.23**

(Source: FSI, 2013)

1.3 Tropical Wet Evergreen Forests of North East India

The north eastern region of the country comprising of eight states *viz*., Arunachal Pradesh, Assam, Manipur, Meghalaya, Mizoram, Nagaland, Tripura and Sikkim is endowed with rich forest resources. The region, which constitutes only 7.98 percent of the geographical area of the country, covers nearly one-fourth of its forest cover. The total forest cover of the region is 172, 592 km², which covers 65.83 percent of its geographical area in comparison to the national forest cover of 21.23 percent (FSI, 2013).

Tropical wet evergreen forests in the north eastern states of India cover an area of ca. 7445.6 km² (Table 1.1) (FSI, 2013) with an annual rainfall of about 2500 mm (Upadhyay & Rai, 2013). The monthly maximum temperature does not exceed 32°C and the mean minimum for January is close to 10°C, the absolute minimum being a little under 5°C. Soils are largely of recent alluvial formation over Tertiary sandstones and shales with the latter outcrop on the hills carrying a similar type of forest (Champion & Seth, 1968).

In tropical wet evergreen forests, *Dipterocarps macrocarpus* and *Shorea assamica* occur scattered and in patches, attaining great girths upto 7 m and heights upto 50 m. They stand over a closed evergreen canopy at about 30 m in which *Mesua ferrea* (with large girths of up to 4 m) and *Vatica lanceaefolia* tend to dominate among the larger number of other species. Underwood as well as shrub layers do exist but the ground is practically bare. Climbers are copious as well as epiphytes, lianas, palms and canes (Champion & Seth, 1968). Due to its biological richness, the region has been identified as one of the 35 biodiversity hotspots of the world (Anon., 2015a). Amongst the north east states, Arunachal Pradesh with a geographical area of 83,743 km² is the largest and shares ca. 2.5% of the total geographical land mass of the country with 15.76% of Indian Himalayan region and 43.62% of the Biological Hotspot (Gosai, 2008; Gosai *et al*., 2009; Sharma *et al*., 2015) with rainfall between 1500 mm to 3100 mm (Gosai *et al*., 2010).

Table 1-2 Area (km2) covered by the tropical wet evergreen forests of North East India (FSI, 2013)

States	Tropical Wet Evergreen Forest			Total (km²)
	Very Dense Forest (VDF) (km²)	Moderately Dense Forest (MDF) (km²)	Open Forest (OF) (km²)	
Arunachal Pradesh	506.9	298.5	184.3	989.7
Assam	276.5	2162.5	812.8	3251.8
Meghalaya	99.7	823.7	2214.3	3137.7
Nagaland	-	17.2	49.2	66.4
Total	883.1	3301.9	3260.6	7445.6

Tropical wet evergreen forests of north east India have a Malayan affinity and its flora comprises of several species including *Alpinia* spp., *Altingia excelsa*, *Amomum* spp., *Amoora wallichii*, *Ampelocissus (Vitis) latifolia*, *Artocarpus chaplasha*, *Bambusa pallida*, *Clerodendron*, *Canarium* spp., *Dalbergia stipulacea, Dendrocalamus hamiltonii*, *Dipterocarpus macrocarpus*, *Dysoxylum procerum*, *Eugenia* spp., *Garcinia cowa*, *Ixora* spp., *Livistona jenkinsiana*, *Laportea*, *Mesua ferrea*, *Myristica* spp., *Michelia* spp., *Pinang* spp., *Phrynium* spp., *Piper* spp., *Pseudostachyum polymorphum*, *Shorea assamica*, *Stereospermum personatum*, *Thunbergia grandiflora*, *Talauma* spp., *Vatica lanceifolia etc*. (Champion & Seth, 1968).

1.4 Vegetation Characteristics and Optical Remote Sensing

The canopy of a tropical forest is however considered to be layered or stratified and different forest formations have different numbers of strata (Fig. 1.1). Strata (layers or storeys) are sometimes easy to see in the forest or in a profile diagram, and sometimes not (Whitmore, 1975).

In general, the estimation of the structural attributes in a forest ecosystem (e.g. aboveground biomass - AGB) can be assessed through the measurement of tree diameter at breast height (DBH) (Keller *et al.,* 2001). However, processes involving direct estimation of AGB through DBH on ground is quite expensive, time-consuming, and sometimes destructive (Hiratsuka *et al.,* 2003).

Remote sensing thus offers all-inclusive spatial and temporal coverage and has the latent to save money, time, and effort in AGB estimation (Dhanda, 2013) besides providing a global perspective on seasonal and inter-annual changes in vegetation productivity (Huete *et al.,* 2006; Saleska *et al.,* 2007). The seasonal greening of tropical forests could however be attributed to synchronous canopy leaf turnover (Huete *et al.,* 2006; Doughty & Goulden, 2008; Brando *et al.,* 2010), as young leaves reflect more near-infrared (NIR) light than the older leaves they replace (Toomey *et al.,* 2009), or seasonal increases in green leaf area (Myneni *et al.,* 2007; Doughty & Goulden, 2008; Samanta *et al.,* 2012). Generally, leaf-level response increases the photosynthetic capacity of tropical forests, resulting in higher net primary production (NPP) as photosynthetically active radiation (PAR) increases during dry months (Saleska *et al.,* 2003; Huete *et al.,* 2006; Brando *et al.,* 2010).
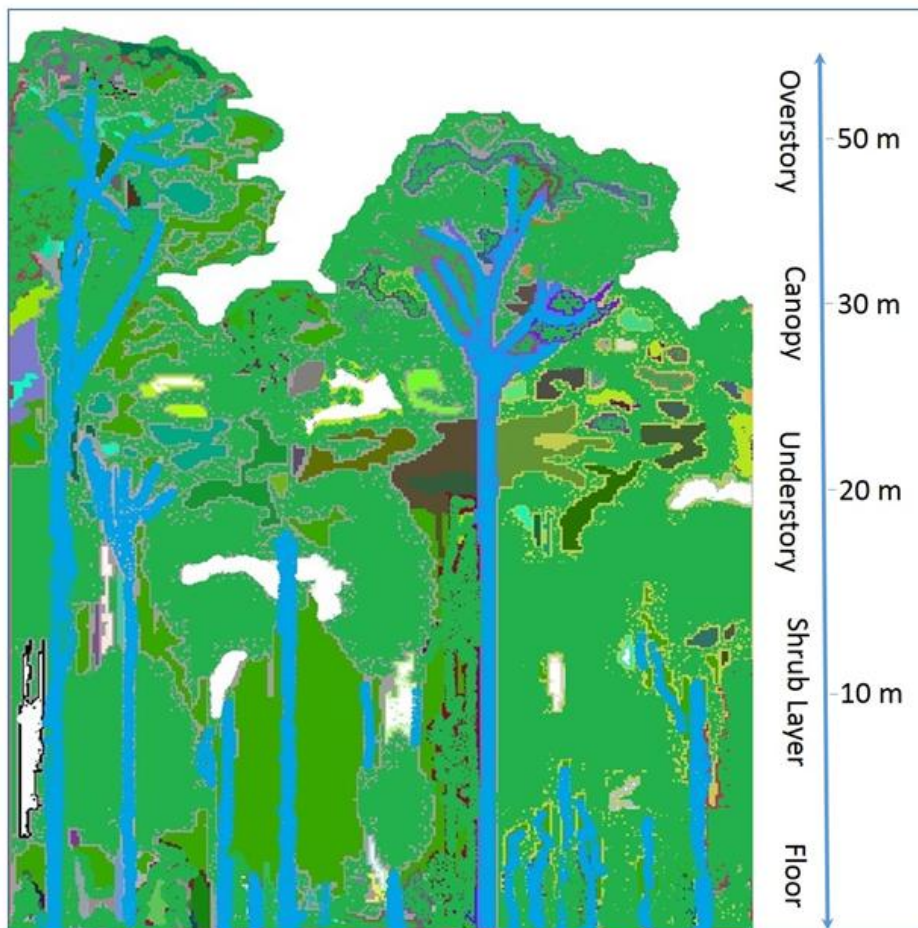
Fig. 1-1 Stratification of tropical evergreen forest (schematic).

Satellite monitoring of vegetation phenology has often made use of a vegetation index such as NDVI since it is related to the amount of green leaf biomass (Lillesand & Keifer, 2000). Vegetation products generated from Moderate Resolution Imaging Spectroradiometer (MODIS) on board Terra and Aqua offer an unprecedented opportunity for researchers to develop long-term records of vegetation phenology at spatial scales as small as 250 m (Ghilain *et al*., 2014). The MODIS products intend to give reliable, spatial and temporal comparisons of global vegetation

conditions that can be used to monitor photosynthetic activities' (Running *et al.*, 1994; Justice *et al.*, 1998). MODIS Vegetation Indices (VIs) *viz.*, Normalized Difference Vegetation Index (NDVI) and Enhanced Vegetation Index (EVI), are produced expansively over land surface at 1km and 500 m resolutions and 16 day compositing periods. While NDVI is chlorophyll sensitive, EVI is more responsive to canopy structural variations, including leaf area index (LAI), canopy type, vegetation physiognomy, and canopy design (Gao *et al.*, 2000). The two VIs, however, complement each other in global vegetation studies and mend upon the revealing of vegetation changes and mining of forest canopy biophysical parameters (Huete *et al.*, 2002).

1.5   Vegetation Characteristics and LiDAR

LiDAR (Light Detection and Ranging) is an active sensor that unswervingly processes the vertical component of vegetation and has the potential to measure the structural vegetation attributes (Lefsky *et al.,* 2002). An active optical sensor, such as the Geoscience Laser Altimeter System (GLAS) on the Ice, Cloud and Land Elevation Satellite (ICESat) emits a light pulse of known intensity and duration (Zwally *et al.,* 2002; Brenner *et al.,* 2003). The pulse is transmitted, absorbed and scattered at various depths throughout the vegetation canopy by leaves and branches and the returned waveform therefore provides facts on canopy structure and height (Drake *et al.,* 2003; Lefsky *et al.,* 2005; Rosette *et al.,* 2008). Spaceborne LiDAR has the ability to obtain vegetation parameters at much higher biomass levels (Drake *et al.,* 2003) and the scattered energy is returned to the sensor from all the intercepted surfaces within the illuminated area (footprint), meaning that the returned waveform represents both the canopy vertical profile and surface topography (Morton *et al.*, 2014). As a whole, forests do represent a very complex structure where both small and large scale structural heterogeneity contributes to canopy reflectance (North, 1996) thus creating the necessity for modelling approach.

1.6   Radiative Transfer Modelling and Forest Light Interaction Model (FLIGHT)

Canopy reflectance modelling is centered on the principle of radiative transfer (Chandrasekhar, 1960) that relates to the alteration in radiation intensity (I_v) along a ray path to local absorption (k_v) and volume emission (j_v) (Weisstein, 1996):

$$\frac{1}{k_v}\frac{dI_v}{ds} = -I_v + \frac{j_v}{k_v} \quad \text{... (Eq. 1.1)}$$

Radiative transfer equation is a monochromatic equation to calculate the radiance in a single layer of Earth's atmosphere using a discrete ordinate or a Monte Carlo method. This method depends upon repeated random sampling and uses three distinct problem classes' *viz.*, optimization, numerical integration and probability distribution to obtain numerical results. The accrued existing intensity allows the calculation of reflectance for view directions quantized over a hemisphere (Anon., 2015c). Monte Carlo technique takes into account the leaf dimension that leads to the formation of the canopy 'hot-spot effect' and it gives the possibility to supplement it with both structural and the optical parameters like specular reflection component in the scattering phase function besides estimating the contribution of the canopy hotspot effect for the radiance of the multiple scattered photons (Antyufeev & Marshak, 1990). However, this technique is known for its limitations wherein the forest canopy structure is discontinuous in nature and the foliage elements show a three-dimensional distribution (North, 1996).

Forest Light Interaction Model (FLIGHT) is based on Monte Carlo simulation technique for photon transport that simulates the observed reflectance response of three-dimensional vegetation canopies. It allows precise simulation of multiple scattering within the canopy, including interactions within crowns as well as between distinct crowns, trunks and the ground surface. This

is however done by simulating the photon free path within a canopy representation and then simulating the chain of scattering events incurred by a photon in its path from the source to the receiver or to its absorption (North, 1996; Disney *et al.*, 2000; Barton & North, 2001).

1.7   Motivation and Problem Statement

Passive Remote Sensing over the years has proven its efficiency in demarcating various forest types, isolating individual trees, and evaluating forest density (Dhanda, 2013). But the generic problem using passive remote sensors to infer canopy structure is that different canopy structures can lead to the same spectral and bidirectional response; the inversion of biophysical parameters in these cases is however a non-unique problem with more than one solution and this inhibits unambiguous estimation of canopy parameters. It is however important to note that optical remote sensing in North East India faces challenging issues such as frequent cloud cover in the wet season. Furthermore, Aerosol Optical Depth (AOD) caused by biomass burning in North East India are high during the dry seasons (Badrinath *et al.*, 2004). Additionally, various artefacts generated in the MODIS data processing stream (*e.g.*, atmospheric correction, cloud removal, surface reflectance retrieval, composting), the bidirectional reflectance distribution function (BRDF) of different land cover types and variation in sun-angle may also contribute to seasonal variations of surface reflectance and vegetation indices (Xiao *et al.*, 2006) such as Enhanced Vegetation Index (EVI) and Normalized Difference Vegetation Index (NDVI) besides others. Thus the incongruity in optical remote sensing metrics can never be ruled out.

Incidentally, for the broad-footprint waveform LiDAR instruments, such as GLAS and proposed replacement missions, the returned waveform may be multifaceted due to the potential effects of terrain and of varying vegetation canopy at different heights of surface properties, such as canopy structure and topography, and sensor characteristics, such as pulse temporal duration and spatial extent (Morton *et al.*, 2014). Thus the three-dimensional radiative transfer model FLIGHT (North, 1996) could be used to model waveform LiDAR interaction at scales suitable for ICESat interpretation. The method allows accurate simulation of multiple scattering in the canopy, including interface within crowns, trunks and the ground surface (North, 1996). The model offers a consistent link from LiDAR derived structure to full canopy optical response and vegetation photosynthesis (Barton and North, 2001; Alton *et al.*, 2005 & 2007). The model is seemly used in parameter retrieval, for example using look-up table (LUT) based inversion methods (North, 2002) and finally, it helps to explore the theoretical potential of biophysical parameter retrieval from satellite waveform LiDAR (Morton *et al.*, 2014). Thus, the auxiliary work forms a desirable need to validate the model against any major forest type and to explore the sensitivity of reflectance in that representative forest type.

1.8   Research Identification

The study aims to integrate the information derived from LiDAR and optical remote sensing metrics to evaluate the potential mechanisms for the structural and apparent greenness in tropical wet evergreen forests of North East India, including increases in leaf area or leaf reflectance using a sophisticated FLIGHT radiative transfer model. The objectives therefore are summed up as follows:

1.9   Research Questions
   ❖ Does the seasonal variation in vegetation indices reflect the true change in greenness and structure of tropical wet evergreen forests?
   ❖ Do the LiDAR metrics represent true canopy structure at footprint level?

❖ Does the simulated forest structure using FLIGHT Radiative Transfer Model differ from LiDAR derived metrics?

❖ How can the seasonality in greenness and structure of tropical wet evergreen forests be better predicted?

1.10 Research Objectives

The objectives of this research focused upon:

1. Analysis of temporal variation in vegetation indices for tropical wet evergreen forests;
2. Retrieval of biophysical parameters and leaf area index at ICESat footprint level;
3. Simulation of photon trajectories in tropical wet evergreen forests using FLIGHT Radiative Transfer Model and
4. Optimization of LiDAR derived metrics using FLIGHT, and normalization of vegetation indices at temporal scales.

Review of Literature

_____

2.1   Rationale of the Study

In recent decades, the extent of forests in Asia has changed drastically. In 1990s, the region encountered a net forest decline of 0.7 million hectares per year, while in the last decade the forest area increased by a normal of 1.4 million hectares per year. The planted forest area also substantially increased through afforestation schemes mainly as a result of large-scale plantation drive been adopted in these countries. The area of primary forests decreased in all the Asian sub-regions in the last decade, in spite the fact that the area selected for conservation of biodiversity increased in the sub-regions in the extent to which forests were set aside for soil and water protection. The area of productive forests also declined over the last decade (Anon., 2010).

Thus, an exploratory study of natural resources, basically for forest is a prerequisite for planning and development for well-being of a society. In the prior times, information on forest inventory was collected only by field methods. But for the tropical ecosystems, the varied nature and complexity in structure supplemented with inaccessibility for ground truthing has always been a challenging task. With an advent of the remote sensing technology, approximation on forest inventory has become easy, fast and cost effective (Unni *et al.,* 1991). Various studies have been undertaken in India with respect to forest cover type mapping, forest cover monitoring using satellite remote sensing data through visual and digital image processing techniques (Kushwaha, 1990; Sudhakar *et al.,* 1992; Joshi *et al.,* 2002; Nandy *et al.*, 2003; Nandy *et al.*, 2007; Nandy & Kushwaha, 2011; Kumar *et al.*, 2014). Nonetheless, for the tropical ecosystems of North East India, such studies through optical remote sensing are limited while no studies have yet been undertaken to assess the structure of the forests through the usage of LiDAR technology.

2.2   Vegetation Characteristics Assessment

Assessment of vegetation phenology utilizing remotely sensed data has a long history (Sayn-Wittgenstein, 1961; Rouse *et al.*, 1973; Rea & Ashley, 1976) with more recent studies making use of satellite data to examine the potential effects of climate change on phenology (e.g., Myneni *et al.*, 1997; Zhang *et al.*, 2004). Canopy reflectance of vegetation is 'causally' associated to leaf area index of the canopy and co-varies with aboveground biomass (Curran, 1981). It is possible to use remote sensing canopy reflectance models for estimating vegetation, woody biomass and productive potential (Roy, 1989; Franklin & Hiernaux, 1991; Gosai, 2009; Heyojoo & Nandy, 2014; Kushwaha *et al.*, 2014; Manna *et al.*, 2014; Yadav & Nandy, 2015).

NOAA-AVHRR data is probably most extensively used dataset to study vegetation dynamics on continental scale. It has shown its efficacy to represent net primary productivity (Warrick *et al.*, 1986). Multistage approach using wide swath and narrow swath satellite NOAA and IRS-1A or 1B has been suggested for national biomass mapping. While NOAA-AVHRR data provides distribution of forest cover type (Roy & Kumar, 1986), satellite like Landsat, SPOT and IRS provide broad vegetation type distribution based on major species composition, canopy density and site conditions. These have been widely studied in Indian context (Roy *et al.* 1986; Unni *et al.,* 1986; Roy *et al.,* 1991; Ravan *et al.,* 1995; Roy & Ravan, 1996).

Vegetation phenology, as used and calculated with remote sensing related research, refers to the relationship between climate and periodic development of photosynthetic biomass. Precise estimates of canopy phenology are critical to enumerating carbon and water exchange between

forests and the atmosphere and its response to climate change. The biophysical and radiometric principles of using a satellite-based vegetation index or related measures (e.g., leaf area index) to detect vegetation phenology, in general, are well established (Rea and Ashley, 1976; Huete *et al*., 2002). However, the paradigm of intricacy increases for stratified and complex ecosystems thus warranting a need for detailed study using satellite-based vegetation data products.

2.3   Remote Sensing Metrics: Vegetation Indices

U.S. Earth Observing System (EOS) programme studies the role of terrestrial vegetation in large-scale global processes with the goal of understanding how the earth functions as a system. This necessitates an understanding of the worldwide distribution of vegetation types as well as their biophysical and structural properties and spatial/temporal variations. Vegetation Indices (VI) are vigorous, pragmatic measures of vegetation activity at the land surface. They are intended to improve the vegetation reflected signal from measured spectral responses by combining two (or more) wavebands, frequently in the red (0.6 - 0.7 μm) and NIR wavelength (0.7-1.1 μm) areas (Solano *et al*., 2010).

MODIS VI products (MOD13) provide unswerving, spatial and temporal assessments of world vegetation environments which might be used to scrutinize the Earth's terrestrial photosynthetic vegetation activity in support of phenological, change detection, and biophysical elucidations. Gridded vegetation index maps portraying spatial and temporal variations in vegetation activity are derived at 16-day and monthly intervals for precise seasonal and inter-annual scrutiny of the earth's terrestrial vegetation (Huete *et al*., 1999).

Two VI products are made globally for land areas. The initial product is the standard Normalized Difference Vegetation Index (NDVI), which is referred to as the continuity index to the existing NOAA-AVHRR derived NDVI. There is a +27-year NDVI global data set (1981-2009) from the NOAA-AVHRR series, which could be prolonged by MODIS data to provide a long term data record for use in operational monitoring studies. The next VI product is the Enhanced Vegetation Index (EVI), with improved sensitivity over high biomass regions and improved vegetation monitoring capability through a de-coupling of the canopy background signal and a reduction in atmosphere influences. The two VIs match each other in global vegetation studies and improve upon the extraction of canopy biophysical parameters wherein a new compositing scheme reduces angular as well as sun-target-sensor variations (Solano *et al*., 2010).

Gridded Vegetation Indices (VI) maps often use MODIS surface reflectance corrected for molecular scattering, ozone absorption, besides aerosols that serves as input to VI equations. They include quality assurance (QA) flags with statistical data that specifies the quality of the VI product and input data. The MODIS VI products are currently shaped at 250 m, 500 m, 1 km and 0.05 degree spatial resolutions. For assembly purposes, MODIS VIs are produced in tile units that are approximately 1200-by-1200 km, and mapped in the Sinusoidal (SIN) grid projection. Only tiles comprising of land features are treated, with the aim to lessen processing and disk space inevitabilities. When mosaicked, all tiles shield the native Earth and it deserves a special mention that the global MODIS-VI can thus be produced in every 16 days as well as in every calendar month (Solano *et al*., 2010).

Recent ecological studies have highlighted the significance of the Normalized Difference Vegetation Index as an index linking vegetation to animal performance. NDVI (Running, 1990) is derived from the red: near-infrared (NIR) reflectance ratio, where NIR and red are the quantities of near-infrared and red lights respectively reflected by the vegetation and captured by the sensor of the satellite. The formulation is centered on the fact that chlorophyll absorbs red whereas the mesophyll leaf structure scatters NIR. NDVI values range from -1 to +1, where negative values correspond to an absence of vegetation (Myneni, 1995). The relationship between the NDVI and

vegetation productivity is well recognized, and the link amidst this index and the fraction of absorbed photosynthetic active radiation intercepted (fAPAR) has been well documented, theoretically (Sellers *et al.*, 1992) and empirically (Asrar *et al.*, 1984). Moreover, direct effects of climatic conditions on biomass and phenological patterns of vegetation as assessed by the use of the NDVI have been reported for many ecosystems (Nemani *et al.*, 2003; Roerink *et al.*, 2003; Zhou *et al.*, 2003; Zhao and Schwartz, 2003; Yu *et al.*, 2003; Wang *et al.,* 2003), as have the feedback effects of vegetation on local climate (Zhang *et al.,* 2003).

The use of NDVI in recent ecological studies has outlined its possible key role in future research of environmental change in an ecosystem context. Studying ecosystem responses to increased surface temperature over the northern hemisphere is a major focus of the scientific community (Stenseth *et al.*, 2002; Walther *et al.*, 2002). Moreover, human activity has profoundly affected ecosystems (e.g. via habitat destruction and biodiversity reduction) so that the need to detect and predict changes in ecosystem functioning has never been greater (Naeem *et al.*, 1999). Field data currently available are generally difficult to use for predicting regional or global changes because such data are traditionally collected at small spatial and temporal scales and vary in their type and reliability. Satellite imagery has become a probable 'goldmine' for ecologists in that context as recently underlined by Kerr and Ostrovsky (2003) and Turner *et al.* (2003). Of the information that can be derived from the satellite-collected data (*e.g.* sea surface temperature, ocean colour, and topography (Turner *et al.,* 2003)), data on phenology, and the amount and distribution of vegetation are of prime importance for terrestrial ecologists because vegetation strongly influences animal distributions and dynamics. However, NDVI has been criticized because of the following perceived defects:

❖ Differences between the "true" NDVI, as would be measured at the surface, and that actually determined from space are sensitive to attenuation by the atmosphere and aerosols.

❖ The understanding of NDVI to LAI becomes increasingly weak with increasing LAI beyond a threshold value, which is typically between 2 and 3.

❖ Disparities in soil brightness may yield large variations in NDVI from one image to the next (Liu & Huete, 1995).

NASA's MODIS is the only chief data source for the studies of the green-up phenomenon, including the enhanced vegetation index (EVI) (Huete *et al.,* 2006; Brando *et al.,* 2010; Samanta *et al.,* 2012) and leaf area index (LAI) products (Myneni *et al.,* 2007; Samanta *et al.,* 2012). MODIS EVI and LAI products are very sensitive to changes in NIR reflectance (Galvao *et al.,* 2011; Samanta *et al.,* 2012). Cowling and Field (2003) examined the sensitivity of LAI to plant resource availability including CO, and suggested the links amongst LAI, canopy development, and primary production used in most of the ecosystem models to examine the effects of climate change. Zhang *et al.* (2004) used time series EVI to estimate phenological transition times from a curvature rate-of change function coupled with MODIS land surface temperature data. They established that there is a crucial need to couple field measurements and reflectance data to understand how species level responses to climate effects may influence large-scale studies, especially using satellite data with pixels containing mixed species. Schwartz *et al.* (2002) compared three methods using satellite data for determining the onset of greenness of a deciduous broad leaf stand at the Harvard forest in Massachusetts and concluded that each of the methods perform reasonably well when compared to field measurements. Several mechanisms could however generate an increase in NIR reflectance of Amazon forests; increases in MODIS EVI or LAI alone are therefore insufficient to isolate the biophysical basis for the Amazon green up phenomenon (Doughty & Goulden, 2008; Samanta *et al.,* 2012). Thus, a thorough study in all the major tropical ecosystems is warranted.

The periodicity of sunlight and precipitation regulates net primary productivity in the tropical forests (Saleska *et al.,* 2003). Earlier studies have suggested that light is more limiting than

water for tropical forest productivity (Nemani *et al.,* 2003), unswerving with greening of Amazon forests during the dry season in satellite data (Huete *et al.,* 2006; Myneni *et al.,* 2007; Doughty & Goulden, 2008; Brando *et al.,* 2010; Samanta *et al.,* 2012). The role of tropical rainforests such as Amazon in the global carbon budget, however, remains indefinite (Gatti *et al.,* 2010; Chevalier *et al.,* 2011; Pan *et al.,* 2011; Davidson *et al.,* 2012).

Efforts to better restrain the net carbon emissions from tropical forests have focused on the seasonal and inter-annual variability of forest productivity (Saleska *et al.,* 2003; Philips *et al.,* 2009). Inconsistency in Amazon forest productivity is potentially larger than deforestation emissions on yearly basis, yet remains poorly inhibited by field or atmospheric observations (Gatti *et al.,* 2010; Chevalier *et al.,* 2011). At the center of this debate is whether tropical forest productivity is more restricted by sunlight or precipitation (Huete *et al.,* 2006; Saleska *et al.,* 2007; Philips *et al.,* 2009; Brando *et al.,* 2010; Lewis *et al.,* 2011; Davidson *et al.,* 2012). Determining this issue is critical to reducing uncertainties in the contemporary carbon balance of tropical forests (Gatti *et al.,* 2010; Chevalier *et al.,* 2011; Pan *et al.,* 2011) and the probable response of Amazon forests to climate change (Zelazowski *et al.,* 2011; Davidson *et al.,* 2012; Kim *et al.,* 2012). Analogous studies in other tropical eco-regions of the world thus warrants a need.

2.4   LiDAR Remote Sensing Applications in Forestry

LiDAR is an active remote sensing technique that determines ranges (i.e. distances) by taking the product of the speed of light and the time required for an emitted laser to travel to a target object (Lim *et al*., 2003). It is analogous to radar, but using laser light, a breakthrough technology for forestry applications (Dubayah & Drake, 2000). There are basically two categories of LiDAR systems: Discrete Return Device (DRD) which measures time elapsed between emission and return of laser pulse (Hudak *et al*., 2002) resulting in 3D point cloud and Waveform Recording Device (WRD) which captures continuous energy return from every emitted laser pulse (Patenaude *et al*., 2005). On the basis of width of laser pulse, LiDAR is categorized as: large-footprint system having diameter of laser beam greater than 5 m on ground and small-footprint system having diameter less than 50 cm (Bortolot & Wynne, 2005).

LiDAR provides data on three-dimensional forest structures characterizing vegetation height, vertical spreading of canopy, crown volume, sub-canopy landscape, biomass, vertical vegetation diversity and manifold layers, height to live crown, tree density, leaf area index, and physiographic or life form diversity through direct and indirect retrievals. It measures vertical forest structure directly, with accurately estimating height and biomass (Behera & Roy, 2002).

Table 2-1 Potential contributions of LiDAR remote sensing for forestry applications

Forest Characteristic	LiDAR Derivation
Canopy Height	Direct retrieval
Subcanopy Topography	Direct retrieval
Vertical distribution of Intercepted Surfaces	Direct retrieval
Aboveground Biomass	Modeled
Basal Area	Modeled
Mean Stem Diameter	Modeled
Vertical Foliar Profiles	Modeled
Canopy Volume	Modeled
Large Tree Density	Inferred
Canopy cover, LAI	Fusion with other sensors
Life Form Diversity	Fusion with other sensors

Source: Dubayah & Drake, 2000)

LiDAR data have produced accurate estimates of tree height, canopy closure, and aboveground biomass (Lim *et al*., 2003). In combination with an accurate GPS onboard an aircraft, discrete return LiDAR systems provides three-dimensional point clouds of forested areas, from which tree heights and vertical structural measures can be extracted (Lim *et al*., 2003). For direct measurement and estimation of several key forest characteristics, LiDAR remote sensing has vast potential. The direct measurements of large-footprint LiDAR include canopy height, vertical distribution and sub-canopy topography of intercepted surfaces between the canopy top and the ground. From these shortest measurements, other forest structural physiognomies, such as aboveground biomass are inferred (Dubayah *et al*., 2000).

Spaceborne LiDAR with large footprints and full waveform datasets have the advantage of assessing vegetation parameters at unparalleled scales, from regional to continental and global ranges. An outline of the ICESat mission is provided in Schutz *et al.* (2005) while a series of studies using GLAS data have successfully demonstrated the capabilities of GLAS data for estimating forest canopy heights (Lefsky *et al.,* 2007; Rosette *et al.,* 2008) and forest biomass (Lefsky *et al.,* 2005; Nelson *et al.,* 2009).

LiDAR metrics (e.g., canopy height) have been used to accurately estimate basal area (e.g. (Means *et al*., 1999; Drake *et al*., 2002) and mean stem diameter (Drake *et al*., 2002). Like canopy height, the vertical distribution of intercepted surfaces provides a new means to classify vegetation, and provides the basis for estimating other important canopy descriptors, such as aboveground biomass. The vertical distribution of intercepted surfaces has been used to model "canopy height profiles" using assumptions from methods developed to estimate vertical foliage profiles from optical point quadrats (Lefsky *et al*., 1999). In addition, the vertical distribution of intercepted surfaces has also been used to examine the volumetric nature of Douglas fir/western hemlock (Lefsky *et al*., 1999) and tropical wet forest canopy structure (Weishampel *et al*., 2000). It also functions as a predictor of the succession state of a forest (Dubayah *et al*., 1997). However, as the age of the forest stand changes, the vertical distribution of canopy components changes relative to younger stands (Lefsky *et al*., 1999; Dubayah *et al*., 2000). However, for the forest types of tropical regions, wherein the forest structure does not change rapidly, application of LiDAR needs to be tested out.

2.5 ICESat/GLAS LiDAR Data in Forestry Applications

Geoscience Laser Altimeter System (GLAS) onboard NASA's Ice, Cloud, and Land Elevation Satellite (ICESat) from 12 January 2003 (Afzal *et al*., 2007), with huge footprints and full waveform datasets is the first space-borne LiDAR system capable of providing global datasets of the Earth's surface (Schutz *et al*., 2005). GLAS through June 2005 had made over 904 million measurements of the Earth surface and atmosphere on more than 3600 orbits with vertical resolution approaching 3 cm (Abshire *et al*., 2005). The primary purpose of the GLAS instrument was to detect ice-elevation changes in Antarctica and Greenland (Bae & Schutz, 2002). However, the application of these data reached far more aspects than the initial purpose. These data have been used widely in other fields, including stemming sea-ice freeboard, vegetation canopy height, cloud heights, aerosol-height spreading and land-terrain changes (Zwally, 2010). ICESat/GLAS) GLAS provided data since 2003 till 2009, with models to estimate forest structural properties from GLAS data (Harding and Carabajal, 2005; Lefsky *et al*., 2007; Boudreau *et al*., 2008; Rosette *et al*., 2008; Sun *et al*., 2008).

GLAS data have been used in different areas e.g. landscape (Harding and Carabjal, 2005), cloud distribution (Wylie *et al*., 2007), hydrology (Carabjal and Harding, 2006), monitoring of ice-sheets (Kwok *et al*., 2006; Slobbe *et al*., 2008), aerosol distribution and vegetation attributes (Harding and Carabajal, 2005; Lefsky *et al*., 2005, 2007). GLAS products, mainly GLA01 and

GLA14 have been used for land cover classification and biomass estimation (Ranson *et al*., 2004; Lefsky *et al*., 2005; Boudreau *et al*., 2008) and seasonal changes in vegetation (Duong *et al*., 2008) where a large information is retrieved from GLA01 (the 'raw' waveform) (Semwal, 2014).

Couple of studies have shown that the width of GLAS waveform can be utilized for AGB estimation as a part of moderately level homogenous backwoods region (Harding & Carabajal, 2005; Lefsky *et al.,* 2005; Rosette et al. 2008). Harding and Carabajal (2005) changed the waveform with an instrument model as per a high-determination DEM, and afterward contrasted it and the genuine waveform of GLAS; they affirmed that the extraction of biophysical parameters over tree-shrouded zones of low alleviation can be achieved with ICESat data. Lefsky *et al*. (2005) extracted maximum forest height in tropical broadleaf forests, temperate broadleaf forests and temperate needle leaf forests using GLAS waveform data and a knowledge of local topography as well as an above-ground biomass estimation with an empirical method. Sun *et al*. (2008) reported forest height extraction over a forested area in the USA using GLAS data from autumn 2003 to summer 2005 and airborne LVIS data. Dolan *et al*. (2009) derived forest progression rate from GLAS data and Landsat-based disturbance history maps in three regions of the USA, as well as the approximation of above-ground wood productivity from height–biomass allometric relations. Chen (2010) used GLAS data to extract forest canopy height over mountainous areas (with mean slope of around 20°) and pointed out that the direct canopy height from GLAS waveform metrics inclined to be higher than that derived from airborne LiDAR data and that it was difficult to identify signal start time and terrain ground elevation. Lefsky (2010) estimated forest heights over the world with Moderate Resolution Imaging Spectro-radiometer (MODIS) data determining the forest-covered areas and GLAS data estimating height. The efficiency of GLAS LiDAR data for tropical rainforests of Amazon has already been tested and one of the key biophysical parameters as a function of canopy structure has been derived (Morton *et al*., 2014). Analogous studies thus needs a replication in the other key ecoregions of the world.

2.6   Monte Carlo Simulation of Radiative Transfer

Multi-angle remote sensing delivers additional information about vegetation in terms of directional characteristics related to its vertical structure (Verstraete *et al.,* 1996; Diner *et al.,* 1999; Leblanc *et al.,* 1999; Hese *et al.,* 2005) and there have been a number of studies carried out to extract information on optical properties and structure of vegetation from multi-angle data (Deering *et al.,* 1999; Sandmeier and Deering, 1999; White *et al.,* 2001; Zhang *et al.,* 2002a,b; Chen *et al.,* 2003; Gao *et al.,* 2003; Cierniewski *et al.,* 2004; Rautiainen *et al.,* 2004). However, the aptitude of multi-angle remote sensing for retrieving vegetation background optical properties has not been systematically investigated. The involvement of the background to the total reflectance changes with view angle as the probability of viewing the background decreases with increasing view zenith angle (Canisius & Chen, 2007). At nadir, the background contribution is the largest, while at the largest view zenith angle, the contribution of the vegetation is the largest. Assuming that the reflected radiance from the canopy changes little on the perpendicular plane, the total bidirectional reflectance would then decrease with increasing view zenith angle (Canisius & Chen, 2007).

Monte Carlo simulation is a flexible technique that permits very precise estimation of light interception and bidirectional reflectance (Disney *et al*., 2000). The technique indulges inspecting of the photon free-path within a canopy depiction, and simulation of the scattering event at every interactions. Through iterations, we obtain accurate treatment of light interception and multiple dispersions between foliage components and the ground surface. Overlapping vegetation crowns and multiple dispersions within and between distinctive crowns and the ground surface are thus modelled. The extreme challenge however of displaying LiDAR interaction is the additional consideration of time dependency of the response, controlled by varying path length over multiple

interactions forming the return, and the temporal spread of the incoming pulse (North *et al., 2008*). Such Radiative Transfer Models are often used in terrestrial remote sensing as tools for examining the physical interaction of electromagnetic radiation with earth surface features. Such models have been used to demonstrate how LiDAR signals vary with the vertical structure of vegetation (Sun & Ranson, 2000; Ni-Meister *et al.*, 2001; Koetz *et al*., 2006; Yin *et al*., 2013).

2.7   Forest Light Interaction Model (FLIGHT)

Forest Light Interaction Model (FLIGHT) is a Monte Carlo numerical simulation of optical and near-infrared photons propagating through either a one-dimensional (1-D) homogeneous or 3-D heterogeneous leaf canopy and has been described to simulate satellite waveform LiDAR collections (North, 1996; North *et al*., 2010) and has been used to examine the uncertainty of these data for vegetation structure and topography (Rosette *et al.,* 2010). It has also been used to examine the sensitivity of LiDAR to site specific conditions such as topography, canopy and ground reflectance (Rosette *et al*., 2013). In LiDAR simulations, the model calculates the probability distribution of return of a photon emitted from the laser as a function of time, and has been corroborated by comparing model simulations with field and satellite observations (North *et al.*, 2010; Morton *et al.*, 2014) and through comparisons with other radiative transfer models (Widlowski *et al.*, 2007). For the simulation of discrete photon returns for photon counting LiDAR, the expected energy distribution is quantized, and stochastic Poisson sampling is used to calculate the expected number of returned photons at each time interval. Solar noise due to photons originating from solar scattering from land and atmosphere is calculated, and included implicitly within the simulation by increasing energy within each bin. The LiDAR sensor is characterized using wavelengths, pulse duration, emitted energy per pulse, IFOV, and sensor 'dead' time. Footprint dimensions are determined using sensor altitude, beam divergence and viewing geometry. Atmospheric effects of signal delay or pulse broadening are not represented, however atmospheric transmittance is accounted for, giving attenuation of the signal by fixed gases and aerosols using coefficients derived from the 6S radiative transfer model (Vermote, *et al*., 1997).

The original model (North, 1996) traces photon trajectories forwards from the source until absorption in the canopy or leaving the canopy boundary, when energy was accumulated in bins defined for each solid angle of exit. Consequently, the model was advanced to sample paths from a given view direction to intercepted surfaces, and to accrue the radiance inputs from these surfaces (Disney *et al.,* 2000; Barton & North, 2002). The final method is more appropriate for LiDAR calculation, as it is possible to competently estimate return for infinitesimal angles; this is necessary for LiDAR as viewing is made at the retro-reflection direction or 'hot-spot', where the reflectance changes very significantly with small changes in view angle (North *et al.,* 2008).

The tropical forests of North East India as has been described in the previous Chapter represent a very complex structure where structural heterogeneity contributes to canopy reflectance. The present study therefore intend to evaluate the potential mechanisms for the seasonal green-up phenomenon and consistent structure in these forests, using a sophisticated Forest Light Interaction (FLIGHT) radiative transfer model coupled with independent satellite observations from LiDAR and optical sensors.

<div align="right">

Chapter 3

</div>

Study Area and Materials/Data Used

_____

3.1 Study Area

3.1.1 Location

ICESat GLAS footprints falling in the tropical eco-regions of North East India representing the Tropical Wet Evergreen forests were selected for extensive study (Fig. 3.1). ICESat footprint pairs on the tropical wet evergreen forests (27°22´32.7´´-27°36´04.8´´N latitude and 96°30´10.9´´-96°32´18.2´´E longitude) were found to fall in the Changlang district of Arunachal Pradesh, which harbours one of the renowned protected areas of India- the Namdapha National Park. The Park covers an area of about 1985 km^2 with an elevation range of 250-4571 m AMSL of which about 177 km^2 is buffer zone (Barbhuiya *et al*., 2008).

3.1.2 Climate

The region experiences three seasons- winter (November to February), spring (March to April), monsoon (May to September). The average precipitation ranges from 2000 mm to 4300 mm with a mean annual temperature of 21° C (Barbhuiya *et al*., 2008).

3.1.3 Drainage, Vegetation and Soils

The major perennial rivers flowing through the study area includes the *Noa-Dihing, Deban, Namdapha,* and *Burma-Nala*. Further, there are innumerable seasonal rainfed streams and streamlets that inundate the thick vegetation consisting of various species like *Ailanthus grandis, Altingia excelsa, Castanopsis indica, Duabanga sonneriatioides, Dipterocarpus macrocarpus, Dysoxylum binectariferum, Mesua ferrea, Taluma hodgsonii, Terminalia myriocarpa, Vatica lancefolia,* and *Shorea assamica* besides others. The forest soil entails of coarse, loose, poorly amalgamated ferruginous, bluish grey sand and grey clay with layers of pebbles (Barbhuiya *et al*., 2008). The area is represented by tall, dense and multi-layered forests (Champion & Seth, 1968).

Data availability (LiDAR and collateral) coupled with accessibility of the Protected Area representing the undisturbed wet evergreen forests in addition to available timeframe served as the guiding factors for the choice of study area.

3.2 Materials/Data Used

3.2.1 Materials

A. Satellite Data

- ICESat GLAS Data Products (*GLA01* and *GLA14*) (NSIDC, 2003-2008)
- MODIS- EVI, LAI & NDVI products
- MODIS Terra/Aqua Daily Surface Reflectance Data
- MODIS BRDF Adjusted Surface Reflectance Data
- Shuttle Radar Topography Mission (SRTM) Data
- Tropical Rainfall Measuring Mission (TRMM) Data
- Google Earth Imagery

B. *Ancillary data*
- Ground truth
- Topographic maps

C. *Software*
- IDL 6.3, MATLAB R2012
- ArcGIS 10.2
- ERDAS IMAGINE 2014

D. *Instruments*
- Global Positioning System (GPS)
- Laser rangefinder
- Plant canopy imager (CI-100)
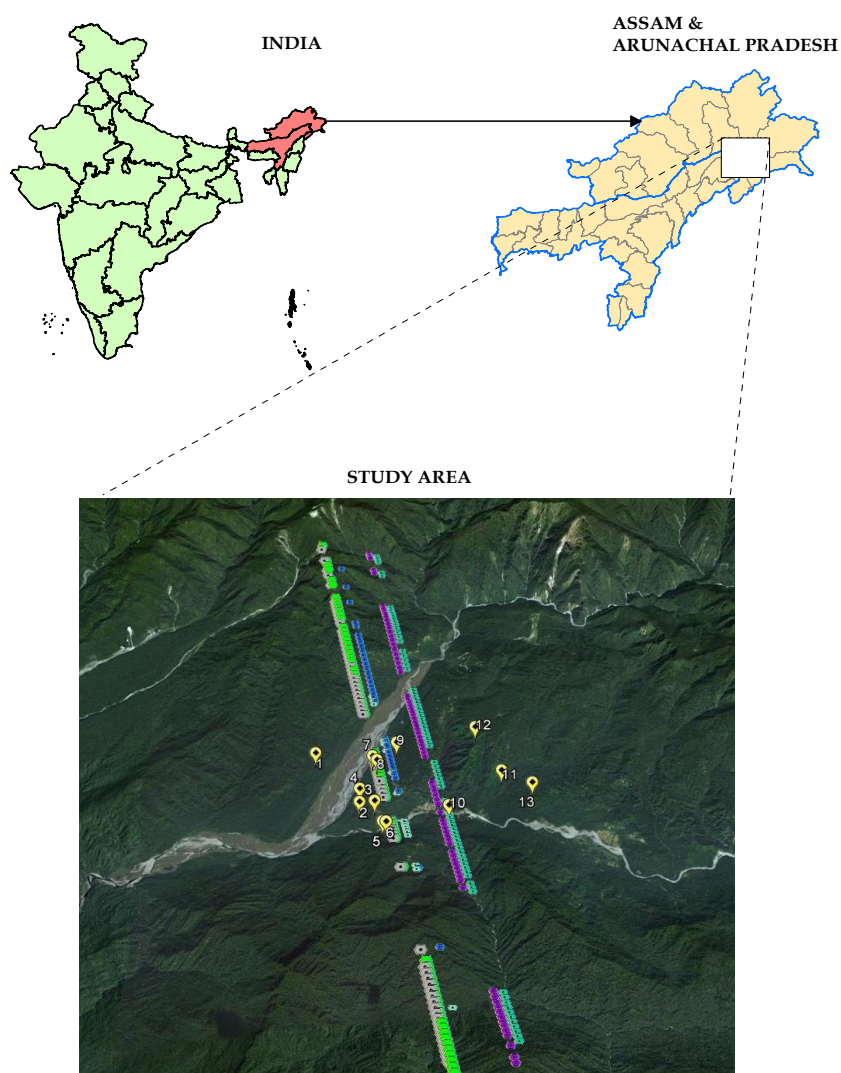
Fig. 3-1 Location of the study area with ICESat GLAS footprints

3.2.2 Satellite Data

3.2.2.1 ICESat/GLAS data

GLAS has fifteen data products (GLA01 to GLA15) (Table 3.1), of which two data products (GLA01 and GLA14) of release 33 were used. The relevant specifications are mentioned in Table 3.2.

3.2.2.2 GLA01

GLA01 is a Level-1A altimetry data that features transmitted and received waveforms from the GLAS instrument. It contains all altimetry information transmitted from the spaceship, as well as the long and short waveforms. The quantity of received samples is sometimes 200 or 544. These modifications at the frame boundary are nominally set by the onboard surface-type mask. In traditional operations, GLAS receives 200 samples over sea, ice and oceans, while 544 samples are recorded over ice sheets and the land. The transmit pulse, received echo samples, and connected digitizer addresses are transported from Level-0 telemetry without calibration or unit changes. This is the sole product that contains the altimeter transmitted and received waveforms, which can be needed by altimetry scientists envisaging the instrument health (Anon., 2015b).

3.2.2.3 GLA14

GLA14 is a Level-2 altimetry information that has surface elevations for land surface. Data additionally includes the laser footprint geolocation and reflectance besides geodetic, instrument, and atmospheric corrections for range measurements (Anon., 2015b).

Table 3-1 Standard GLAS data products.

Product Name	Product Long Name
GLA01	L1A Global Altimetry Data
GLA02	L1A Global Atmosphere Data
GLA03	L1A Global Engineering Data
GLA04	L1A Global Laser Pointing Data
GLA05	L1B Global Waveform-based Range Corrections Data
GLA06	L1B Global Elevation Data
GLA07	L1B Global Backscatter Data
GLA08	L2 Global Planetary Boundary Layer and Elevated Aerosol Layer Heights
GLA09	L2 Global Cloud Heights for Multi-layer Clouds
GLA10	L2 Global Aerosol Vertical Structure Data
GLA11	L2 Global Thin Cloud/Aerosol Optical Depths Data
GLA12	L2 Antarctic and Greenland Ice Sheet Altimetry Data
GLA13	L2 Sea Ice Altimetry Data
GLA14	L2 Global Land Surface Altimetry Data
GLA15	L2 Ocean Altimetry Data

(Source: http://nsidc.org/data/icesat/data.html#glas-hdf5)

Table 3-2 ICESat/GLAS specifications

Sl.No.	ICESat/GLAS Parameter	Specification on Land Surface
1.	Wavelength	1064 nm
2.	Laser pulse rate	40 Hz
3.	Average footprint diameter	~70 m
4.	Laser pulse width	4 ns
5.	Vertical sampling resolution	0.15 m
6.	Surface ranging accuracy	5 cm
7.	Footprint geolocation accuracy	6m
8.	Footprint spacing along track	~ 170 m
9.	Laser beam divergence	110 µrad

(Source: Duong, 2010)

3.2.2.4 *Periodicity of ICESat/GLAS data used*

GLAS shots used in this study were acquired for the period (2003-2008) comprising of 6 satellite passes and total footprints of about 1573 Nos. (Fig. 3.1). Data was downloaded from the data portal of National Snow and Ice Data Center (NSIDC) through ICESat/GLAS data sub-setter (NSIDC, 2011) (Tables 3.3 & 3.4).

Table 3-3 GLAS data products with their source

Product Name	Data Source
GLA01	http://nsidc.org/forms/glas_subset_form.html
GLA14	http://reverb.echo.nasa.gov/reverb/#utf8=%E2%9C%93&spatial_map=satellite&spatial_type=rectangle

Table 3-4 GLAS Data products used for the study period (2003-2008)

Product Name	Data Description
GLA01	GLAS/ICESat L1A Global Altimetry Data V034
GLA14	GLAS/ICESat L2 Global Land Surface Altimetry Data V034

3.2.2.5 *MODIS Vegetation Index Products: NDVI and EVI*

MODIS vegetation indices, available on 16-day intervals and at multiple spatial resolutions, gives a consistent spatial and temporal comparisons of vegetation canopy greenness, a complex property of leaf area, chlorophyll and canopy structure. Vegetation indices were derived from atmospherically-corrected reflectance within the red, near-infrared, and blue wavebands. NDVI provides continuity across the time-series record for historical and climate applications, while EVI reduces canopy-soil variations and improves sensitivity over dense vegetation conditions. The two products more effectively illustrate the global range of vegetation states and processes. Vegetation Indices (VI's) are retrieved from daily, atmosphere-corrected, bidirectional surface reflectance. The

VI's use a MODIS-specific compositing technique that supports product quality assurance metrics to get rid of low quality pixels (Solano *et al*., 2010).

3.2.2.6 Periodicity and Nature of MODIS Vegetation Index Product Data Used

MODIS Product Data of EVI and NDVI were downloaded for the period (2003-2008) over the study area. Data was downloaded from the data portal source as given in Table 3.5.

Table 3-5 MODIS data source

Product Name	Product Abbreviation	Data Source
MODIS Vegetation Index Products: NDVI and EVI (16 day interval data)	MOD13A2	http://reverb.echo.nasa.gov/reverb/
MODIS-Terra Daily Surface Reflectance Data	MOD09GA	http://reverb.echo.nasa.gov/reverb/
MODIS-Aqua Daily Surface Reflectance Data	MYD09GA	http://reverb.echo.nasa.gov/reverb/
MODIS- BRDF Adjusted Surface Reflectance Data (8 day interval data)	MCD43B4	http://reverb.echo.nasa.gov/reverb/

3.2.2.7 MODIS- Terra/Aqua Daily Surface Reflectance Data

MOD09 (MODIS Surface Reflectance) is a seven-band product figured from the MODIS Level 1B land bands 1 (620-670 nm), 2 (841-876 nm), 3 (459-479), 4 (545-565 nm), 5 (1230-1250 nm), 6 (1628-1652 nm), and 7 (2105-2155 nm) (Table 3.6). This product is an estimate of the surface spectral reflectance for every band as it would have been measured on the ground surface as if there were no scattering or absorption. It corrects the effects of atmospheric gases, aerosols, and skinny cirrus clouds (Vermote and Kotchenova, 2008).

3.2.2.8 Periodicity and Nature of MODIS Daily Surface Reflectance Data Used

Daily surface reflectance data at 1 km spatial resolution from the Terra and Aqua MODIS sensors were downloaded for the period (2003-2008) over the study area. Data was downloaded from the data portal source as shown in Table 3.5.

3.2.2.9 MODIS- BRDF Adjusted Surface Reflectance Data

MODIS Nadir BRDF Adjusted reflectance (NBAR) product (MCD43B4) provides 1-kilometer reflectance data adjusted through the bidirectional reflectance distribution function (BRDF) of MCD43B1 to model values as if they were obtained from a nadir view. MCD43B4 reflectance represents the best characterization of the surface attainable from the inputs offered over a 16-day duration. The MCD43B4 NBAR is provided as a level-3 gridded product within the sinusoidal projection. Each Terra and Aqua data breeds this product, providing the very best likelihood for quality input file and designating it as an "MCD," meaning "Combined," product (Schaaf *et al*., 2012).

3.2.2.10 Periodicity and Nature of MODIS BRDF Adjusted Surface Reflectance Data Used

MODIS/Terra+Aqua Nadir BRDF-Adjusted Reflectance 16-Day L3 Global 1km SIN Grid V005 was downloaded for the period (2003-2008) over the study area. Data was downloaded from the data portal source as shown in Table 3.5.

Table 3-6 Description of the 36-bands in a full MODIS scene

Band	Range (nm) reflected	Range nm emitted	Key use
1	620-670		Absolute Land cover Transformations, Vegetation Chlorophyll
2	841-876		Cloud Amount, Vegetation Land Cover Transformation
3	459-479		Soil/Vegetation Difference
4	545-565		Green Vegetation
5	1230-1250		Leaf/Canopy Differences
6	1628-1652		Snow/Cloud Differences
7	2105-2155		Cloud Properties, Land Properties
8	405-420		Chlorophyll
9	438-448		Chlorophyll
10	483-493		Chlorophyll
11	526-536		Chlorophyll
12	546-556		Sediments
13h	662-672		Atmosphere, Sediments
13l	662-672		Atmosphere, Sediments
14h	673-683		Chlorophyll Fluorescence
14l	673-683		Chlorophyll Fluorescence
15	743-753		Aerosol Properties
16	862-877		Aerosol Properties, Atmospheric Properties
17	890-920		Atmospheric Properties, Cloud Properties
18	931-941		Atmospheric Properties, Cloud Properties
19	915-965		Atmospheric Properties, Cloud Properties
20		3.660-3.840	Sea Surface Temperature
21		3.929-3.989	Forest Fires and Volcanoes
22		3.929-3.989	Cloud Temperature, Surface Temperature
23		4.020-4.080	Cloud Temperature, Surface Temperature
24		4.433-4.498	Cloud Fraction, Troposphere Temperature
25		4.482-4.549	Cloud Fraction, Troposphere Temperature
26	1.360-1.390		Cloud Fraction (Thin Cirrus), Troposphere Temperature
27		6.535-6.895	Mid Troposphere Humidity
28		7175-7.475	Upper Troposphere
29		8.400-8.700	Surface Temperature
30		9.580-9.880	Total Ozone
31		10.780-11.280	Cloud Temperature, Forest Fires & Volcanoes, Surface Temperature
32		11.770-12.270	Cloud Height, Forest Fires & Volcanoes, Surface Temperature
33		13.185-13.485	Cloud Fraction, Cloud Height
34		13.485-13.785	Cloud Fraction, Cloud Height
35		13.485-14.085	Cloud Fraction, Cloud Height
36		14.085-14.385	Cloud Fraction, Cloud Height

(Source: https://lpdaac.usgs.gov/lpdaac/products/modis_overview)

3.2.2.11 *Shuttle Radar Topography Mission (SRTM) Data*

SRTM is a global effort led by the U.S. National Geospatial-Intelligence Agency (NGA) and the U.S. National Aeronautics and Space Administration (NASA) that obtained digital elevation models on a near-global scale from 56° S to 60° N (Nikolakopoulos *et al*., 2006) to generate the foremost complete high-resolution digital topographical information of Earth. The elevation models derived from the SRTM data are however utilized in geographic data systems and can be freely downloaded in .hgt file format. The elevation models are set into tiles, each covering one degree of latitude and one degree of longitude, named as per their south western corners. It

follows that "n45e006" stretches from 45°N 6°E to 46°N 7°E and "s45w006" from 45°S 6°W to 44°S5°W. For the entire world, only 3 arcsecond (90 m) data are downloadable (Rexer *et al.,* 2014). The dimensions of the 3 arc second tiles are 1201 x 1201 and the SRTM elevations are relative to WGS84 ellipsoid (Hennig *et al.*, 2001).

3.2.2.12 Periodicity and Type of Shuttle Radar Topography Mission (SRTM) Data Used
Digital elevation data (90 m resolution) was obtained from CGIAR-CSI http://srtm.csi.cgiar.org/SELECTION/inputCoord.asp for the study site (Tile X: 55 and Tile Y: 08 in GeoTiff format).

3.2.2.13 Tropical Rainfall Measuring Mission (TRMM) Data
TRMM is a collaborative space mission of NASA and Japan launched on November 27, 1997 to assess the tropical rainfall and study the Earth as a global system. With the fast depleting fuel to maintain the orbital altitude, the spacecraft has been turned off on April 09, 2015. Tools on board TRMM include precipitation radar (PR), TRMM Microwave Imager (TMI), Visible and Infrared Scanner (VIRS), Clouds and the Earth's Radiant Energy Sensor (CERES) and Lightning Imaging Sensor (LIS).

3.2.2.14 Periodicity and Type of Tropical Rainfall Measuring Mission (TRMM) Data Used
TRMM 3B43v6 Product Data at a monthly interval at 0.25° latitude-longitude spatial resolution covering the tropical wet evergreen regions of the study area were used from EOSDIS Home http://disc.sci.gsfc.nasa.gov/SSW/ (3B43.030101.6.G3.nc to 3B43.081201.6A.G3.nc).

3.2.3   Google Earth Imagery
Google Earth Imagery was used extensively to overlay the LiDAR footprints and locate the accessibility of the footprint location for ground verification.

Chapter 4

Methodology
_____

This Chapter contains ICESat/GLAS data processing techniques followed by field inventory. Procedure followed for MODIS data analysis is explained thereafter followed by forest structure simulation using FLIGHT Radiative Transfer Model.
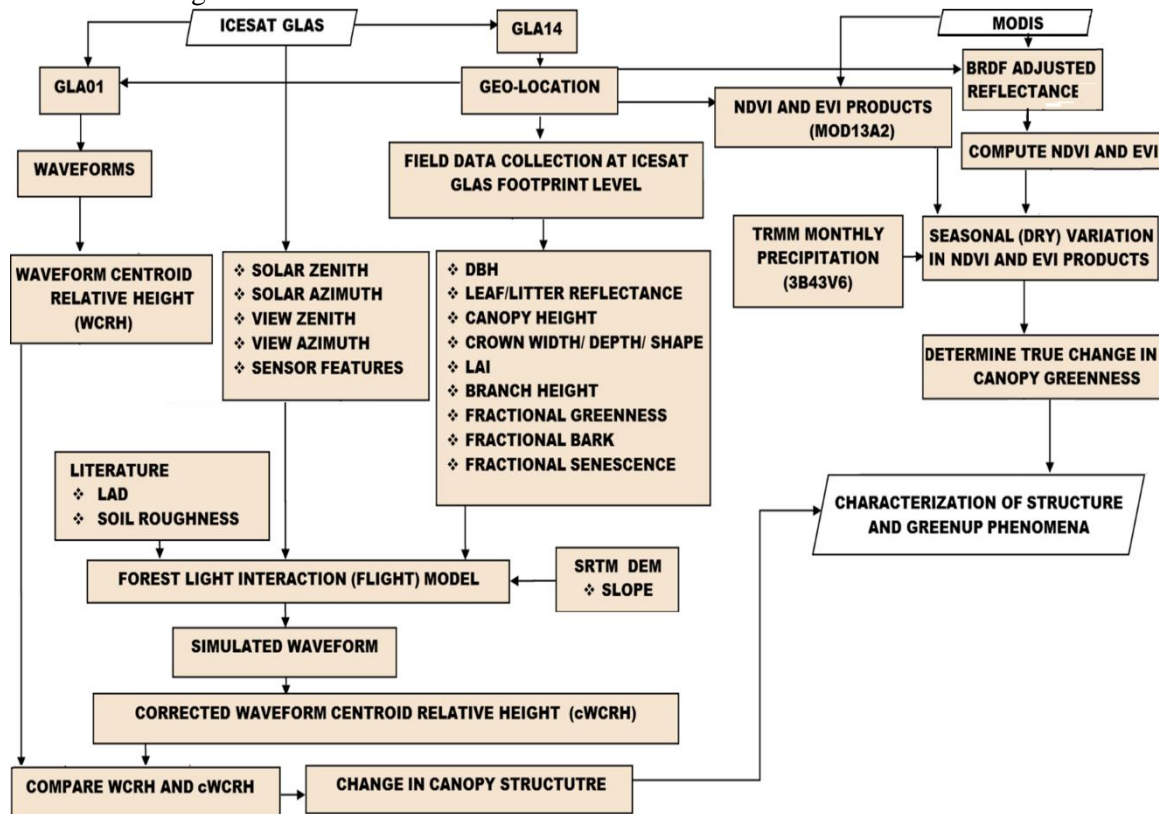
Fig. 4-1 Paradigm of the Study

4.1   ICESat/GLAS Data Processing

The standard methodology for downloading of ICESat/GLAS data and processing is available at NSIDC website (http://nsidc.org/data/icesat). The procedure followed for data processing is listed as under:

- Out of the 15 GLAS data products, two data products (GLA01 and GLA14) of Release 33 were used.
- Relevant data was downloaded with the help of known coordinates from NSIDC website (http://nsidc.org.data/icesat).
- Elevation as well as information related to geolocation were extracted from GLA14 data using NSIDC GLAS Altimetry Elevation Extraction Tool (NGAT).
- GLA14 product includes UTC time at which the waveform from a footprint is recorded and this UTC time is utilized to extract the raw waveforms from the GLA01 file.
- The GLA01 product that pops up in SCF_VISUALIZER is provided by NSIDC. The IDL Virtual Platform initializes the icesatvis_ds.sav file (to run the visualizer via the IDL Virtual Machine) that is provided by NSIDC to open the SCF_VISUALIZER. Window showing the raw waveform in the visualizer is in Fig.4.1.

- The waveform received has two values: Volts on the 'Y' axis and response bins of interval 1 nanosecond on the 'X' axis. Received as well as transmitted waveforms along with the respective sensor gains (in dB) are shown in the curve (Fig. 4). Estimates for mean and standard deviation of background noise are also available from the waveform window. IUTC time that uniquely recognizes the waveform is shown on the upper right corner. Predicted coordinates however can only be had from the GLA14 product. The waveform is later exported in form of a text file to be used for retrieval of biophysical parameters.
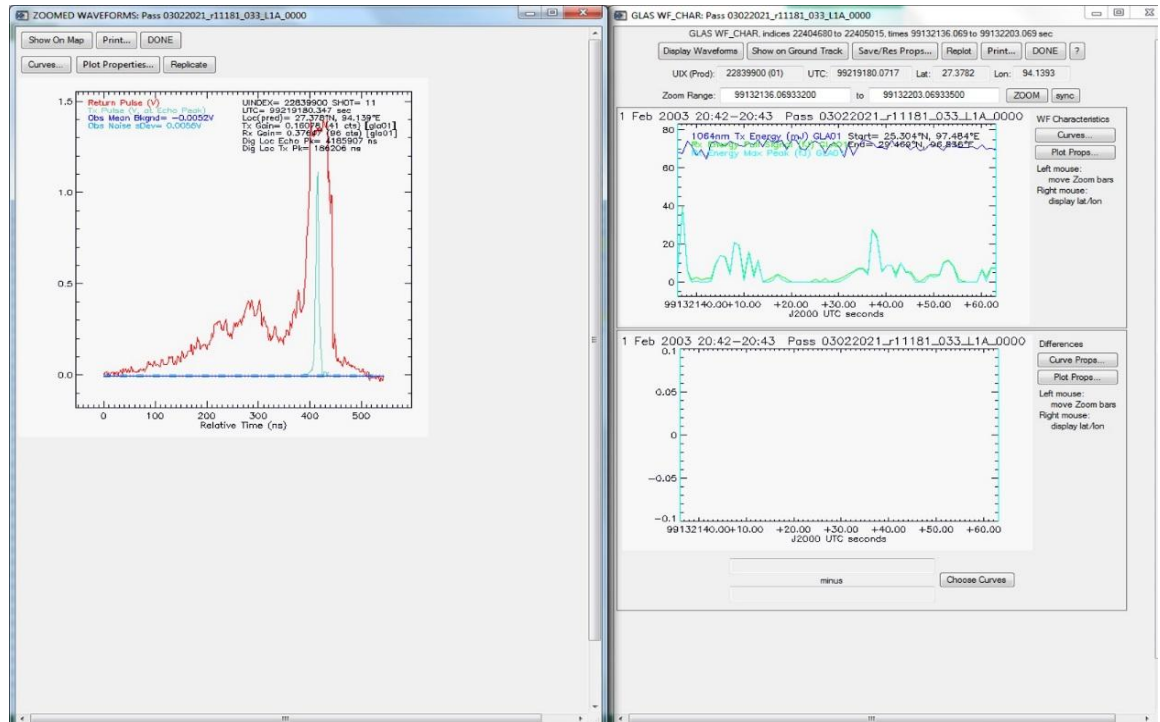
Fig. 4-2 Raw Waveform

4.2 Waveform Conversion

ICESat/GLAS data (GLA01) is generally provided in binary format (∗.DAT) that needs to be converted into ASCII format in an IDL platform developed by National Snow and Ice Data Center (NSIDC, 2007b).

4.3 Waveform Normalization

After the regeneration of the wave, the voltage waveform is then normalized by allocating the amplitude with the whole received energy. The tenacity of this operation is to form the waveform comparable, since different waveforms are captured at different time periods. Due to different climate or changes within the behavior of the laser device, the quantity of return energy could vary with time and the ground surface. This operation makes it attainable for cross check of the relative energy levels from numerous waveforms (Duong *et al.*, 2006). Normalization process is completed by dividing the received energy V_i at the moment *i* by the total energy V_T, calculated with the help of the following Eq. 4.1

$$V_T = \sum_{i=1}^{M} V_i \qquad \text{…………………………………………………..(Eq. 4.1)}$$

Then the normalization is described by Eq. 4.2 as

$$V_{Norm}(i) = {V_i}/{V_T} \qquad \text{………………………………….....……………..…(Eq. 4.2)}$$

Where, 'M' is the no. of waveform bins, which is 544 and 1000 in this present study.

4.4 Detection of effective waveform signal

A waveform detector system constantly measures the return signal. Therefore, it becomes essential to extract actual waveform signal from the continual datum (Duong, 2010). This method is enforced by considering the position of the amplitude of the GLAS waveform signal that firstly exceeds a certain noise level threshold. In the present study, it was observed during the visualization of the data that the actual waveforms signal (Fig. 4.13) often start after 720th bins (720 ns) within 1000 bins. Hence, the first 720 bins have been used for the calculation of mean (M_N) and standard deviation (δ_N) of the noise, as expressed within the equation (4.3) and (4.4).

$$M_N = \sum_{i=1}^{720} V_i / 720 \qquad \dots\dots\dots\dots\dots\dots\dots\dots\dots\dots\dots\dots\dots\dots\text{(Eq. 4.3)}$$

$$\delta_N = \sqrt{\sum_{i=1}^{720}(V_i - M_n)^2 / 720 - 1} \qquad \dots\dots\dots\dots\dots\dots\dots\dots\dots\dots\dots\dots\text{(Eq. 4.4)}$$

Where, (V_i) is the amplitude of the (i^{th}) bin in the waveform. The threshold value T_n for distinguishing between noise and actual signal is determined as the mean plus four times the standard deviation (Lefsky *et al*., 2005) as described in Equation (4.5). The signal value at that part of the waveform that is below the threshold is set to zero.

$$T_n = \mu_n + 4 * \sigma_n \qquad \dots\dots\dots\dots\dots\dots\dots\dots\dots\dots\dots\dots\dots\dots\text{(Eq.4.5)}$$

This also contributes to smooth differentiation of more noisy waveforms from the less noisy ones.
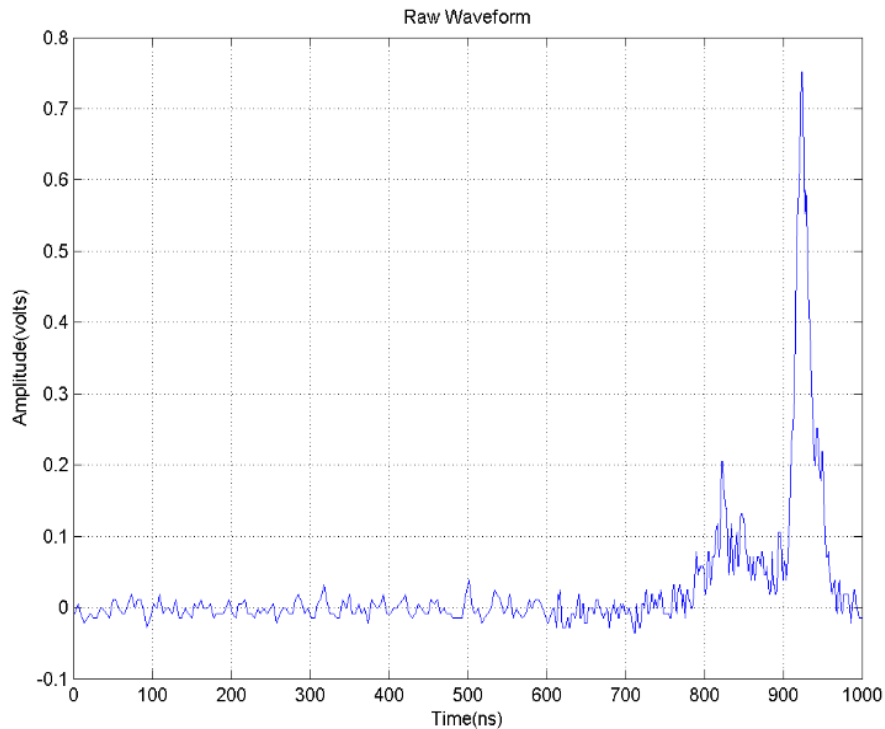
Fig. 4-3 GLAS waveform signal defined based on threshold value

4.5 Waveform Smoothing

The smoothing of the waveform is very important to eliminate the noise and ensure initial estimates for the waveform parameters like estimating the locations and amplitudes of the peaks within the waveform that further smoothens the voltage waveform through a Gaussian filter (Duong, 2010). Due to the noisy nature of many waveforms, estimation of initial values from the raw waveform

signal ends up in large number of modes with a low amplitude and a slender width. Therefore, it becomes necessary to smooth the waveforms so as to induce a smaller variety of modes. Although numerous smoothing algorithms do exist in MATLAB user library, yet Gaussian filter was used for smoothening during the present course of study.

4.6 Waveform Gaussian Fitting

Gaussian Decomposition technique was used for waveform processing with the help of MATLAB code wherein the transmitted waveform $W_x(t)$ (Fig.4.3) is assumed to have a bell shape and modeled as Gaussian function as follows:

$$W_x(t) = A_x * e^{-(t-x)^2/2\sigma_x^2} \qquad \dots\dots\dots\dots\dots\dots\dots\dots\dots\dots\dots\dots\dots(Eq.4.6)$$

Where, A_x is the amplitude of transmitted pulse, T_x is the mean value demonstrating the peak location and σ_x represents width of transmitted pulse at half power. The received waveform is modeled as a sum of Gaussian components.
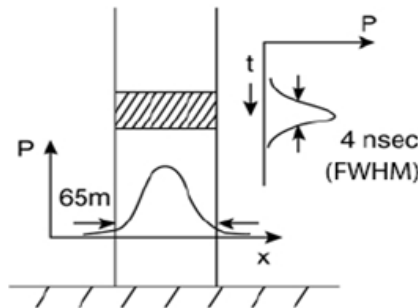
Fig. 4-4 A transmited pulse of the ICESat laser altimetry System

Gaussian decomposition assumes that both the transmitted and received waveforms are Gaussian in nature (Fig.4.15) and can be fitted reasonably well using Gaussian peaks.
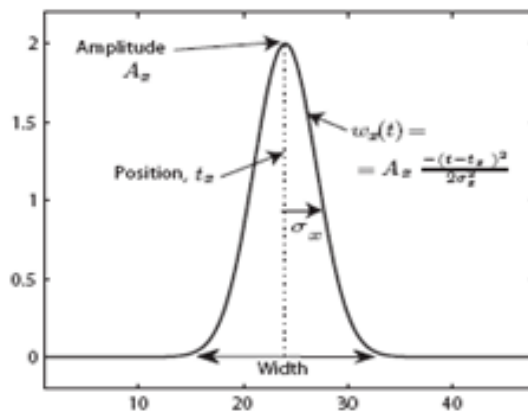
Fig. 4-5 Gaussian function used to describe the transmitted pulse

Each Gaussian element is presumed to result from the interaction of the transmitted pulse with a specific object on the earth surface inside the footprint. The full waveform W(t) is represented as in the following Fig. 4.6.

$$w(t) = \varepsilon + \sum_{n=1}^{N} w_n(t), \text{ with } W_n = A_n * e^{-(t-T_x)^2/2\sigma_x^2} \quad \dots\dots\dots\dots(Eq.4.7)$$

25

where ε a noise term, $w_n(t)$ is the nth Gaussian component, N is the total number of components or the number of different reflecting layers inside the footprint.
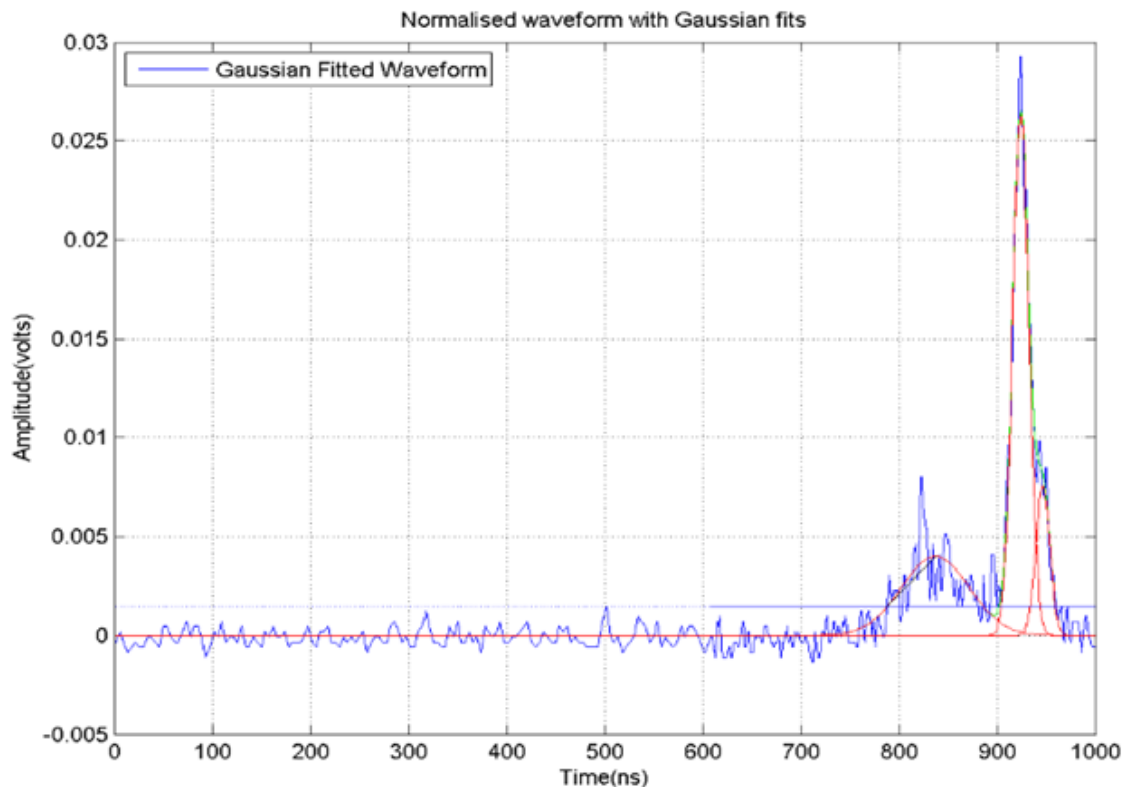
Fig. 4-6 Gaussian fitted waveform along with the raw waveform in blue

The curve was smoothened repeatedly by Gauss fit function in MATLAB and then it fits the smoothened curve with Gaussian components. Here, the user has to provide the number of peaks been desired as input. The number of peaks was intentionally kept less than 6 and the final selection of the number of peaks was made with the help of MATLAB Code based on the least RMS error between the fitted curve and the smoothened curve. In addition, the Code also implements the following 4 conditions of fitting:

i.   The number of Gaussians to 6.
ii.   The minimum distance between neighbouring peaks to 1.5m.
iii. The minimum sigma width of a peak to 30cm.
iv.   The minimum amplitude of an individual peak to be in equal to the noise threshold (Duong, 2010)

Likewise, the code was also developed for Gaussian fitting of the transmitted pulse. After fitting, it is generally presumed that the last peak is the ground peak. Sometimes, this is not the case and the waveform has a tail bit longer than the usual, caused by cloud conditions. This effect is often referred to as the *Ringing Effect* (Fricker *et al.*, 2005). Fig. 4.17 shows the Gaussian fitting waveform with some GLAS waveform parameters.
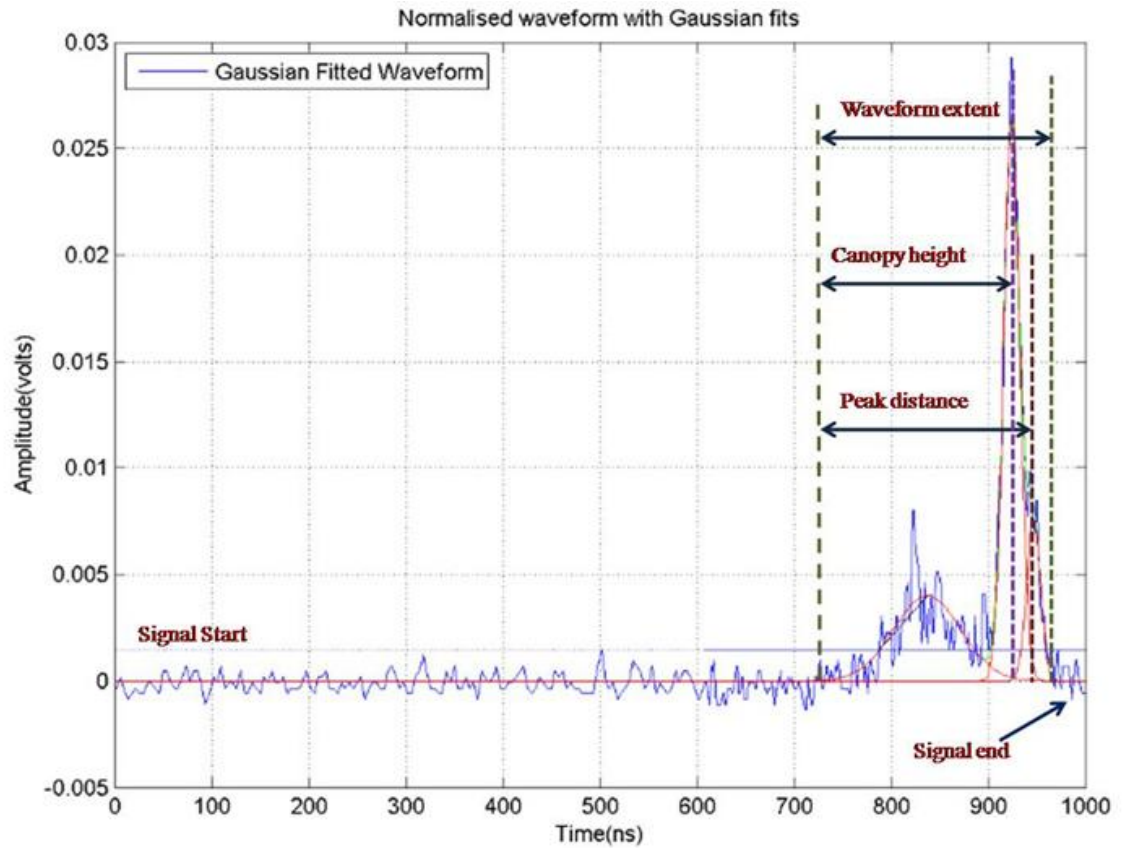
Fig. 4-7 Gaussian fitted waveform along with GLAS waveform parameters

4.7   Laying of ICESat Footprints on the Google Earth Imagery

With the help of the coordinates generated through the processing of GLA14 data, shape files of the footprints were created and overlaid on Google Earth Imagery. This later helped for tracing the location and accessibility of the footprints during ground verification at ICESat footprint level. The generated shape files also helped in the extraction of values from different layers used throughout the period of study.

4.8   Retrieval of Biophysical Parameters at GLAS Footprint level

Biophysical parameters using MATLAB code were generated as described by Duong (2010) (Appendix I). Out of these parameters, 18 parameters were pertinent excluding *pstart, pend, wcanopy* and *wground* which were selected for biomass prediction. The description of the parameters is shown in Appendix-I.

Besides the above parameters as mentioned above, the waveform centroid relative height (WCRH) was used in this study to assess changes in relative height of median energy within the waveform (Morton *et al.*, 2014).

$$WCRH = \frac{CE - S_e E}{S_s E - S_e E} \dots\dots\dots\dots\dots\dots\dots\dots\dots\dots\dots\dots\dots\dots\dots\dots\dots\text{(Eq.4.8)}$$

where CE corresponds to the waveform centroid elevation, $S_s E$ is the signal start elevation and $S_e E$ is the signal end elevation as determined by thresholds defined for the alternate (land) waveform processing schemes.

27

4.9   LAI Estimation from GLAS waveform

Following the retrieval of biophysical parameters, GLAS waveform parameters, such as canopy return energy (*eCanopy*) and ground return energy (*eGround*) were used for calculating LAI with the help of gap-fraction formula given by Beer Lambert's law for a tree canopy (Richardson *et al*., 2009; Zhao & Popescu, 2009; Luo *et al*., 2013).

Diminution of the transmission of a light beam through the tree canopy can be described by Beer–Lambert's equation of light annihilation considered as a function of LAI (Richardson *et al*., 2009)

$$I = I_0 e^{-kL}$$ …………………………………………………………… (Eq.4.9)

Where L denotes LAI, *I* is the light intensity below the canopy, I_0 is the light intensity attaining the top of the canopy, while *k* is the extinction coefficient that depends upon the leaf inclination angle dispersal as well as the direction of illuminating beam. With known values of *k*, *L* can be estimated based on the gap fraction (I/I_0) as:

$$L = -\frac{1}{k} \ln\left(\frac{I}{I_0}\right)$$ ……………………………………………………… (Eq.4.10)

One of the specific characteristic of a LiDAR waveform is that the ratio of ground return energy to its total energy illuminated (I/I_0) is always proportional to the gap fraction (Lefsky *et al*., 1999) and is considered as the probability of light beam crossing the canopy layer without any collision (Gower *et al*., 1999). Hence, the gap fraction may be replaced with the fraction of the return energy transmitted through the canopy layer to the total return energy. Thus, *eCanopy* or the canopy return energy is calculated by adding up the waveform return energy reflected from the canopy layer.

Usually, reflectance at GLAS wavelengths differs between canopy and forest ground covered with litter mass (Lefsky *et al*., 1999). Reduction of this reflectance differential on the accuracy of LAI estimation, the total energy ratio needs adjustment. Hence, a factor of 2 was used as an optimal height threshold to separate ground and canopy return energy (Lefsky *et al*., 1999). Following this, for each GLAS waveform, E_r (ground to total energy ratio) was derived by taking the ratio of the ground return energy and the total waveform return energy given as:

$$E_r = \frac{nG_R}{C_R + nG_R}$$ ……………………………………………………… (Eq. 4.11)

In the present study, for calculation of LAI, E_r was used instead of I/I_0 (Richardson *et al*., 2009; Solberg, 2010). Hence Equation 4.10 becomes

$$L = -\frac{1}{k} \ln(E_r)$$ ……………………………………………………… (Eq.4.12)

4.10   Delineation of Tropical Wet Evergreen Forest at GLAS Footprint Level

Intersection of GLAS Footprints over the tropical wet evergreen forests of North East India was done and the area delineated.

4.11   Vegetation Indices at GLAS Footprint Level

- ❖ MODIS vegetation indices, such as EVI and NDVI available on 16-day interval were downloaded, extracted, re-projected and then clipped with the study area boundary and then with the region of interest *i.e.* area representing the tropical wet evergreen forests of North East India.

❖ ICESat GLAS Footprints were then overlaid on the Imagery of Vegetation Indices data products ranging from 2003-2008 and the point values in each layer were extracted in ArcGIS for further interpretation.

4.12 MODIS-BRDF Adjusted Surface Reflectance Data

❖ MODIS BRDF Adjusted Surface Reflectance Data available on 8-day interval were downloaded, extracted, re-projected and then clipped with the study area boundary and then with the region of interest *i.e.* area representing the tropical wet evergreen forests of North East India.

❖ ICESat GLAS Footprints were then overlaid on each of the Imagery ranging from 2003-2008 and the point values in each layer were extracted in ArcGIS for further interpretation.

4.13 Collection of Field Data

Location and mode of accessibility of the footprints were traced initially with the help of Google Earth Imagery. Footprint centers on the ground were traced during January'2015 and May'2015 with the help of a handheld Trimble Juno GPS and a high resolution Google Imagery (Fig. 3.1). Altogether 19 footprints could be traced on the ground, the location of which are shown in Fig. 3.1. Based on the study by Dhanda (2013), 20 m radius circular plots were selected for vegetation height assessment. Once the center of the GLAS footprint was located, the sampling plots were laid and the diameter as well as height of the trees in those plots were noted down and marked upon. It may also be noted that field data was collected six years following the last LiDAR data availability (August 2009). Since the study plots being climax forests within the Protected Area Network (Namdapha National Park), it has not changed as been validated by field observations and Google imagery.

4.14 Monte Carlo Simulation of Radiative Transfer Model

This technique of Monte Carlo assessment of photon transport proceeds by sampling *n* rays over the instrument IFOV. For each ray:

1. One has to find the intersection with the first surface facet (leaf/bark/soil).
2. The facet illumination is considered as the sum of direct and diffuse incoming light. The diffuse light term is calculated by recursive sampling of higher scattering orders. Radiance input is defined according to the standard rendering equation, depending on facet orientation with respect to illumination, and optical properties.
3. For each facet and scattering order, both the radiance inputs and the total return path length to the sensor are calculated. The path length is equivalent to time of signal. For efficiency, ground leaving radiance for unit incoming signal is initially recorded.
4. The radiance is binned into m bins according to path length, whose width is defined by the sensor model temporal sampling. The final steps accounts for detector characteristics and pulse width.
5. The radiance values are converted into absolute power (mW) recorded in each temporal bin, dependent on the sensor aperture A_r, distance to sensor P_z and atmospheric round-trip transmission T_{RTstm}. The effect of pulse width is modelled by Gaussian convolution of the resultant output array, with amplitude dependent on emitted pulse energy E_{trans}. The estimation error decreases as $n^{0.5}$ (North *et al*., 2008).

4.15 Simulation of photon trajectories using FLIGHT Radiative Transfer Model

Simulation of photon trajectories using FLIGHT requires the following combined input parameters both from Field as well as Sensor (Tables 4.1,4.2).

Table 4-1 LiDAR sensor model (North et al., 2008).

Name	Units	Meaning	Value
(P_x, P_y, P_z)	m	Sensor position relative to scene centre	(0,0,600000)
θ_0	deg	Sensor zenith angle	0
$\emptyset_0$	deg	Sensor azimuth angle	0
s1	ns	Emitted RMS pulse width assuming Gaussian (1sd)	5
q_T	rad	Half-width angle of beam divergence, Gaussian (1sd)	0.00011
IFOV	rad	Detector IFOV	0.0004
A_T	m^2	Detector telescope area	0.709
T_{RTstm}	-	Roundtrip atmospheric trans.	0.8 (532nm) 0.9 (1024nm)
E_{trans}	mJ	Total pulse energy	32 (532nm); 72 (1064nm)
Δ_t	ns	Recording bin width	1

Surface reflectance is estimated from the LiDAR return as:

$$\rho_{surf} = \frac{\pi E_{rec} R^2}{E_{trans} A_t T_{RTatm}} \qquad \text{...(Eq. 4.9)}$$

where, E_{rec} (pJ) is calculated as

$$E_{rec} = \sum_{i=1}^{m} L_i \Delta_t \qquad \text{...(Eq. 4.10)}$$

where, energy is accumulated in m sample bins, where each sample bin I has accumulated power $L_i (mW)$, and the bins correspond to temporal increment Δ_t ns. (North *et al.,* 2008).

Table 4-2 FLIGHT canopy input parameters (North et al., 2008).

Name	Units	Meaning	Value
PAI	m^2/ m^2	Plant area index (one sided)/ Leaf area index	*
LAD	-	Leaf angle distribution	*
F_c	-	Crown fractional cover	*
F_b	-	Fraction of bark	*
E_{xy}	m	Ellipsoid horizontal radius	*
E_z	m	Ellipsoid vertical eccentricity	*
D_1	m	Leaf size diameter	*
DBH	m	Trunk diameter at breast height	*
S_r	0-1	Soil roughness	*
S_y	Deg	Terrain slope (yz plane)	*
H_{min}, H_{max}	m	Min/max height to crown start	*
ρ_L	-	Leaf reflectance	*
τ_L	-	Leaf transmittance	*
ρ_S	-	Soil reflectance	*

*To be determined from field observations

4.16 Execution of FLIGHT Radiative Transfer Model

Once the inputs to FLIGHT are finalized, the input text file in the C-Program file needs to be updated accordingly (Table 4.3) following which .exe file is executed on Windows platform (Fig. 4.8.1, Fig. 4.8.2).

Table 4-3 Input parameters used for execution of FLIGHT.

Input Variables	Inputs	Description
'f' or 'I' or 's' or 'r'	MODE	Mode of operation: Forwards ('f'), image ('i'), solid-object image ('s'), reverse ('r')
1 or 3	ONED_FLAG	Dimension of model: '0' or '3' means 3D Representation, '1' means 1D representation
0.0 0.0	SOLAR_ZENITH, VIEW_ZENITH	Source zenith and View zenith (degrees). (Negative value for source => diffuse beam only)
0.0 0.0	SOLAR_AZIMUTH, VIEW_AZIMUTH	Source azimuth and View azimuth angles (degrees)
2	NO_WAVEBANDS	Number of wavebands simulated
25000	NO_PHOTONS	Number of photon paths simulated
3	TOTAL_LAI	Mean one-sided total foliage area index for scene (m^2/m^2)
0.85 0.0 0.15	FRAC_GRN, FRAC_SEN, FRAC_BARK	Foliage composition: FRAC_GRN, FRAC_SEN, FRAC_BARK
0.015 0.045 0.074 0.1 0.123 0.143 0.158 0.168 0.174	LAD[1-9]	Leaf angle distribution, giving angle between normal to leaves and vertical, expressed as fraction lying within 10 degree bins 0-10, 10-20, 20-30... 80-90
0	SOIL_ROUGH	Soil roughness index (0-1). Lambertian soil given by 0, rough (mean slope 60 degree) given by 1
-1.1	AER_OPT	Aerosol optical thickness at 555nm (A negative value means direct beam only)
0.05	LF_SIZE	Leaf size (radius, approximating leaf as circular disc).
0.6	FRAC_COV	Fraction of ground covered by vegetation (on vertical projection, and approximating crowns as opaque)
For 3D case only:		
10	GROUND_SLOPE (degrees)	Degree of slope derived from SRTM data
'e' or 'c' or 'f'	CROWN_SHAPE	'e' for ellipsoid, 'c' for cones, 'f' for field data in file crowns.dat
10.0 10.0	E_{xy}, E_z	Crown radius(E_{xy}), and center to top distance (E_z). For cones, (E_z) gives crown height, while for ellipsoids it gives half of the crown height.
5.0 10.0	MIN_HT, MAX_HT	Min and Max height to first branch. Crowns randomly distributed between these ranges. Total canopy height will be the sum of this value and crown height
2	DBH	Trunk Diameter at Breast Height (DBH). Trunks approximated as cones from ground to top of crown. A zero value indicates trunks should not be modelled (resulting in faster calculation)
NB: All distances are specified in meters while angles are in degrees. For the 1D case, canopy height is assumed to be 1m, and LF_SIZE should be scaled in proportion, in range 0-1.		

FLIGHT model then executes on Windows platform as follows:
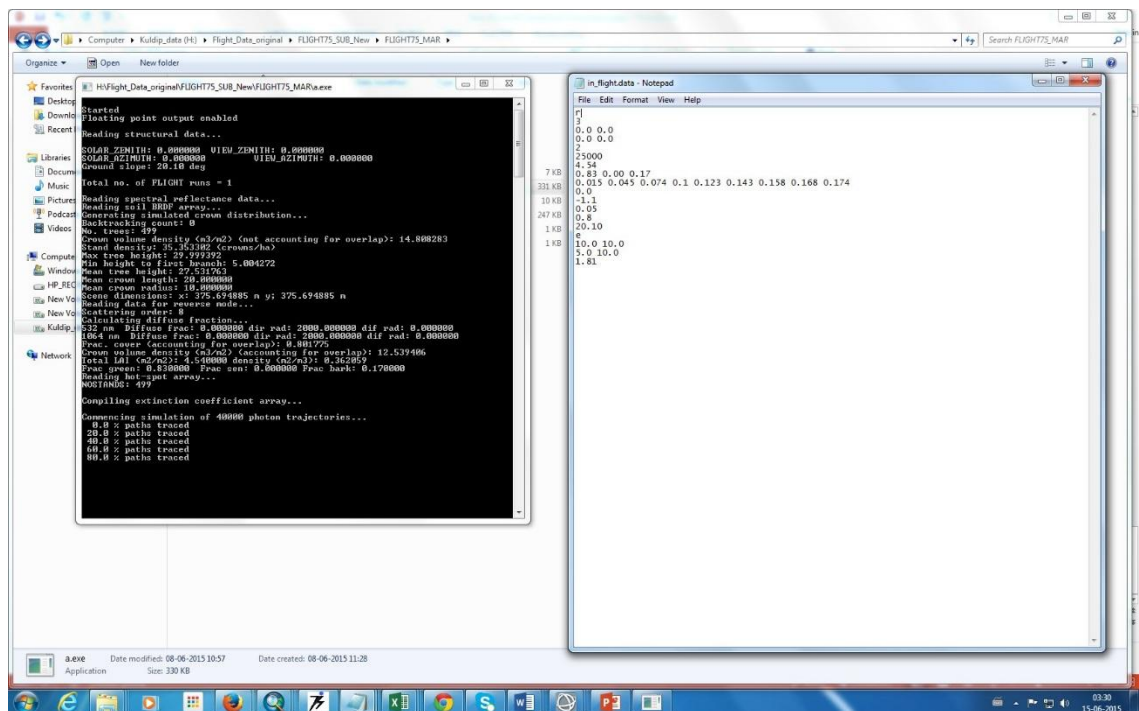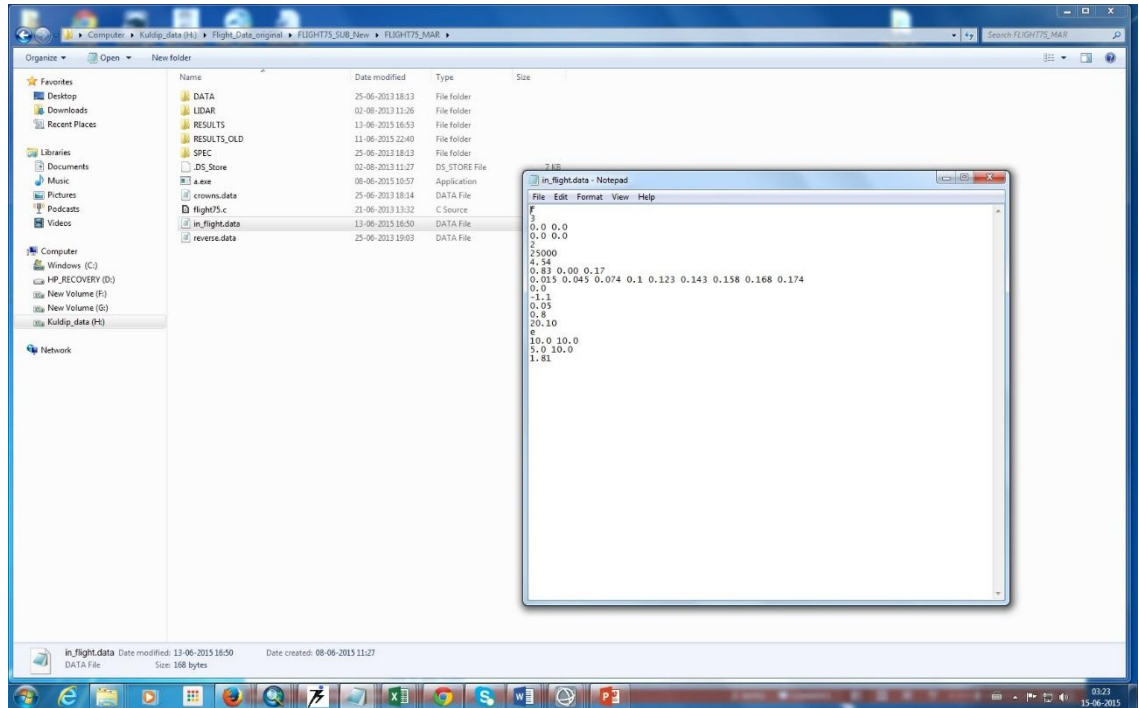
Fig. 4.8.1 Execution of FLIGHT model
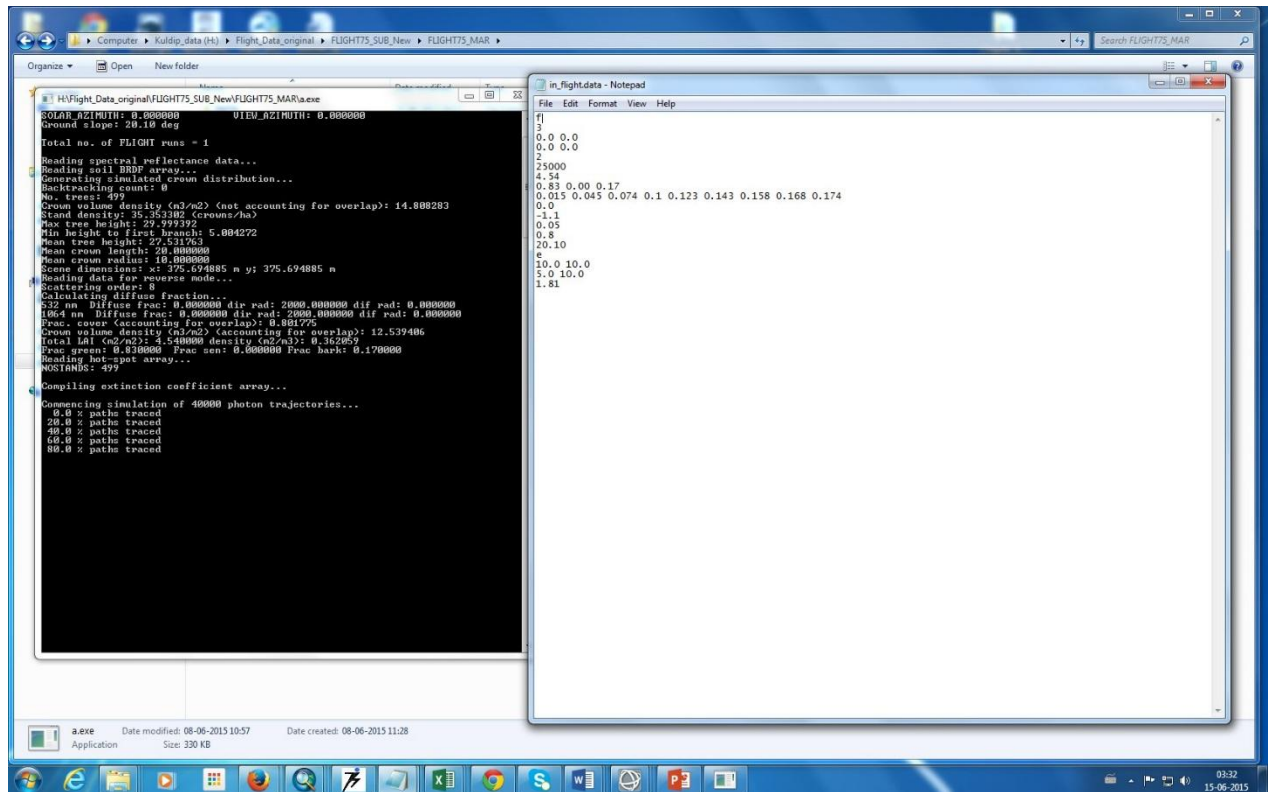
Fig. 4-8 Execution of FLIGHT model

The C Program file in Windows platform executes in two modes mainly:
1. forward ('f') mode and
2. reverse ('r') mode

In forward ('f') mode, the photons are traced as they enter the top of the canopy, scatter off the ground and/or canopy foliage, and then are either absorbed or escape to the sky while the reverse ('r') mode estimates the irradiances on leaf surfaces using Monte Carlo sampling (Alton *et al*., 2005).

All the outputs generated are stored in the Results Directory for further interpretation.

Results and Discussion

_____

5.1   Delineation of Tropical Wet Evergreen Forest

Vegetation Type Map prepared by FSI (2013) was used to delineate the tropical wet evergreen forests of North East India (Figure 5.1)
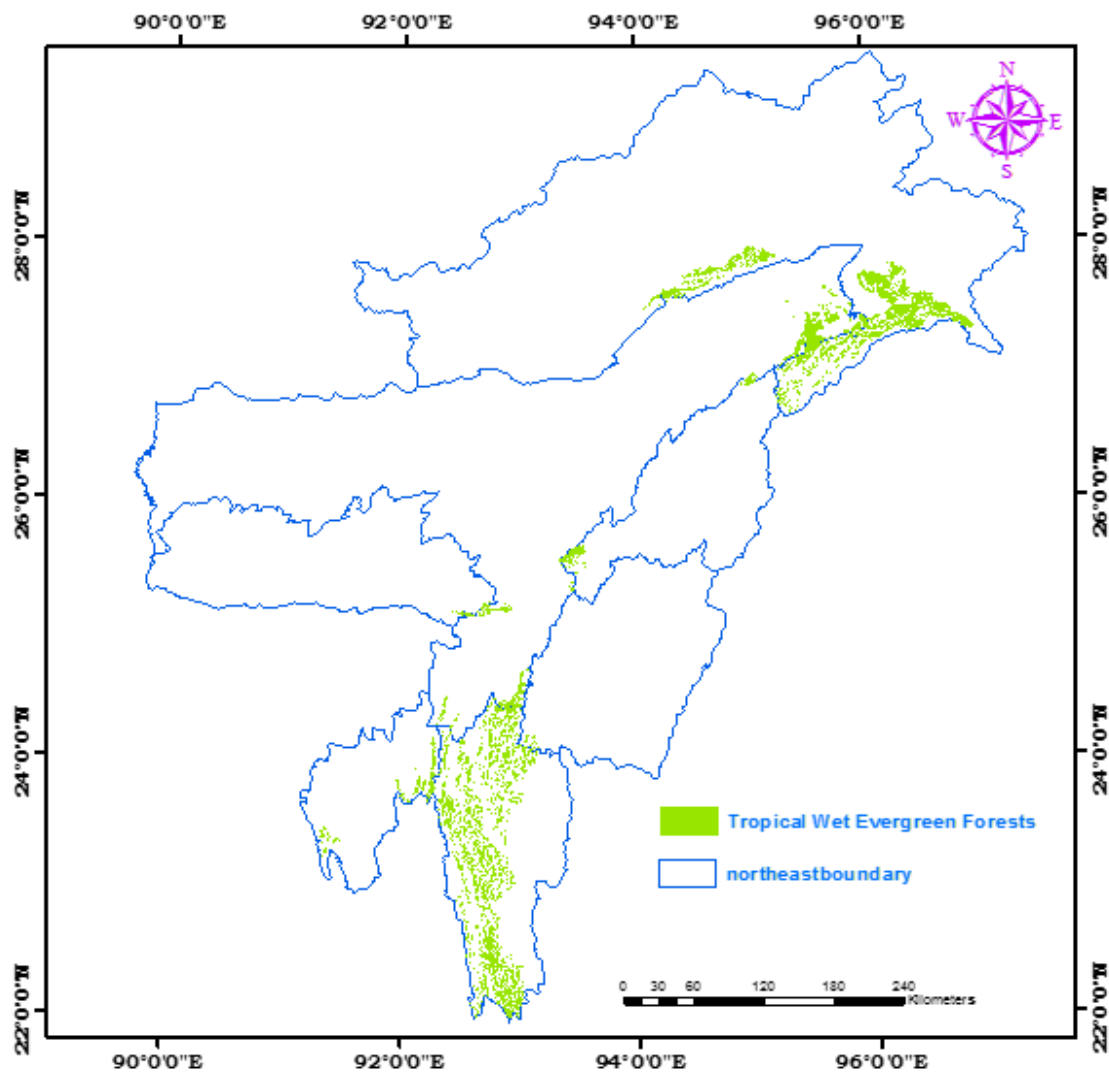
Fig. 5-1 Distribution of Tropical Wet Evergreen Forest in North East India

Tropical wet evergreen forests in North East India covers an area of 7445.6 km^2 (FSI, 2013). The present study however focused on the tropical wet evergreen forests of Arunachal Pradesh.

5.2   Delineation of Geolocation at ICESat footprint level

Altogether 06 passes (Fig. 5.2) 'representing three prominent seasons of different years were observed to pass through the Study Area (Table 5.1)

Table 5-1 Description of the ICESat footprints over the study area

| Seasons	Date	Number of Footprints
Winter	29th February'2004	20
	29th February'2008	94
Summer	30th May'2004	36
	05th June'2006	30
Autumn	06th November'2006	88
	26th November'2008	124
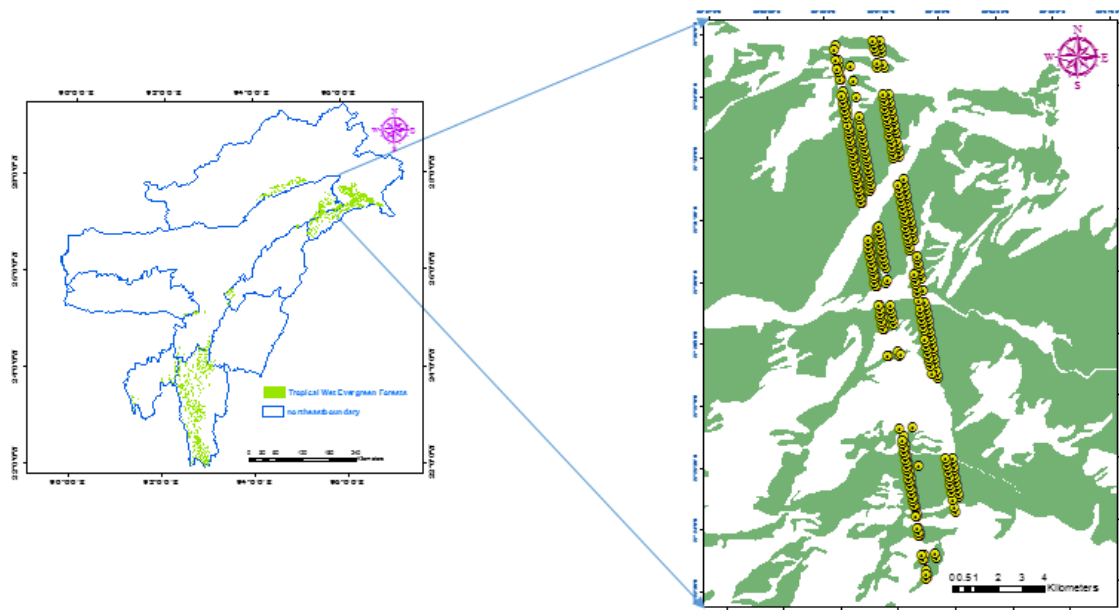
Fig. 5-2 GLAS footprints overlaid on tropical wet evergreen forests

5.3   Changes in Greenness at ICESat Footprint Level

Passive optical multispectral and multiangular remote sensing has been extensively used to estimate land surface variables (Roberts, 2001; Liang, 2007). MODIS EVI and NDVI data was analyzed between 2003 and 2008 (Table 5.2; Fig.5.3). Interestingly, it showed a sharp decline during the dry months (November to March). This is in accordance to the findings of Morton *et al.* (2014) for Amazon forests. Although, in some instances, EVI and NDVI data do not match. Since both are vegetation indices of the growing season and/or dry season the trend should match. Due to this discrepancy, precipitation data derived from TRMM was examined (Fig. 5.3). Comparing NDVI and EVI values with precipitation, it was observed that EVI and NDVI show low values in

the monsoon period which differs from the phenological characteristics of tropical evergreen forests. In high precipitation time NDVI and EVI do not show the actual greenness of the study area. Also in dry season, EVI and NDVI show large declination in few years and over all variation of EVI and NDVI were large (0.2-0.54 for EVI and 0.35 to 0.9 for NDVI). This nature of EVI and NDVI implies either the forest losses its tropical evergreen characteristics due to mixing up with other kind of forest or there is a problem in datasets itself.

Table 5-2 Vegetation indices and TRMM mean monthly precipitation at ICESat Footprint level (2003-2008)

Months	EVI	NDVI	TRMM Mean Precipitation
January_2003	0.41775	0.842763	0.063734
February_2003	0.379747	0.835422	0.193615
March_2003	0.355203	0.795078	0.101397
April_2003	0.289606	0.778119	0.345559
May_2003	0.386425	0.757194	0.269746
June_2003	0.420775	0.7638	0.573266
July_2003	0.28365	0.472259	0.684425
August_2003	0.487306	0.644331	0.381503
September_2003	0.535591	0.782053	0.25869
October_2003	0.466966	0.807119	0.199453
November_2003	0.446556	0.876194	0.016007
December_2003	0.468175	0.864947	0.057286
January_2004	0.452241	0.866991	0.084806
February_2004	0.362194	0.8506	0.209796
March_2004	0.201203	0.824644	0.380071
April_2004	0.249488	0.677888	0.434968
May_2004	0.378378	0.65005	0.692644
June_2004	0.368025	0.505409	0.47901
July_2004	0.290331	0.353581	0.823979
August_2004	0.512919	0.755084	0.310291
September_2004	0.414613	0.743272	0.267615
October_2004	0.454616	0.851847	0.242859
November_2004	0.469791	0.875747	0.008108
December_2004	0.453209	0.859216	0.048573
January_2005	0.420388	0.849188	0.076479
February_2005	0.418388	0.817866	0.330278
March_2005	0.357709	0.715928	0.615597
April_2005	0.297122	0.721531	0.314549
May_2005	0.402519	0.744791	0.218626
June_2005	0.368025	0.687619	0.195877
July_2005	0.290331	0.583369	0.436176
August_2005	0.512919	0.51425	0.299058
September_2005	0.414613	0.883178	0.12994
October_2005	0.454616	0.8973	0.131336
November_2005	0.469791	0.882013	0.068693

Months	EVI	NDVI	TRMM Mean Precipitation
December_2005	0.453209	0.861647	0.010959
January_2006	0.420388	0.853834	0.002336
February_2006	0.389006	0.806813	0.555728
March_2006	0.336803	0.776616	0.227433
April_2006	0.337925	0.742178	0.220484
May_2006	0.450272	0.800453	0.44421
June_2006	0.440622	0.785316	0.373253
July_2006	0.521109	0.839194	0.537343
August_2006	0.47865	0.892978	0.181058
September_2006	0.457891	0.7551	0.200672
October_2006	0.485006	0.879578	0.052699
November_2006	0.463778	0.877775	0.081523
December_2006	0.401213	0.850238	0.048722
January_2007	0.396663	0.8535	0.036142
February_2007	0.369766	0.840734	0.075712
March_2007	0.4084	0.812825	0.074291
April_2007	0.319688	0.7681	0.20148
May_2007	0.484559	0.766822	0.230988
June_2007	0.529613	0.778097	0.298321
July_2007	0.490069	0.694719	0.376753
August_2007	0.475116	0.867178	0.397546
September_2007	0.372738	0.635472	0.613445
October_2007	0.499731	0.895038	0.151472
November_2007	0.49215	0.881347	0.080205
December_2007	0.455906	0.864891	0.013884
January_2008	0.459869	0.854013	0.052043
February_2008	0.384359	0.812281	0.053299
March_2008	0.343072	0.792597	0.268735
April_2008	0.339006	0.774181	0.268821
May_2008	0.438169	0.772019	0.388636
June_2008	0.309209	0.417759	0.243365
July_2008	0.471081	0.681597	0.270951
August_2008	0.441372	0.749663	0.299001
September_2008	0.462966	0.867453	0.109161
October_2008	0.5038	0.878828	0.12729
November_2008	0.464028	0.877088	0.005143
December_2008	0.461859	0.852056	0.00217

During field survey, *Ailanthus grandis, Altingia excelsa, Castanopsis indica, Duabanga sonneriatioides, Dysoxylum binectariferum, Mesua ferrea, Taluma hodgsonii, Terminalia myriocarpa, Vatica lancefolia, Shorea assamica* and *Dipterocarpus macrocarpus* species were identified. These are well known species of tropical evergreen forest. So the focus was laid on datasets. To verify the results obtained from MOD13A2 NDVI and EVI products, MODIS- BRDF Adjusted Surface Reflectance Data (MCD43B4) was used. BRDF gives the reflectance of a target

as a function of illumination geometry and viewing geometry. It depends on wavelength and is determined by the structural and optical properties of the surface, such as shadow-casting, multiple scattering, mutual shadowing, transmission, reflection, absorption and emission by surface elements, facet orientation distribution and facet density (Strahler *et al*., 1999). The shape of the BRDF contains information about subpixel surface heterogeneity and can thus improve land cover classification (Pinty *et al.,* 2002). So, it is expected that MODIS- BRDF reflectance data can give better results than MOD13A2 NDVI and EVI products. EVI and NDVI were calculated from MCD43B4 reflectance data for dry season (November to March) as MOD13A2 products showed decrease in greenness. Removing artefacts of changing sun-sensor geometry in EVI and NDVI derived from MCD43B4 reflectance data for dry seasons eliminated the appearance of decreasing trend (Fig.5.4). EVI showed more consistency than NDVI (Fig.5.4). This is in agreement to the studies done for Amazon forests (Morton *et al*., 2014)
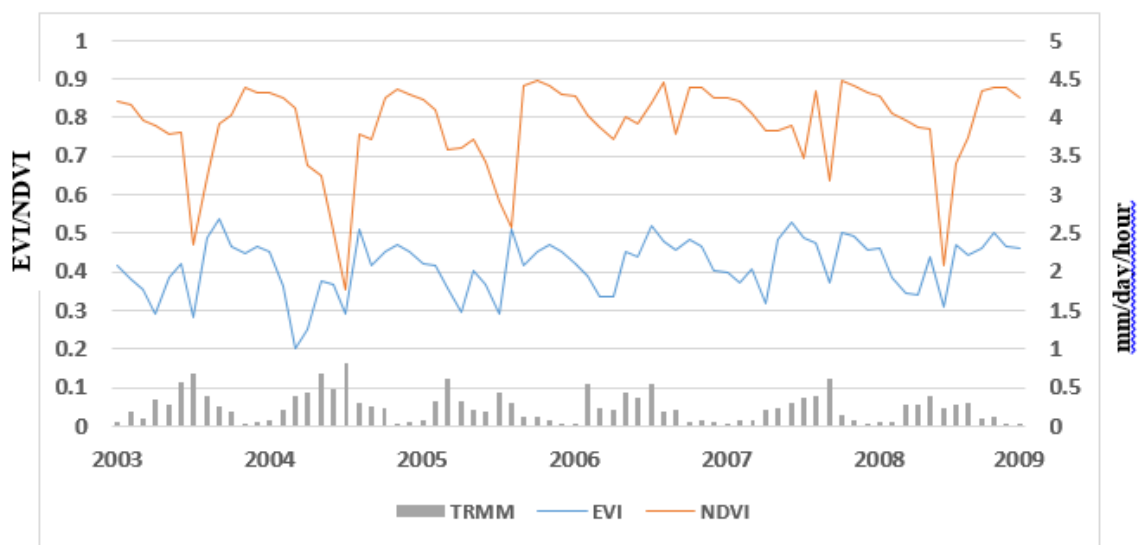

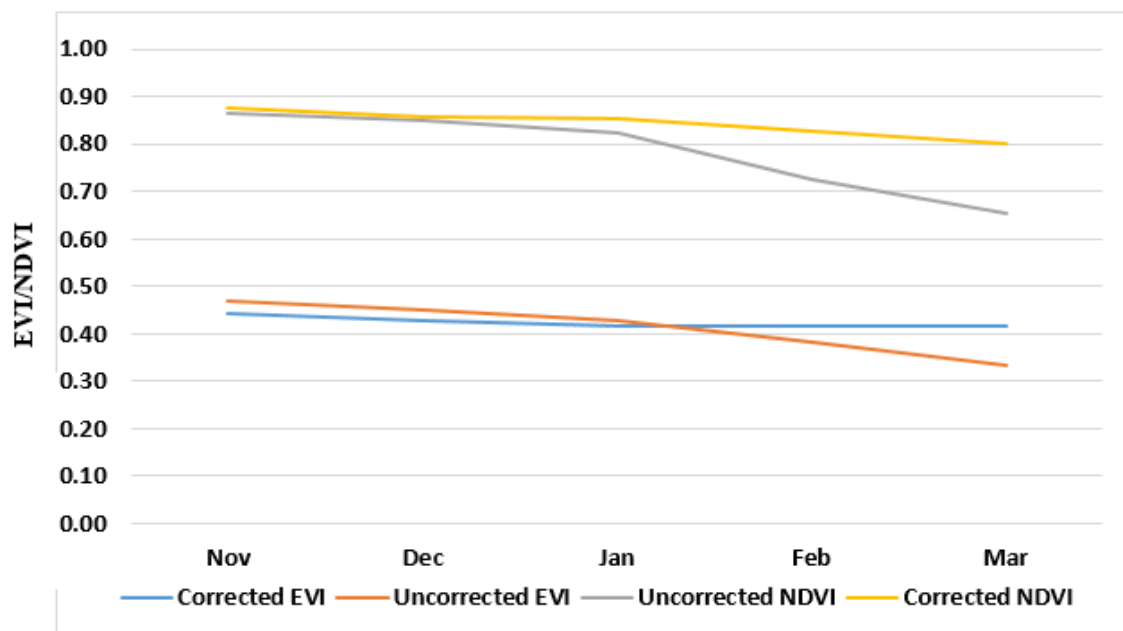**Fig. 5-3 Inter seasonal and inter annual variability of NDVI and EVI from tropical evergreen forest**

Fig. 5-4 Seasonal variation of NDVI and EVI for uncorrected and corrected MODIS data from tropical evergreen forest (2003-2008)

5.4   Changes in LAI at ICESat Footprint Level

Different bio-physical parameters across the vertical forest structure of tropical wet evergreen forests of North East India were retrieved from ICESat/GLAS LiDAR data for the dry months (2003-2008) (Table 5.3). LAI derived from ICESat Data and from Field observations through Plant Canopy Imager was analysed and showed high correlation (r=0.89) (Fig. 5.5). Using the same relation, LAI was generated for remaining ICESat/GLAS footprints wherein field data are either missing or the collection of field data was not possible.

For forests with medium to high biomass, LiDAR has the potential to estimate LAI with higher precisions than multispectral images (Zhao and Popescu, 2009). In this study, a strong relation was also found between field measured DBH and LAI (r=0.68) (Fig. 5.6). Using regression technique, DBH was generated for the remaining footprints of the study area since both DBH and LAI form valuable inputs for FLIGHT.

Thus, the present study using ICESat (Ice, Cloud and land Elevation Satellite)/GLAS full-waveform data, confirms the study of Luo *et al*.(2013), and endorses the possibility of LAI estimation for highly inaccessible forest areas.

Table 5-3 List of different bio-physical parameters retrieved from ICESat/GLAS

| Date	lat	lon	wstart	wend	wcentroid	eEcho	eground	ecanopy	WCRH	LAI
06 Nov 2006	27.39	96.53	538	788	680	34.66	2.19	32.48	0.43	4.08
06 Nov 2006	27.40	96.53	602	771	667	27.85	13.42	14.43	0.62	5.00
06 Nov 2006	27.41	96.53	593	800	676	52.69	35.08	17.61	0.60	4.48
06 Nov 2006	27.42	96.53	602	824	693	74.76	10.15	64.61	0.59	6.29
06 Nov 2006	27.49	96.52	688	885	793	37.65	5.83	31.82	0.47	3.83
06 Nov 2006	27.49	96.52	647	967	872	101.51	6.24	95.27	0.30	5.45
06 Nov 2006	27.50	96.52	739	915	843	93.35	6.98	86.36	0.41	5.81
06 Nov 2006	27.50	96.52	682	923	811	93.99	9.31	84.68	0.46	4.99
06 Nov 2006	27.51	96.52	603	795	702	85.36	17.25	68.11	0.48	6.83
06 Nov 2006	27.51	96.52	597	828	712	69.12	4.20	64.91	0.50	6.50
06 Nov 2006	27.51	96.52	586	818	713	67.68	8.05	59.63	0.45	6.42
06 Nov 2006	27.54	96.51	590	804	702	75.74	1.80	73.94	0.48	5.03
06 Nov 2006	27.55	96.51	602	804	687	97.28	12.13	85.15	0.70	6.69
26 Nov 2008	27.39	96.54	660	897	789	6.55	3.81	2.75	0.46	2.56
26 Nov 2008	27.41	96.53	693	925	847	7.90	1.00	6.91	0.34	2.00
26 Nov 2008	27.42	96.53	743	954	948	6.99	5.49	1.50	0.03	8.65
26 Nov 2008	27.48	96.52	675	966	886	5.89	2.81	3.08	0.27	3.68
26 Nov 2008	27.49	96.52	729	919	853	13.39	4.03	9.36	0.35	2.62
26 Nov 2008	27.49	96.52	786	923	879	13.58	0.62	12.96	0.32	3.30
26 Nov 2008	27.50	96.52	712	960	860	10.99	2.26	8.72	0.40	3.70
26 Nov 2008	27.51	96.52	635	948	770	5.33	1.96	3.37	0.57	6.17
26 Nov 2008	27.51	6.52	648	886	721	8.70	0.95	7.75	0.69	2.10
26 Nov 2008	27.51	96.52	657	840	781	11.45	0.34	11.12	0.32	2.91
26 Nov 2008	27.51	96.52	698	922	862	11.51	0.84	10.67	0.27	5.20
26 Nov 2008	27.53	96.51	722	945	779	10.48	1.99	8.49	0.74	3.40
26 Nov 2008	27.53	96.51	698	916	857	9.82	1.02	8.80	0.27	2.63
26 Nov 2008	27.54	96.51	734	928	812	8.65	2.23	6.42	0.60	2.45
26 Nov 2008	27.57	96.51	719	940	836	4.36	0.30	4.06	0.47	2.07
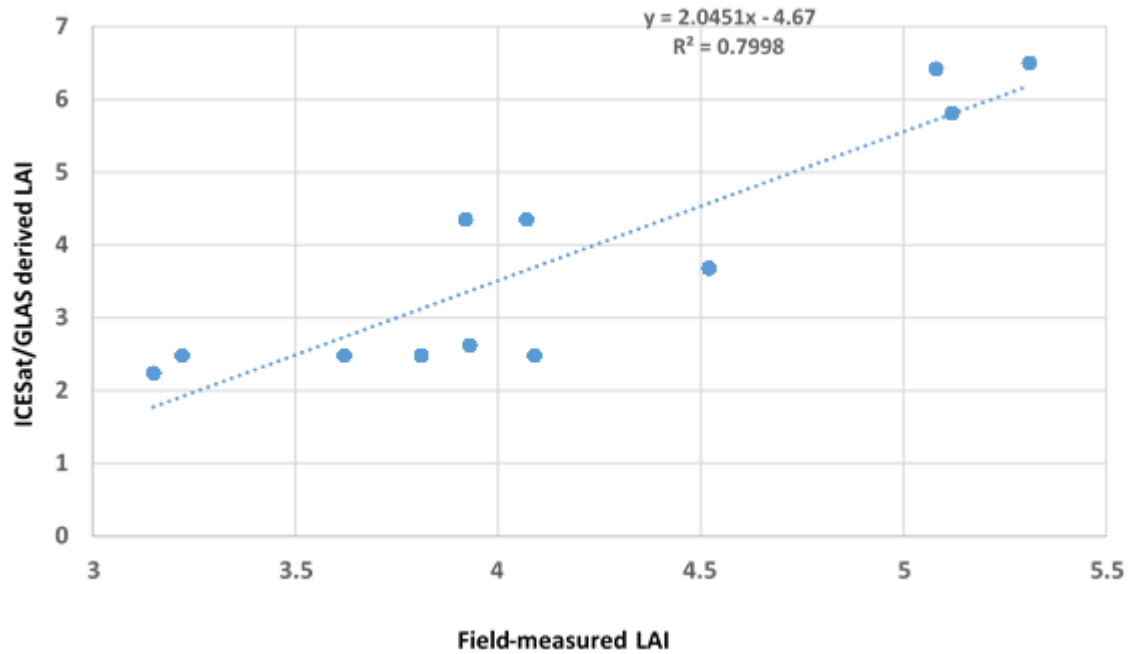
Fig. 5-5 Relationship of field measured LAI with ICESat/GLAS derived LAI
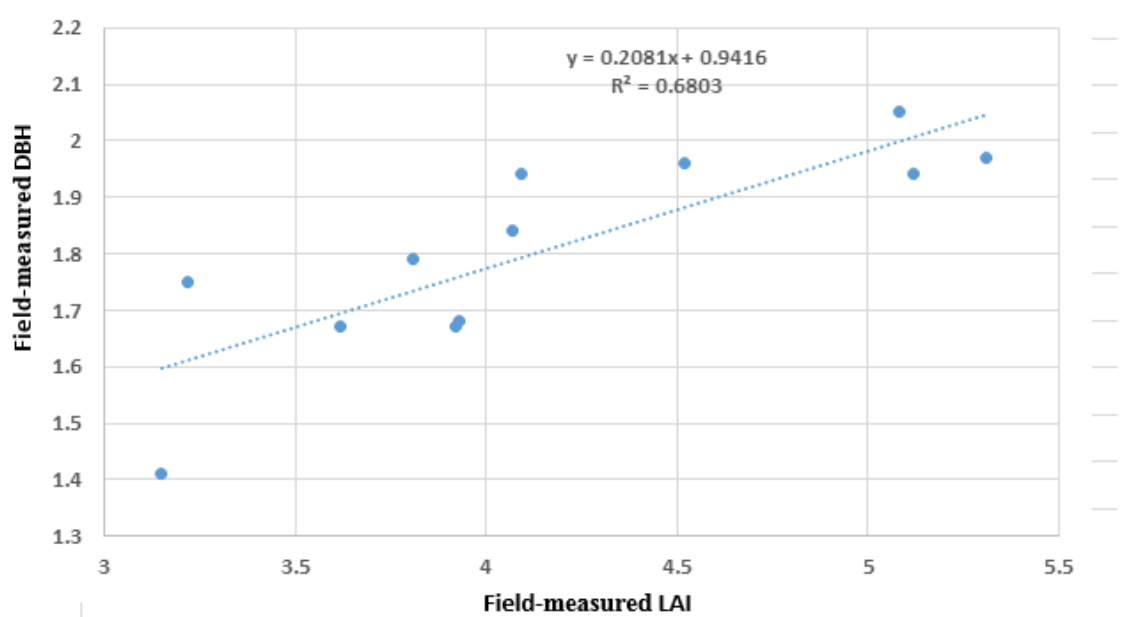

Fig. 5-6 Relationship of field measured LAI with DBH

5.5   Changes in Canopy Structure at ICESat Footprint Level

GLA01 full waveform data was analysed to investigate the seasonal change of canopy structure. Each GLA01 waveform contains information about various bio-physical parameters including stand height, LAI and vertical distribution of the canopy structure within footprint. The integrated energy from the return waveform can be normalized by the outgoing laser energy to estimate apparent reflectance at 1064 nm were considered in the present study. Apparent reflectance corresponds to the footprint retro-reflectance multiplied by the square of atmospheric transmission to account for the two-way travel path. The WCRH was used in this study to assess changes in the relative height of median energy within the waveform. GLAS footprints over the forest cover types were selected based on time series of dry season (Figs. 5.7, 5.8, 5.9 & 5.10).
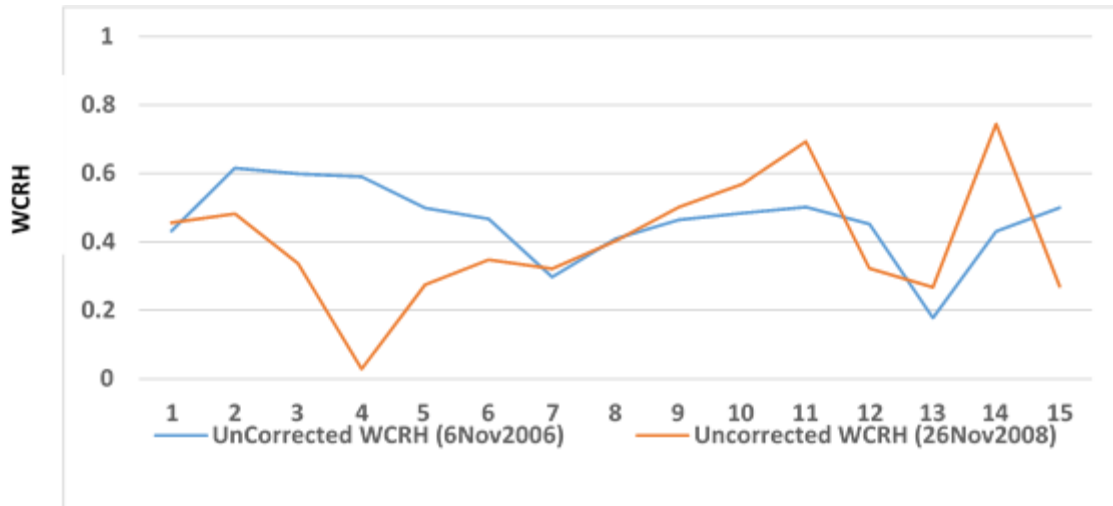
Fig. 5-7 Derived WCRH from GLA01 data of 6th November 2006 and 26th November 2008

Fig 5.7 shows major fluctuation in WCRH (from raw GLA01 data) of the two intervals in a same forest type. As the forest is in mature stage and there was no significant change observed in MODIS BRDF datasets, further investigation was proceed using FLIGHT model. By use of regressed LAI and DBH, slope (from SRTM) as well as other field parameters Monte Carlo simulation was performed (North, 1996). It was observed that after the simulation (corrected) modified WCRH showed consistency of canopy structure (Figure 5.8).
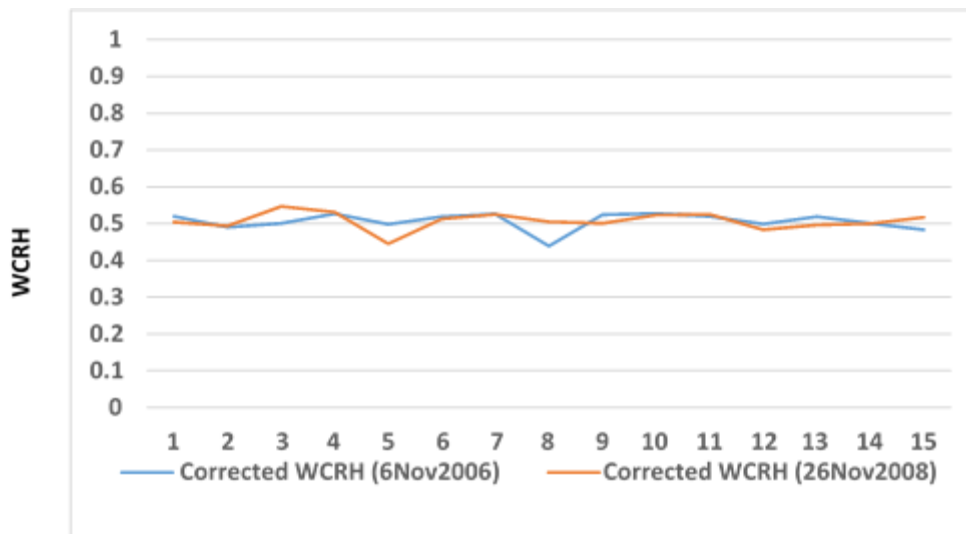

Fig. 5-8 Modified WCRH from GLA01 data of 6th November 2006 and 26th November 2008

Figs. 5.9 and 5.10 show the corrected (after simulation) and uncorrected (without simulation) WCRH of the two intervals. It clearly shows that the observed canopy structure maintains consistency over time.
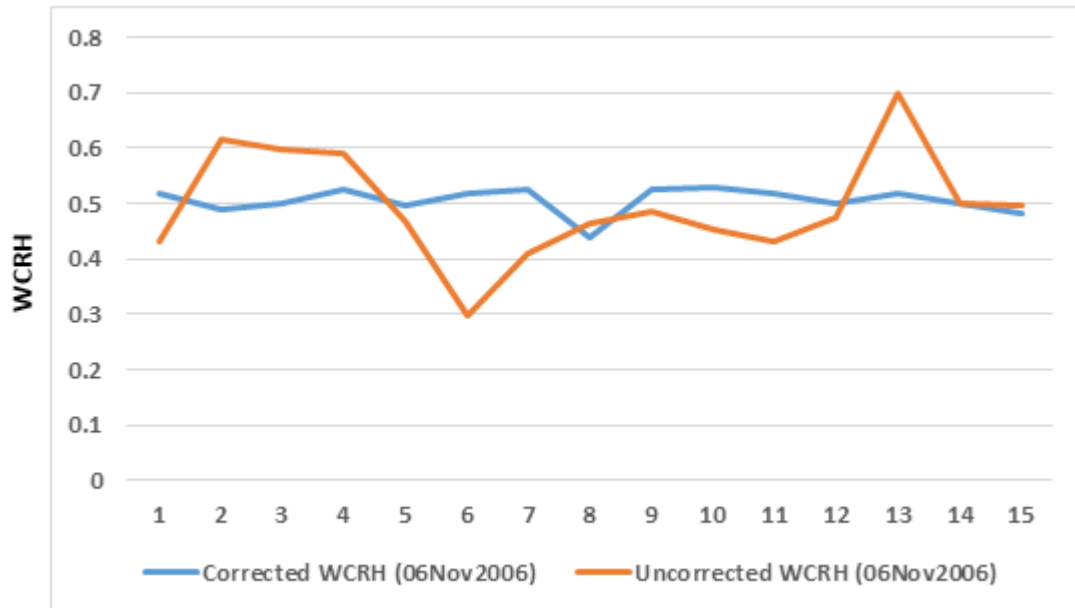
Fig. 5-9 Corrected (After Simulation) and Uncorrected (Without Simulation) WCRH GLA01
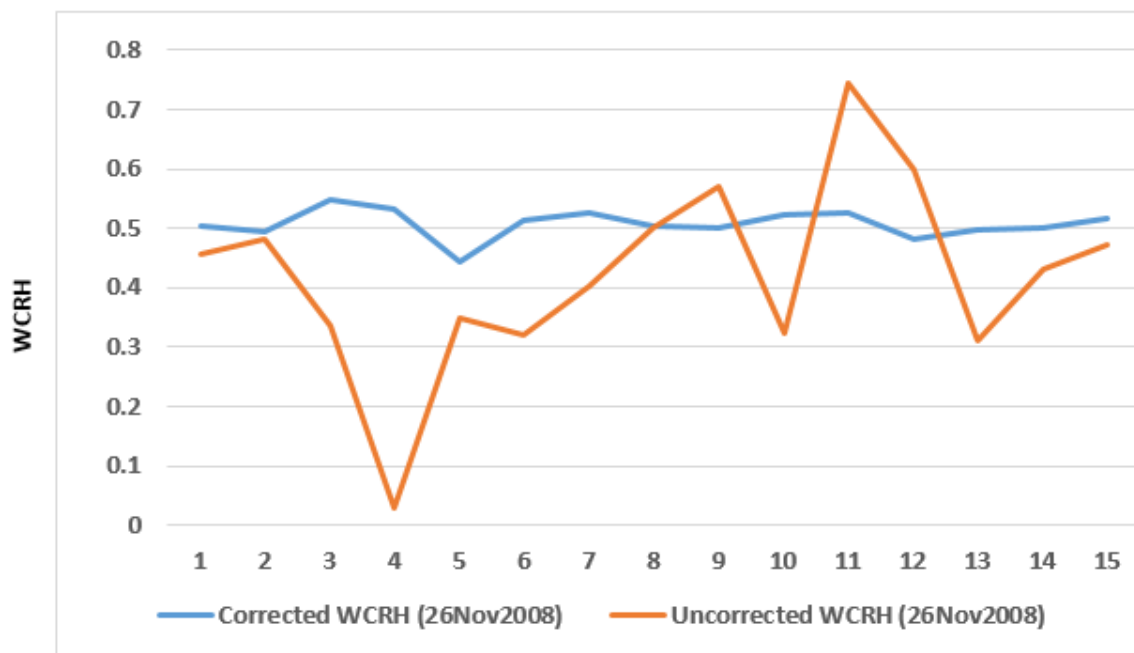

Fig. 5-10 Corrected (After Simulation) and Uncorrected (Without Simulation) WCRH GLA01

LiDAR with larger footprints brighten an area with a diameter of numerous meters (up to 70 m in ICESat/GLAS) (Duong, 2010). The returned signal encompasses the normal height distribution of intercepting surfaces over the footprint area, weighted by reflectivity and energy distribution across the footprint (Harding *et al*., 2001). This measured profile is connected to the actual foliage profile *vis-a-vis* leaf orientation, clumping of vegetation (Ni-Meister *et al*., 2001) and the mixture of green and non-green vegetation elements (Weiss *et al*., 2004). The technique of deriving foliage profiles from measured energy distributions however, takes only sole variations in reflectivity between foliage and soil; and extinction within the canopy and therefore underestimates leaf area in clumped canopies (Harding *et al*., 2001). FLIGHT model in the present study attempts to rectify such inaccuracies (Fig. 5.4).

One of the important characteristics of FLIGHT Radiative Transfer model is that it can represent multiple scattering of light within the canopy and with the surface of the ground; simulate the return signal efficiently at multiple wavebands, and model the effects of topography (North, 1996, Morton *et al*., 2014). In the present study, GLAS dataset was used to investigate the seasonal variation in canopy structure of tropical wet evergreen forests, that serves as one of the controlling factors of reflectance (Heyder, 2005); suggesting a potential to retrieve structural parameters from remote sensing measurements. Thus, as is evident from the present study, the correction of bidirectional reflectance effect has eliminated the seasonal changes in surface reflectance during the dry seasons of tropical wet evergreen forests (Fig. 5.4), unswerving with independent LiDAR observations and model simulations with unchanging canopy structure in the study area (Figs., 5.9, 5.10).

Chapter 6

Conclusions and Recommendations

_____

6.1   Conclusion

The present study deals with the assessment of LiDAR and optical sensor metrics with respective representations of structure and greenness in a tropical wet evergreen forests of North East India. At ICESat footprints, the vegetation indices derived from the MODIS BRDF products showed steadiness for tropical wet evergreen forests in dry seasons in contrast to MODIS Vegetation Indices product data for the same. Waveform Centroid Relative Height (WCRH) too showed temporal inconsistencies at ICESat Footprint Level. However, once the simulation of photon trajectories was induced through FLIGHT, WCRH showed consistency both at spatial and temporal scales. The novelty of the research was to address the inaccuracies of LiDAR and optical sensor metrics thus claiming evenness in structure and greenness in tropical wet evergreen forest across all seasons. The study obtained throughout success in achieving the desired objectives and in posing justification to all the research queries.

Research Question 1: Does the seasonal variation in vegetation indices reflect the true change in greenness and structure of tropical wet evergreen forests?

No, the seasonal variation in vegetation indices do not at all reflect the change in greenness and forest structure. The changing trend observed from MODIS product data is however due to the change in sun-senor geometry that can be better addressed through the usage of MODIS BRDF Adjusted Reflectance data.

Research Question 2: Do the LiDAR metrics represent true canopy structure at footprint level?

Answer: No, the LiDAR metrics do not represent the true canopy structure at the footprint level. The inaccuracies of the metrics can however be improved through simulation of photon trajectories using FLIGHT Radiative Transfer Model.

Research Question 3: Does the simulated forest structure using FLIGHT Radiative Transfer Model differ from LiDAR derived metrics?

For tropical ecosystems having an inherent climax nature, the simulated forest structure shows steadiness across all seasons at footprint level inconsistent with the LiDAR derived metrics. Thus, simulation using FLIGHT provides an accurate picture of the forest structure.

Research Question 4: How can the seasonality in greenness and structure of tropical wet evergreen forests be better predicted?

For tropical wet evergreen forests, seasonality in greenness can be better predicted using the BRDF corrected surface reflectance data. For vegetation structure however, simulated metrics derived from FLIGHT Radiative Transfer Model using Monte Carlo simulation of photon transport, mend the errors at footprint level.

6.2   Recommendations

❖ The present study was undertaken for one of the representative climax forest type in North East India. Results however may vary with other forest types and thus warrants a thorough investigation.

❖ BRDF Adjusted Surface Reflectance data improved the accuracy for Vegetation Indices of tropical wet evergreen forests as compared to Vegetation Indices product data at footprint level. However, for more improved accuracy, there is an utmost need for per-pixel correction of Daily Surface Reflectance data accounting for all the variations in sun-sensor geometry across all seasons.

❖ FLIGHT provides forward modelling of BRDF while MODIS BRDF product is an inversion BRDF, using both semi-empirical approach as well as actual multi-angle reflectance. The need of the hour is however to test the accuracy of such approaches, and if inaccurate, then improvement of the same for better prediction in greenness.

****

References

_____

Abshire, J.B., Sun, X., Riris, H., Sirota, J.M., McGarry, J.F., Palm, S., Yi, D. & Liiva, P. (2005). Geoscience Land Altimeter System (GLAS) on the ICESat Mission: On-orbit measurement performance. *Geophysical Research Letters,* 32, L21S02. 10.1029/2005GL024028.

Afzal, R.S. Yu, A.W., Dallas J.L., Melak A., Lukemire A.T., Ramos-Izqueirdo L. & Mamakos W. (2007). The Geoscience Laser Altimeter System (GLAS) Laser Transmitter, *IEEE Journal of Selected Topics in Quantum Electronics*, Vol. 13, No. 3, p. 511.

Alton, P. B., North, P. R. & Los, S. O. (2007). The impact of diffuse sunlight on canopy light-use efficiency, gross photosynthetic product and net ecosystem exchange in three forest biomes. *Global Change Biology*, 13(4), 776-787.

Alton, P. B., North, P., Kaduk, J. & Los, S. (2005). Radiative transfer modeling of direct and diffuse sunlight in a Siberian pine forest. *Journal of Geophysical Research: Atmospheres* (1984–2012), 110(D23).

Anonymous, (2009) "Rainforests.net – Variables and Math". Retrieved 4 January 2009.

Anonymous,(2001).The Global Forest Resources Assessment 2000 (FRA 2000): Main Report. Rome: Food and Agriculture Organization (FAO). Forestry Paper no. 140.

Anonymous, (2007). Natural vegetation in India and its classification. In: Remote Sensing and Geographic Information System Application for Natural Resources Management in Forestry and Ecology. Lecture Notes: Volume I, IIRS, Dehradun.

Anonymous, (2010). Global Forest Resources Assessment 2010 (FRA 2010): Main Report. Rome: Food and Agriculture Organization (FAO). Forestry Paper No. 163.

Anonymous,(2015a) https://en.wikipedia.org/wiki/Biodiversity_hotspot. Retrieved on 14 July 2015

Anonymous,(2015c) https://en.wikipedia.org/wiki/Atmospheric_radiative_transfer_codes. Retrieved on 13 July 2015.

Anonymous,(2008). http://www.globalchange.umich.edu/globalchange1/current/lectures/kling/rainforest/ /rainforest.html. Retrieved on 14 March 2008.

Anonymous,(2015b) https://nsidc.org/data/docs/daac/glas_icesat_l1_l2_global_altimetry.gd.html. Retrieved on 13 May 2015.

Antyufeev, V. S. & Marshak, A. L. (1990). Monte Carlo method and transport equation in plant canopies. *Remote Sensing of Environment*, *31*(3): 183-191.

Asner, G.P., Palace, M., Keller, M., Pereira, R., Silva, J.N.M. & Zweede, J.C. (2002). Estimating canopy structure in an Amazon forest from Laser Range Finder and IKONOS satellite observations. *Biotropica*, 34(4): 483-492.

Asrar, G., Fuchs, M., Kanemasu, E. T. & Hatfield, J. L. (1984). Estimating absorbed photosynthetic radiation and leaf area index from spectral reflectance in wheat. *Agronomy Journal*, *76*(2): 300-306.

Baccini, A., Goetz, S.J., Walker, W.S., Laporte, N.T., Sun, M., Sulla-Menashe, D., Hackler, J., Beck, P.S.A., Dubayah, R., Friedl, M.A., Samanta, S. & Houghton, R.A. (2012). Estimated carbon dioxide emissions from tropical deforestation improved by carbon-density maps. *Nature Climate Change*, 2: 182-185.

Badarinath, K. V. S., Latha, K. M., Chand, T. K., Gupta, P. K., Ghosh, A. B., Jain, S. L., Gera, B.S., Singh, R., Sarkar, A.K., Singh, N., Parmar, R.S., Koul, S., Kohli, R., Nath, S., Ojha,

V.K. & Singh, G. (2004). Characterization of aerosols from biomass burning—a case study from Mizoram (Northeast), India. *Chemosphere*, 54(2): 167-175.

Bae, S. & B.E. Schutz. (2002). Precision attitude determination (PAD). GLAS algorithm theoretical basis document. Version 2.2. Austin, TX: Center for Space Research, University of Texas, Austin.

Barbhuiya, A. R., Arunachalam, A., Nath, P. C., Khan, M. L. & Arunachalam, K. (2008). Leaf litter decomposition of dominant tree species of Namdapha National Park, Arunachal Pradesh, North East India. *Journal of Forest Research*, 13(1): 25-34.

Barton, C. V. M. & North, P. R. J. (2001). Remote sensing of canopy light use efficiency using the photochemical reflectance index: Model and sensitivity analysis. *Remote Sensing of Environment*, *78*(3): 264-273.

Behera, M. D. & Roy, P. S. (2002). LiDAR remote sensing for forestry applications: The Indian context. *Current Science*, 83(11): 1320-1327.

Bortolot, Z. J. & R. H. Wynne (2005). Estimating forest biomass using small footprint LiDAR data: An individual tree-based approach that incorporates training data. *ISPRS Journal of Photogrammetry and Remote Sensing*, 59(6): 342-360.

Boudreau, J., Nelson, R. F., Margolis, H. A., Beaudoin, A., Guindon, L. & Kimes, D. S. (2008). Regional aboveground forest biomass using airborne and spaceborne LiDAR in Québec. *Remote Sensing of Environment*, 112(10): 3876–3890.

Brando, P.M., Goetz, S.J., Baccini, A., Nepstad, D.C., Beck, P.S.A. & Christman, M.C.(2010). *Proceedings of the National Academy of Sciences of the United States of America,* 107(33): 14685-14690.

Bre´on, F.M., Maignan, F., Leroy, M., & Grant, I. (2002). Analysis of hot spot directional signatures measured from space. *Journal of Geophysical Research*, 107(D16, 4282): 1-15.

Brenner, A. C., Zwally, H. J., Bentley, C. R., Csatho, B. M., Harding, D. J., Hofton, M. A., Minster, J.B., Roberts, L., Saba, J., Thomas, R. & Yi, D. (2003). Derivation of range and range distributions from laser pulse waveform analysis for surface elevations, roughness, slope, and vegetation heights. *Algorithm Theoretical Basis Document*, 4*:* 26-32.

Bruijnzeel, L. A. & Veneklaas, E. J. (1998). Climatic conditions and tropical montane forest productivity: the fog has not lifted yet. *Ecology*, 79(1): 3-9.

Canisius, F. & Chen, J.M. (2007). Retrieving forest background reflectance in a boreal region from Multi-angle Imaging SpectroRadiometer (MISR) data. *Remote Sensing of Environment,* 107: 312-321.

Carabajal, C.C. & Harding, D.J. (2006). SRTM C-Band and ICESat Laser Altimetry Elevation Comparisons as a Function of Tree Cover and Relief. *Photogrammetric Engineering & Remote Sensing,* 72 (3): 287–298.

Champion, S. H. & Seth, S. K. (1968). Revised Forest Types of India. Government of India Publications, New Delhi.

Chandrasekhar, S. (1960). Radiative heat transfer. Dover Publications, New York, 11: 11-12.

Chen, J.M., Liu, J., Leblanc, S. G., Lacaze, R. & Roujean, J. L (2003). Multi-angular optical remote sensing for assessing vegetation structure and carbon absorption. *Remote Sensing of Environment,* 84: 516-525.

Chen, Q. (2010). Retrieving vegetation height of forests and woodlands over mountainous areas in the Pacific Coast region using satellite laser altimetry. *Remote Sensing of Environment*, *114*(7): 1610-1627.

Chevallier, F., Deutscher, N.M., Conway, T. J., Ciais, P., Ciattaglia, L., Dohe, S., Fröhlich, M., Gomez-Pelaez, A. J., Griffith, D., Hase, F., Haszpra, L., Krummel, P., Kyrö, E., Labuschagne, C., Langenfelds, R., Machida, T., Maignan, F., Matsueda, H., Morino,

I., Notholt, J., Ramonet, M., Sawa, Y., Schmidt, M., Sherlock, V., Steele, P., Strong, K., Sussmann, R., Wennberg, P., Wofsy, S., Worthy, D., Wunch, D. & Zimnoch, M. (2011). Global CO_2 fluxes inferred from surface air-sample measurements and from TCCON retrievals of the CO_2 total column. *Geophysical Research Letters*, 38(L24810): 1-5.

Cierniewski, J., Gdala, T. & Karnieli, A. (2004). A hemispherical directional reflectance model as a tool for understanding image distinctions between cultivated and uncultivated bare surfaces. *Remote Sensing of Environment*, 90: 505-523.

Curran, P. J. (1981). Multispectral remote sensing for estimation of biomass and productivity; In *Plants and Daylight Spectrum* (ed.) H Smith (New York: Academic Press) 65-69 pp.

Davidson, E. A., Araújo, A. C., Artaxo, P., Balch, J.K., Brown, I.F., Bustamante, M.M.C., Coe, M.T., DeFries, R.S., Keller, M., Longo, M., Munger, J.W., Schroeder, W., Soares-Filho, B.S., Souza, C.M. & Wofsy, S.C.(2012). The Amazon basin in transition. *Nature,* 481(7381): 321-328

Deering, D.W., Eck, T.F. & Banerjee, B. (1999). Characterization of the reflectance anisotropy of three boreal forest canopies in spring-summer. *Remote Sensing of Environment*, 67:205-229.

Dhanda, P. (2013). Optimising Parameters Obtained From Multiple Sensors For Biomass Estimation At ICESat Footprint Level Using Different Regression Algorithms. *M.Tech. Thesis*, IIRS, Dehradun.

Diner, D.J., Asner, G.P., Davies, R., Knyazikhin, Y., Muller, J.P., Nolin, A.W., Pinty, B., Schaaf, C.B. & Stroeve, J.(1999). New directions in Earth observing: Scientific applications of multi-angle remote sensing. *Bulletin of the American Meteorological Society*, 80: 2209-2228.

Disney, M. I., Lewis, P. & North, P. R. J. (2000). Monte Carlo ray tracing in optical canopy reflectance modelling. *Remote Sensing Reviews*, 18(2-4): 163-196.

Dolan, K., Masek, J. G., Huang, C., & Sun, G. (2009). Regional forest growth rates measured by combining ICESat GLAS and Landsat data. *Journal of Geophysical Research: Biogeosciences (2005–2012)*, 114(G2).

Doughty, C.E & Goulden, M.L. (2008). Seasonal patterns of tropical forest leaf area index and CO_2 exchange. *Journal of Geophysical Research*, 113, G00B06.

Drake, J.B., Dubayah, R.O., Knox, R.G., Clark, D.B. & Blair, J.B. (2002). Sensitivity of largefootprint LiDAR to canopy structure and biomass in a neotropical rainforest. *Remote Sensing of Environment*, 81: 378–392.

Drake, J.B., Knox, R.G., Dubayah, R.O., Clark, D.B., Condit, R., Blair, J.B. & Hofton, M. (2003). Aboveground biomass estimation in closed canopy neotropical forests using LiDAR remote sensing: Factors affecting the generality of relationships. *Global Ecology and Biogeography*, 12(2): 147–159.

Dubayah, R. O. & Drake, J. B. (2000). LiDAR remote sensing for forestry. *Journal of Forestry*, 98(6): 44-46.

Dubayah, R., Knox, R., Hofton, M., Blair, J. B. & Drake, J. (2000). Land surface characterization using LiDAR remote sensing. *Spatial Information for Land use Management*, 25-38.

Dubayah, R., Prince, S., JaJa, J., Blair, J. B., Bufton, J. L., Knox, R., Luthcke, S.B., Clarke, D.B. & Weishampel, J. (1997). The vegetation canopy LiDAR mission. *Land satellite information in the next decade II: Sources and applications*.

Duong,V.H. (2010). Processing and Application of ICESat Large Footprint Full Waveform Laser Range Data. Technische Universiteit, Delft, 213.

Duong, H., Pfeifer, N. & Lindenbergh, R. (2006). Full-waveform analysis: ICESat laser data for land cover classification. *Remote Sensing: From Pixels to Processes*. Enschede, the Netherlands: ISPRS Commission VII Mid-term Symposium.

Duong, H., Pfeifer, N. & Lindenbergh, R. (2006). Full waveform analysis: ICESat laser data for land cover classification. *International Archives of Photogrammetry, Remote Sensing and Spatial Information Sciences*, 36: 30-35.

Feldpausch, T. R., Banin, L., Phillips, O.L., Baker, T.R., Lewis, S.L., Quesada, C.A., Affum-Baffoe, K., Arets, E.J.M.M., Berry, N.J., Bird, M., Brondizio, E.S., Camargo, P., Chave, J., Djagbletey, G., Domingues, T.F., Drescher, M., Fearnside, P.M., Franc, M.B., Fyllas, N.M., Lopez-Gonzalez, G., Hladik, A., Higuchi, N., Hunter, M.O.,Iida, Y., Salim, K.A., Kassim, A.R., Keller, M., Kemp, J., King, D.A., Lovett, J.C., Marimon, B.S., Marimon-Junior, B.H., Lenza, E., Marshall, A.R., Metcalfe, D.J., Mitchard, E.T.A., Moran, E.F., Nelson, B.W., Nilus, R., Nogueira, E.M., Palace, M., Patino, S., Peh, K. S.H., Raventos, M.T., Reitsma, J.M., Saiz, G., Schrodt, F., Sonke, B., Taedoumg, H.E., Tan, S., White, L., W¨oll, H. & Lloyd, J. (2011). Height-diameter allometry of tropical forest trees. *Biogeosciences*, 8: 1081-1106.

Fittkau, E. J. & Klinge, H. (1973). On biomass and trophic structure of the central Amazonian rain forest ecosystem. *Biotropica,* 2-14.

Franklin, J. & Hiernaux, P. H. Y. (1991). Estimating foliage and woody biomass in Sahelian and Sudanian woodlands using a Remote Sensing model. *International Journal of Remote Sensing*, 12:1387-1404.

Fricker, H.A., Bassis, J.N., Minster, B. & MacAyeal, D.R. 2005. ICESats new perspective on ice shelf rifts: The vertical dimension. *Geophysical Research Letters*, 32. L23S08, doi:10.1029/2005GL025070.

FSI (2013). India State of Forest Report 2013, Forest Survey of India Dehradun.

Galvão, L.S., dos Santos, J.R., Roberts, D.A., Breunig, F.M., Toomey, M. & de Moura, Y.M. (2011). On intra-annual EVI variability in the dry season of tropical forest: A case study with MODIS and hyperspectral data. *Remote Sensing of Environment*, 115: 2350-2359.

Gao, F., Schaaf, C.B., Strahler, A.H., Jin, Y., & Li, X. (2003). Detecting vegetation structure using a kernel-based BRDF model. *Remote Sensing of Environment,* 86:198-205.

Gao, X., Huete, A. R., Ni, W. & Miura, T. (2000). Optical–biophysical relationships of vegetation spectra without background contamination. *Remote Sensing of Environment*, 74(3): 609-620.

Gatti, L. V., Miller, J. B., D'Amelio, M. T. S., Martinewski, A., Basso, L. S., Gloor, M. E. , Wofsy, S. & Tans, P. (2010). Vertical profiles of CO_2 above eastern Amazonia suggest a net carbon flux to the atmosphere and balanced biosphere between 2000 and 2009. *Tellus,* 62B: 581-594.

Ghilain, N., De Roo, F. & Gellens-Meulenberghs, F. (2014). Evapotranspiration monitoring with Meteosat Second Generation satellites: improvement opportunities from moderate spatial resolution satellites for vegetation. *International Journal of Remote Sensing*, 35(7).

Gong, D.Y. & Shi, P.J. (2003). Northern hemispheric NDVI variations associated with large-scale climate indices in spring. *International Journal of Remote Sensing,* 24: 2559–2566.

Gosai, K. (2008). Studies on the dynamics of soil microbial biomass and nitrogen mineralization associated with tillage practices in rainfed agricultural systems. *Ph.D. Thesis*, Assam University, Silchar, Assam, India.

Gosai, K. (2009). Woody biomass assessment in Yachuli circle, Lower Subansiri, Arunachal Pradesh using remote sensing, GIS and spectral modeling, *P.G.Diploma Dissertation*, IIRS, Dehradun.

Gosai, K., Arunachalam, A. & Dutta, B. K. (2009). Influence of conservation tillage on soil physicochemical properties in a tropical rainfed agricultural system of northeast India. *Soil and Tillage Research*, 105(1): 63-71.

Gosai, K., Arunachalam, A., & Dutta, B. K. (2010). Tillage effects on soil microbial biomass in a rainfed agricultural system of northeast India. *Soil and Tillage Research*, 109(2), 68-74.

Gower, S.T. (1999). Direct and indirect estimation of LAI, fAPAR and net primary production of terrestrial ecosystems. *Remote Sensing of Environment*, 70(1): 29–51.

Harding, D. J., Lefsky, M. A., Parker, G. G. & Blair, J. B. (2001). Laser altimeter canopy height profiles: Methods and validation for closed-canopy, broadleaf forests. *Remote Sensing of Environment,* 76(3): 283-297.

Harding, D.J. & Carabajal, C.C. (2005). ICESat waveform measurements of within-footprint topographic relief and vegetation vertical structure. *Geophysical Research Letters*, 32 (L21210): 1-4.

Hemery, G.E., Savill, P.S. & Pryor, S.N. (2005). Applications of the crown diameter-stem diameter relationship for different species of broadleaved species. *Forest Ecology and Management*, 215: 285-294.

Hese, S., Lucht, W., Schmullius, C., Barnsley, M., Dubayah, R., Knorr, D., Neumann, K., Riedel, T. & Schroter, K. (2005). Global biomass mapping for an improved understanding of the CO_2 balance-The earth Observation Mission Carbon-3D. *Remote Sensing of Environment,* 94:94-104.

Heyder, U. (2005). Vertical forest structure from ICESat/GLAS LiDAR data. *Masters Thesis,* Department of Geography, University College, London, 155:12-50.

Heyojoo, B.P. & Nandy, S. (2014). Estimation of above-ground phytomass and carbon in tree resources outside the forest (TROF): A geo-spatial approach. *Banko Janakari* 24 (1): 34-40.

Hilker, T., Coops, N.C., Hall, F.G., Nichol, C.J., Lyapustin, Andrew Black, T.A., Wulder, M.A., Leuning, R., Barr, A., Hollinger, D.Y., Munger, B. & Tucker, C.J. (2011). Inferring terrestrial photosynthetic light use efficiency of temperate ecosystems from space. *Journal of Geophysical Research*, 116 (G03014): 1-11

Hiratsuka, M., Toma, T., Yamada, M., Heriansyah, I. & Morikawa, Y. (2003). . A general allometric equation for estimating biomass in *Acacia mangium* plantations." *Proceedings of the 2003 International Conference on Tropical Forests and Climate Change: Carbon Sequestration and Clean Development Mechanism: held on 21-22 October, 2003, Traders Hotel, Manila, Philippines*. University of the Philippines Los Banos. College of Forestry and Natural Resources, Manila, Philippines, 2004.

Hudak, A. T., Lefsky, M. A., Cohen, W. B. & Berterretche, M. (2002). Integration of LiDAR and Landsat ETM+ data for estimating and mapping forest canopy height. *Remote Sensing of Environment*, 82(2): 397–416.

Huete, A., Didan, K., Miura, T., Rodriguez, E.P., Gao, X. & Ferreira, L.G. (2002). Overview of the radiometric and biophysical performance of the MODIS vegetation indices. *Remote Sensing of Environment*, 83: 195-213.

Huete, A., Justice, C. & Van Leeuwen, W. (1999). MODIS vegetation index (MOD13). *Algorithm Theoretical Basis Document*, 3, 213.

Huete, A.R., Didan, K., Shimabukuro, Y.E., Ratana, P., Saleska, S.R., Hutyra, L.R., Yang, W., Nemani, R.R. & Myneni, R. (2006). Amazon rainforests green-up with sunlight in dry season. *Geophysical Research Letters,* 33(L06405): 1-4.

Hunter, M.O., Keller, M., Victoria, D. & Morton, D.C. (2013). Tree height and tropical forest biomass estimation. *Biogeosciences*, 10: 8385-8399.

Hyde, P., Dubayah, R., Peterson, B., Blair, J. B., Hofton, M., Hunsaker, C., Knox, R. & Walker, W. (2005). Mapping forest structure for wildlife habitat analysis using waveform LiDAR: Validation of montane ecosystems. *Remote Sensing of Environment,* 96(3–4): 427–437.

Hyde, P., Nelson, R., Kimes, D. & Levine, E., (2007). Exploring LiDAR–RaDAR synergy predicting aboveground biomass in a south-western ponderosa pine forest using LiDAR, SAR, and InSAR. *Remote Sensing of Environment*, 106(1): 28–38.

Jiang, Z., Huete, A.R., Didan, K. & Miura, T. (2008). Development of a two-band enhanced vegetation index without a blue band. *Remote Sensing of Environment*, 112: 3833-3845.

Jingyong, Z., Wenjie, D., Congbin, F. & Lingyun, W. (2003). The influence of vegetation cover on summer precipitation in China: a statistical analysis of NDVI and climate data. *Advances in Atmospheric Sciences,* 20(6): 1002-1006.

Joiner, J., Yoshida, Y., Vasilkov, A.P., Yoshida, Y., Corp, L.A. & Middleton, E.M., (2011). First observations of global and seasonal terrestrial chlorophyll fluorescence from space. *Biogeosciences*, 8: 637-651.

Joshi, P.K., Rashid, H. & Roy, P.S. (2002). Landscape dynamics in Hokersar wetland, Jammu and Kashmir, an application of geo-spatial approach. *Journal of Indian Society of Remote Sensing* 30 (1 and 2): 1-6.

Justice, D. H., Salomonson, V., Privette, J., Riggs, G., Strahler, A., Lucht, R., Myneni, R., Knjazihhin, Y., Running, S., Nemani, R., Vermote, E., Townshend, J., Defries, R., Roy, D., Wan, Z., Huete, A., van Leeuwen,R., Wolfe, R., Giglio, L., Muller, J.-P., Lewis, P. & Barnsley, M. (1998). The Moderate Resolution Imaging Spectroradiometer (MODIS): Land Remote Sensing for Global Change Research. *IEEE Transactions on Geoscience and Remote Sensing*, 36: 1228–1249.

Keller, M., Palace, M. & Hurtt, G. (2001). Biomass estimation in the Tapajos National Forest, Brazil. Examination of sampling and allometric uncertainties. *Forest Ecology and Management*, 154: 371-382.

Kerr, J.T. & Ostrovsky, M. (2003). From space to species: ecological applications for remote sensing. *Trends in Ecology and Evolution*, 18: 299–305

Kim, Y., Knox, R.G., Longo, M., Medvigy, D., Hutyra, L. R., Pyle, E.H., Wofsy, S.C., Bras, R.L. & Moorcroft, P.R. (2012). Seasonal carbon dynamics and water fluxes in an Amazon rainforest. *Global Change Biology*, 1-12 doi: 10.1111/j.1365-2486.2011.02629.x

Koetz, B., Morsdorf, F., Sun, G., Ranson, K. J., Itten, K. & Allgöwer, B. (2006). Inversion of a LiDAR waveform model for forest biophysical parameter estimation. *IEEE Transactions on Geoscience and Remote Sensing*, 3(1): 49-53.

Kumar, R., Nandy, S., Agarwal, R. & Kushwaha, S.P.S. (2014). Forest cover dynamics analysis and prediction modeling using logistic regression model. *Ecological Indicators* 45: 444–455.

Kushwaha, S. P. S., Nandy, S. & Gupta, M. (2014). Growing stock and woody biomass assessment in Asola-Bhatti Wildlife Sanctuary, Delhi, India. *Environmental Monitoring and Assessment*, 186(9): 5911-5920.

Kushwaha, S.P.S. (1990). Forest type mapping and change detection from satellite imagery. *ISPRS Journal of Photogrammetry and Remote Sensing*, 45:175-181.

Leblanc, S.G., Bicheron, P., Chen, J.M., Leroy, M. & Cihlar, J. (1999). Investigation of directional reflectance in boreal forests with an improved 4-scale model and airborne POLDER data. *IEEE Transaction on Geoscience and Remote Sensing*, 37: 1396-1414.

Lefsky, M. A., Cohen, W. B., Acker, S. A., Parker, G. G., Spies, T. A. & Harding, D. (1999). LiDAR remote sensing of the canopy structure and biophysical properties of Douglas-fir western hemlock forests. *Remote Sensing of Environment*, 70(3): 339-361.

Lefsky, M. A., Cohen, W. B., Parker, G. G. & Harding, D. J. (2002). LiDAR Remote Sensing for Ecosystem Studies LiDAR, an emerging remote sensing technology that directly measures the three-dimensional distribution of plant canopies, can accurately estimate vegetation structural attributes and should be of particular interest to forest, landscape, and global ecologists. *BioScience*, 52(1): 19-30.

Lefsky, M. A., Harding, D.J., Keller, M., Cohen, W.B., Carabjal, C.C., Espirito Santo, F.D. Hunter, M.O. & Oliveira, R. (2005). Estimates of forest canopy height and aboveground biomass using ICESat. *Geophysical Research Letters*, 32(22): L22S02.

Lefsky, M.A., Keller, M., Pang, Y. De Camargo, P.B. & Hunter, M. O. (2007). Revised method for forest canopy height estimation from Geoscience Laser Altimeter System waveforms. *Journal of Applied Remote Sensing*, 1. pp. 013537. doi:10.1117/1.2795724.

Lewis, S.L., Brando, P.M., Phillips, O.L., van der Heijden, G.M.F. & Nepstad, D., (2011). The 2010 Amazon Drought. *Science*, 331: 554.

Liang, S. (2007). Recent developments in estimating land surface biogeophysical variables from optical remote sensing. *Progress in Physical Geography*, 31(5): 501-516.

Lillesand, T. M. & Keifer, R. W. (2000).Remote sensing and image interpretation. New York: John Wiley & Sons, Inc.

Lillesand, T. M., Kiefer, R. W. & Chapman, J. (2000). Remote sensing and image analysis. *John Wiley and Sons, New York*.

Lim, K., Treitz, P., Wulder, M., St-Onge, B. & Flood, M. (2003). LiDAR remote sensing of forest structure. *Progress in Physical Geography*, 27(1): 88-106.

Luo, S., Wang, C., Li, G. & Xi, X. (2013). Retrieving leaf area index using ICESat/GLAS full-waveform data. *Remote Sensing Letters*, 4(8): 745-753.

Mallet, C. & Bretar, F. (2009). Full-waveform topographic LiDAR: State-of-the-art. *ISPRS Journal of Photogrammetry and Remote Sensing*, 64: 1-16.

Manna, S., Nandy, S., Chanda, A., Akhand, A., Hazra, S. and Dadhwal, V.K. (2014). Estimating aboveground biomass in *Avicennia marina* plantation in Indian Sundarbans using high-resolution satellite data. *Journal of Applied Remote Sensing,* 8(1): 083638.

MEA, (2005). Millennium Ecosystem Assessment Report. Available: http://www.maweb.org/en/Synthesis.aspx

Means, J. E., Acker, S. A., Harding, D. J., Blair, J. B., Lefsky, M. A., Cohen, W. B., Harmon, M.E. & McKee, W. A. (1999). Use of large-footprint scanning airborne LiDAR to estimate forest stand characteristics in the western Cascades of Oregon. *Remote Sensing of Environment*, 67(3): 298-308.

Montesano, P.M., Rosette, J., Sun, G., North, P., Nelson, R.F., Dubayah, R.O., Ranson, K.J. & Kharuk, V. (2015). The uncertainty of biomass estimates from modelled ICESat-2 returns across a boreal forest gradient. *Remote Sensing of Environment*, 158: 95-109.

Morton, D. C., Le Page, Y., DeFries, R., Collatz, G. J. & Hurtt, G. C. (2013). Understorey fire frequency and the fate of burned forests in southern Amazonia. *Philosophical Transactions of the Royal Society* B: Biological Sciences, 368(1619), 20120163.

Morton, D.C., DeFries, R.S., Nagol, J., Souza, C.M., Kasischke, E.S., Hurtt, G.C. & Dubayah, R. (2011). Mapping canopy damage from understory fires in Amazon forests using annual time series of Landsat and MODIS data. *Remote Sensing of Environment*, 115: 1706-1720.

Morton, D.C., Nagol, J. Carabajal, C.C. Rosette, J., Palace, M., Cook, B.D. Vermote, E.F., Harding, D.J. & North, P.R.J. (2014). Amazon forests maintain consistent canopy structure and greenness during the dry season. *Nature,* doi:10.1038/nature 13006.

Myneni, R. B. & Hall, F. G. (1995). The interpretation of spectral vegetation indexes. *IEEE Transactions on Geoscience and Remote Sensing,* 33(2): 481-486.

Myneni, R. B., Ramakrishna, R., Nemani, R. & Running, S. W. (1997). Estimation of global leaf area index and absorbed PAR using radiative transfer models. *IEEE Transactions on Geoscience and Remote Sensing,* *35*(6): 1380-1393.

Myneni, R.B., Yang, W., Nemani, R.R, Huete, A.R., Dickinson, R.E., Knyazikhin, Y., Didan, K. Fu, R., Juarez, R.I.N., Saatchi, S.S., Hashimoto, H., Ichii, K., Shabanov, N.V., Tan, B., Ratana, P., Privette, J.L., Morisette, J.T., Vermote, E.F., Roy, D.P., Wolfe, R.E., Friedl, M.A., Running, S.W., Votava, P., Saleous, N.E., Devadiga, S., Su, Y. & Salomonson, V.V. 2007. Leaf seasonal changes swings in leaf area of Amazon forests. (2007). *Proceedings of the National Academy of Sciences of the United States of America,* 107(33): 14685-14690.

Naeem, S., Chapin C.F.S., Costanza, R., Ehrlich, P.R., Golley, F.B., Hooper, D.U., Lawton, J.H., O'Neill, R.V., Mooney, H.A., Sala, O.E., Symstad, A.J. & Tilman, D.(1999). Biodiversity and ecosystem functioning: maintaining natural life support processes. *Issues in Ecology* (4):1–11.

Nandy, S., Joshi, P.K. and Das, K.K. (2003). Forest canopy density stratification using biophysical spectral response modelling. *Journal of the Indian Society of Remote Sensing,* 31(4): 291-297.

Nandy, S., Kushwaha, S.P.S. & Mukhopadhyay, S. (2007). Monitoring the Chilla-Motichur wildlife corridor using geospatial tools. *Journal for Nature Conservation,* 15(4):237-244.

Nandy, S. & Kushwaha, S.P.S. (2011). Study on the utility of IRS 1D LISS-III data and the classification techniques for mapping of Sunderban mangroves. *Journal of Coastal Conservation-Planning and Management* 15(1): 123-137.

Nath, P. C., Arunachalam, A., Khan, M. L., Arunachalam, K. & Barbhuiya, A. R. (2005). Vegetation analysis and tree population structure of tropical wet evergreen forests in and around Namdapha National Park, North East India. *Biodiversity & Conservation*, 14(9): 2109-2135.

Nelson, R., Ranson, K. J., Sun, G., Kimes, D. S., Kharuk, V. & Montesano, P. (2009). Estimating Siberian timber volume using MODIS and ICESat/GLAS. *Remote Sensing of Environment*, 113: 691–701.

Nemani, R.R., Keeling, C.D., Hashimoto, H., Jolly, W.M., Piper, S.C., Tucker, C.J., Myneni, R.B. & Running, S.W. (2010). Climate driven increases in global terrestrial net primary production from 1982 to 1999. *Science,* 300(5625): 1560-1563.

Nepstad, D.C., de Carvalho, C.R., Davidson, E.A., Jipp, P.H., Lefebvre, P.A., Negreiros, G.H., da Silva, E.D., Stone, T.A., Trumbore, S.E. & Vieira, S. (1994). The role of deep roots in the hydrological and carbon cycles of Amazonian forests and pastures. *Nature*, 372: 666-669.

Nepstad, D.C., Tohver, I.M., Ray, D., Moutinho, P. & Cardinot, G. (2007). Mortality of large trees and lianas following experimental drought in an Amazon forest. *Ecology*, 88(9): 2259-2269.

Nikolakopoulos, K. G., Kamaratakis, E. K. & Chrysoulakis, N. (2006). SRTM vs ASTER elevation products. Comparison for two regions in Crete, Greece. *International Journal of Remote Sensing*, 27(21): 4819-4838.

Ni-Meister, W., Jupp, D. L. & Dubayah, R. (2001). Modeling LiDAR waveforms in heterogeneous and discrete canopies. *IEEE Transactions on Geoscience and Remote Sensing, 39*(9), 1943-1958.

North, P., Rosette, J., Suárez, J. & Los, S. (2008). A Monte Carlo radiative transfer model of satellite waveform LiDAR. *SilviLaser*, 31(5), 189-198.

North, P.R.J. (1996). Three-Dimensional Forest Light Interaction Model using a Monte Carlo method. *IEEE Transactions on Geoscience and Remote Sensing,* 34(4): 946-956.

North, P.R.J., Rossette, J.A.B., Suarez, J.C. & Los. S. O. (2010). A Monte Carlo radiative transfer of satellite waveform LiDAR. *International Journal of Remote Sensing,* 31, 1343-1358.

North, R. A. (2002). Molecular physiology of P2X receptors. *Physiological Reviews*, 82(4), 1013-1067.

NSIDC (2009). *ICESat/GLAS data: Tools* [Online]. Available: http://nsidc.org/data/icesat/tools.html

Olson, D. M., Dinerstein, E., Wikramanayake, E. D., Burgess, N. D., Powell, G. V., Underwood, E. C., D´amico, J.A., Itoua, I., Strand, H.E., Morrison, J.C., Loucks, C.L., Allnutt, T.F., Ricketts, T.H., Kura, Y., Lamoreux, J.F., Wettengel, W.W., Hedao, P. & Kassem, K. R. (2001). Terrestrial Ecoregions of the World: A New Map of Life on Earth: A new global map of terrestrial ecoregions provides an innovative tool for conserving biodiversity. *BioScience*, 51(11): 933-938.

Osunkoya, O.O., Omar-Ali, K., Amit, N., Dayan, J., Daud, D.S. & Sheng, T.K. (2007). Comparative height-crown allometry and mechanical design in 22 tree species of Kuala Belalong rainforest, Brunei, Borneo. *American Journal of Botany,* 94(12): 1951-1962.

Palace, M., Keller, M., Asner, G.P., Hagen, S. & Braswell, B. (2008). Amazon Forest Structure from IKONOS Satellite Data and the Automated Characterization of Forest Canopy Properties. *Biotropica*, 40(2): 141-150.

Pan,Y., Birdsey, R. A., Fang, J., Houghton, R., Kauppi, P.E., Kurz, W.A., Phillips, O.L., Shvidenko, A., Lewis, S.L., Canadell, J.G., Ciais, P., Jackson, R.B., Pacala, S.W., McGuire, D., Piao, S., Rautiainen, A., Sitch, S. & Hayes, D. (2011). A large and persistent carbon sink in the world's forests. *Science,* 333:988-993.

Patenaude, G., Milne, R. & Dawson, T. P. (2005). Synthesis of remote sensing approaches for forest carbon estimation: reporting to the Kyoto Protocol. *Environmental Science & Policy*, 8(2): 161-178.

Phillips, O.L., Aragão, Luiz, E.O.C., Lewis, S.L., Fisher, J.B., Lloyd, J., López-González, G., Malhi, Y., Monteagudo, A., Peacock, J., Quesada, C.A.,van der Heijden, G., Almeida, S., Amaral, I., Arroyo, L., Aymard, G., Baker, T.R., Bánki, O., Blanc, L., Bonal, D., Brando, P., Chave, J., de Oliveira, A.C. A., Cardozo, N.D., Czimczik, C.I., Feldpausch, T.R., Freitas, M.A., Gloor, E., Higuchi, N., Jiménez, E., Lloyd, G., Meir, P., Mendoza, C., Morel, A., Neill, D.A., Nepstad, D., Patiño, S., Peñuela, M.C., Prieto, A., Ramírez, F., Schwarz, M., Silva, J., Silveira, M., Thomas, A.S., ter Steege, H., Stropp, J., Vásquez, R., Zelazowski, P., Dávila, E.A., Andelman, S., Andrade, A., Chao, K.J., Erwin, T., Fiore, A.D., Honorio E. C., Keeling, H., Killeen, T.J., Laurance, W.F., Antonio Peña Cruz, A.P., Pitman, N.C.A., Vargas, P.N., Ramírez-Angulo, H., Rudas, A., Salamão, R., Silva, N., Terborgh, J. & Torres-Lezama, A. (2009). Drought sensitivity of the Amazon rainforest. *Science*, 323: 1344-1347.

Pinty, B., Gobron, N., Widlowski, J.L., Lavergne, T. &Verstraete, M.M.(2004). Synergy between 1-D and 3-D radiation transfer models to retrieve vegetation canopy properties from remote sensing data. *Journal of Geophysical Research–Atmospheres,* 109, Art. No. D21205.

Pisek, J., Lang, M., Kuusk, J. (2015). A note on suitable viewing configuration for retrieval of forest understory reflectance from multi-angle remote sensing data. *Remote Sensing of Environment*, 156: 242-246.

Quéré, C.L., Raupach, M.R., Canadell, J.G., Marland, G., Bopp, L., Ciais, P., Conway, T.J., Doney, S.C., Feely, R.A., Foster, P. Friedlingstein, P., Gurney, K., Houghton, R.A., House, J.I., Huntingford, C., Levy, P.E., Lomas, M.R., Majkut, J., Metzl, N., Ometto, J.P., Peters, G.P., Prentice, I.C., Randerson, J.T., Running, S.W., Sarmiento, J.L., Schuster, U., Sitch, S., Takahashi, T., Viovy, N., van der Werf, G.R. & Woodward, F.I., (2009). Trends in the sources and sinks of carbon dioxide. *Nature Geoscience*, 1-6.

Rahman, A.F., Sims, D.A., Cordova, V.D & El-Masri, B.Z. (2005). Potential of MODIS EVI and surface temperature for directly estimating per-pixel ecosystem C fluxes. *Geophysical Research Letters*, 32 (L19404): 1-4.

Ranson, K., Sun, G., Kovacs, K. & Kharuk, V. 2004. Landcover attributes from ICESat GLAS data in Central Siberia. International Geoscience and Remote Sensing Symposium, Anchorage, AK, SEP 20-24, 2004, IGARSS (2004). *IEEE International Geoscience and Remote Sensing Symposium Meetings*, 1-7, 753-756.

Rauste, Y., (2005). Multi-temporal JERS SAR data in boreal forest biomass mapping. *Remote Sensing of Environment,* 97 (2): 263–275.

Rautiainen, M., Stenberg, P., Nilson, T. & Kuusk, A. (2004). The effect of crown shape on the reflectance of coniferous stands. *Remote Sensing of Environment,* 89:41-52.

Ravan, S.A. (1994). Ecological analysis of vegetation from satellite remote sensing at Madhav National Park, Shivpuri (M.P.), Ph.D. Thesis, H N B Garhwal University, Srinagar, Garhwal.

Ravan, S.A., Roy, P. S. & Sharma, C. M. (1995). Space remote sensing for spatial vegetation characterization. *Journal of Bioscience*, 20:427- 438.

Rea, J. & Ashley, M. (1976). Phenological evaluations using Landsat—1 sensors. *International Journal of Biometeorology*, 20(3): 240-248.

Reed, B. C., Brown, J. F., VanderZee, D., Loveland, T. R., Merchant, J. W. & Ohlen, D. O. (1994). Measuring phenological variability from satellite imagery. *Journal of Vegetation Science*, 5(5): 703-714.

Rexer, M. & Hirt, C. (2014). Comparison of free high resolution digital elevation data sets (ASTER GDEM2, SRTM v2. 1/v4. 1) and validation against accurate heights from the Australian National Gravity Database. *Australian Journal of Earth Sciences*, 61(2): 213-226.

Richardson, J.J., Moskal, L.M., Kim, S. (2009). Modeling approaches to estimate effective leaf area index from aerial discrete-return LIDAR. Agric. *Forest Meteorology*, 149(6):1152–1160.

Roberts, G. (2001). A review of the application of BRDF models to infer land cover parameters at regional and global scales. *Progress in Physical Geography*, 25(4): 483-511.

Roerink, G. J., Menenti, M., Soepboer, W. & Su, Z. (2003). Assessment of climate impact on vegetation dynamics by using remote sensing. *Physics and Chemistry of the Earth, Parts A/B/C*, 28(1): 103-109.

Rosette, J. A. B., North, P. R. J. & Suárez, H. C. (2008). Vegetation height estimates for a mixed temperate forest using satellite laser altimetry. *International Journal of Remote Sensing*, 29(5): 1475–1493.

Rosette, J. A. B., North, P. R. J., Suarez, J. C. & Los, S. O. (2010). Uncertainty within satellite LiDAR estimations of vegetation and topography. *International Journal of Remote Sensing*, 31(5): 1325-1342.

Roy, P. S. & Kumar, S. (1986). Advanced Very High Resolution Radiometer (AVHRR) satellite data for vegetation monitoring; *Proceedings on the International Seminar on Photogrammetry and Remote Sensing for developing countries*, New Delhi 11-14 March, 1986.

Roy, P. S. & Ravan, S. A. (1996). Biomass estimation using satellite remote sensing data—an investigation on possible approaches for natural forest. *Journal of Biosciences*, 21(4): 535-561.

Roy, P. S., Ranganath, B, K., Diwakar, P. G., Vohra, T. P. S., Bhan, S. K., Singh, I. J. & Pandian, V. C. (1991). Tropical forest type mapping and monitoring using remote sensing. *International Journal of Remote Sensing*, 12:2205-2225.

Roy, P. S., Saxena K. G. & Kamat, D. S. (1986). Biomass estimation through remote sensing; Remote Sensing Technical Report: 1-78.

Roy, P.S. (1989). Analysis of forest types and monitoring disturbances using thematic mapper data in part of Andaman Nicobar islands. In: National Seminar on status of Indian Forestry Problems and Perspectives, pp 22-28. Haryana Agriculture University, Hisar, India.

Running, S. W., Justice, C. O., Salomonson, V., Hall, D., Barker, J., Kaufmann, Y. J. & Carneggie, D. (1994). Terrestrial remote sensing science and algorithms planned for EOS/MODIS. *International Journal of Remote Sensing*, 15(17): 3587-3620.

Running, S.W. (1990) Estimating primary productivity by combining remote sensing with ecosystem simulation. In Remote Sensing of Biosphere Functioning (Hobbs, R.J. and Mooney, H.A., eds), pp. 65–86, Springer-Verlag.

Saatchi, S.S., Harris, N.L., Brown, S., Lefsky, M., Mitchard, E.T.A., Salas, W., Zutta, B.R., Buermann, W., Lewis, S.L., Hagen, S., Petrova, S., White, L., Silman, M. & Morel. A. (2011). Benchmark map of forest carbon stocks in tropical regions across three continents. *Proceedings of the National Academy of Sciences of the United States of America*, 108 (24): 9899-9904.

Saleska, S.R., Didan, K., Huete, A.R. & da Rocha, H.R. (2007). Amazon forests green-up during 2005 drought. *Science*, 612.

Saleska, S.R., Miller, S.D., Matross, D.M., Goulden, M.L., Wofsy, S.C., da Rocha, H.R., da Camargo, P.B., Crill, P., Daube, B.C., de Freitas, H.C., Hutyra, L., Keller, M., Kirchoff, V., Menton, M., Munger, J.W., Pyle, E.H., Rice, A.H. & Silva, H. (2003). Carbon in Amazon Forests: Unexpected Seasonal Fluxes and Disturbance-Induced Losses. *Science*, 302:1554-1557.

Samanta, A., Knyazikhin, Y., Xu, L., Dickinson, R.E., Fu, R., Costa, M.H., Saatchi, S.S., Nemani, R.R. & Myneni, R.B. (2012). Seasonal changes in leaf area of Amazon forests from leaf flushing and abscission. 2012. *Journal of Geophysical Research*, 117(G01015): 1-13.

Sandmeier, St. & Deering, D.W. (1999). Structure analysis and classification of boreal forests using airborne hyperspectral BRDF data from ASAS. *Remote Sensing of Environment*, 69:281-295.

Sayn-Wittgenstein, L. (1961). Phenological aids to species identification on air photographs. In *Technical Note No*. Department of Forestry and Rural Development. Ottawa. Canada.

Schaaf, C., Liu, J., Gao, F., Jiao, Z., Shuai, Y. & Strahler, A. (2012). Collection 005 change summary for MODIS BRDF/Albedo (MCD43) Algorithms.

Schutz, B.E., Zwally, H.J., Shuman, C.A., Hancock, D. & DiMarzio, J.P. (2005). Overview of the ICESat Mission. *Geophysical Research Letters*, 32(L21S01): 1-4.

Schwartz, M. D., Reed, B. C. & White, M. A. (2002). Assessing satellite-derived start-of-season measures in the conterminous USA. *International Journal of Climatology*, 22(14): 1793-1805.
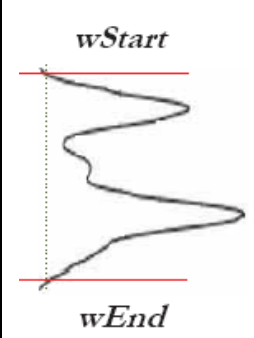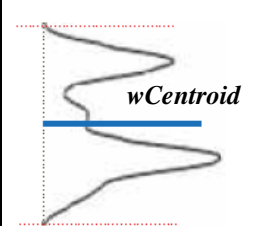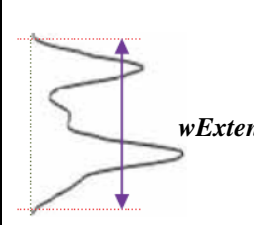
Sellers, P. J., Berry, J. A., Collatz, G. J., Field, C. B. & Hall, F. G. (1992). Canopy reflectance, photosynthesis, and transpiration. III. A reanalysis using improved leaf models and a new canopy integration scheme. *Remote Sensing of Environment*, 42(3): 187-216.

Semwal, M. (2014). Synergistic use of Spaceborne LiDAR and High Resolution Satellite Data for Mapping Aboveground Forest Biomass using Different Modelling Approaches. M.Tech. Thesis, IIRS, Dehradun.

Sharma, D., Gosai, K., Dutta, J., Arunachalam, A. & Shukla, A. K. (2015). Fungal diversity of twelve major vegetational zones of Arunachal Himalaya, India. *Current Research in Environmental & Applied Mycology*, 5(2), 101-119.

Slobbe, D. C., Lindenbergh, R. C. & Ditmar, P. (2008). Estimation of volume change rates of Greenland's ice sheet from ICESat data using overlapping footprints. *Remote Sensing of Environment*, 112(12), 4204-4213.

Solano, R., Didan, K., Jacobson, A. & Huete, A. (2010). MODIS vegetation index user's guide (MOD13 series). *Vegetation Index and Phenology Lab*.

Solberg, S. (2010). Mapping gap fraction, LAI and defoliation using various ALS penetration variables. *International Journal of Remote Sensing*, 31: 1227-1244.

Stenseth, N. C., Mysterud, A., Ottersen, G., Hurrell, J. W., Chan, K. S. & Lima, M. (2002). Ecological effects of climate fluctuations. *Science*, 297(5585): 1292-1296.

Strahler, A.H., Lucht, W., Schaaf, C.B., Tsang, T., Gao, F., Xiaowen, Li, Muller, J.P., Lewis, P. & Barnsley, M.J. (1999). MODIS BRDF/Albedo Product: Algorithm Theoretical Basis Document Version 5.0.

Sudhakar, S., Krishnan, N., Ramana, I.V., Pal, D.K. & Raha, R.K. (1992). Forest cover mapping using IRS-1A LISS-II. *Asian Pacific Remote Sensing Journal*, 4(2):25-30.

Sun, G. & Ranson, K. J. (2000). Modeling LiDAR returns from forest canopies. *IEEE Transactions on Geoscience and Remote Sensing*, 38(6): 2617-2626.

Sun, G., Ranson, K. J., Masek, J., Guo, Z., Pang, Y., Fu, A. & Wang, D. (2008). Estimation of Tree Height and Forest Biomass from GLAS Data. *Journal of Forest Planning*, *13*, 157-164.

Toomey, M., Roberts, D. & Nelson, B. (2009). The influence of epiphylls on remote sensing of humid forests. *Remote Sensing of Environment,* 113: 1787-1798.

Turner, W., Spector, S., Gardiner, N., Fladeland, M., Sterling, E. & Steininger, M. (2003). Remote sensing for biodiversity science and conservation. *Trends in Ecology & Evolution*, 18(6): 306-314.

Unni, N. V. M., Roy, P. S. & Parthasarathy, V. (1986). Evaluation of Landsat and Airborne multispectral data and aerial photograph for mapping forest feature and phenomena in a part of the Godavari Basin. *International Journal of Remote Sensing* 6:419-431

Unni, N.V.M., Jadhav, P.S., Tiwari, R.N., Sudhakar, A.K.S., Ranganath, B.K. & Dabral, S.K. (1991). Remote sensing applications in forestry. *Current Science*, 61(3&4):189-192.

Upadhyay, A. & Rai, R. K. (2013). Case Study: Ken Catchment. In: *Water Management and Public Participation* (pp. 139-152). Springer Netherlands.

Vermote, E. F. & Kotchenova, S. Y. March, (2008). *MOD09 (Surface Reflectance) User's Guide*.

Vermote, E. F., Tanré, D., Deuzé, J. L., Herman, M. & Morcette, J. J. (1997). Second simulation of the satellite signal in the solar spectrum, 6S: An overview. *IEEE Transactions on Geoscience and Remote Sensing,* 35(3), 675-686.

Verstraete, M.M., Pinty, B. & Myneni, R. (1996). Potential and limitation of information extraction on the terrestrial biosphere from satellite remote sensing. *Remote Sensing of Environment,* 58:201-214.
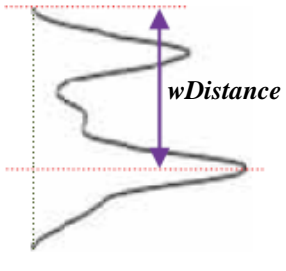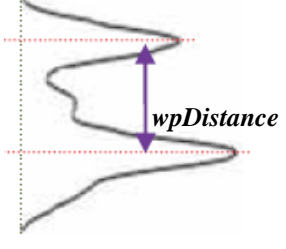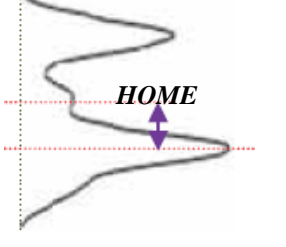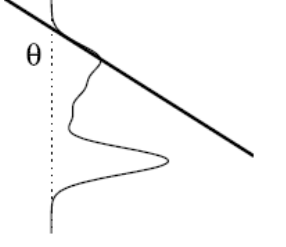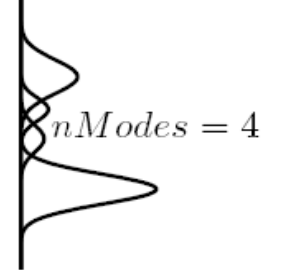
Vourlitis, G. L., Verfaillie, J., Oechel, W. C., Hope, A., Stow, D. & Engstrom, R. (2003). Spatial variation in regional CO2 exchange for the Kuparuk River Basin, Alaska over the summer growing season. *Global Change Biology*, 9(6): 930-941.

Walther, G. R., Post, E., Convey, P., Menzel, A., Parmesan, C., Beebee, T. J., Fromentin, J.M., Guldberg, O.H. & Bairlein, F. (2002). Ecological responses to recent climate change. *Nature*, 416(6879): 389-395.

Wang, J., Rich, P. M. & Price, K. P. (2003). Temporal responses of NDVI to precipitation and temperature in the central Great Plains, USA. *International Journal of Remote Sensing*, 24(11): 2345-2364.

Warrick, R. A., Shugart, H. H., Antonvsky, M. J., Terrant, J. R. & Tucker, C. J. (1986). The effects of increased CO_2 and climatic changes on terrestrial ecosystem, Global perspectives, aims and issues. In *The Greenhouse Effect, Climatic Change and Ecosystems*, (Scope 29) (Eds.) W. Bolin and D. Jagger (New York: John Wiley) 363-392 pp.

Weishampel, J. F., Blair, J. B., Knox, R. G., Dubayah, R. & Clark, D. B. (2000). Volumetric LiDAR return patterns from an old-growth tropical rainforest canopy. *International Journal of Remote Sensing*, 21(2):409-415.

Weiss, M., Baret, F., Smith, G. J., Jonckheere, I. & Coppin, P. (2004). Review of methods for in situ leaf area index (LAI) determination: Part II. Estimation of LAI, errors and sampling. *Agricultural and Forest Meteorology*, 121(1): 37-53.

Weisstein, E.W. (1996). http://www.ericweisstein.com/research/thesis/node40.html

White, P.H., Miller, J.R. & Chen, J.M. (2001). Four-scale linear model for anisotropic reflectance (FLAIR) for plant canopies-Part 1: Model description and partial validation. *IEEE Transactions on Geoscience and Remote Sensing,* 39:1073-1083.

Whitmore, T. C. & Burnham, C. P. (1975). *Tropical rain forests of the Far East*. Clarendon Press.

Widlowski, J. L., Taberner, M., Pinty, B., Bruniquel-Pinel, V., Disney, M., Fernandes, R., Gastellu-Etchegorry, J.P., Gobron, N., Kuusk, A.,T., Lavergne, T., Leblanc, S., Lewis, P.E., Martin, E., Mottus, M., North, P.R.J., Qin, W., Robustelli, M., Rochdi, N., Ruiloba, R., Soler, C., Thompson, R., Verhoef, W., Verstraete, M.M. & Xie, D. (2007). Third Radiation Transfer Model Intercomparison (RAMI) exercise: Documenting progress in canopy reflectance models. *Journal of Geophysical Research: Atmospheres* (1984–2012), 112(D9).

Wylie, D., Eloranta, E., Spinhirne, J. D. & Palm, S. P. (2007). A comparison of cloud cover statistics from the GLAS LiDAR with HIRS. *Journal of Climate*, 20(19): 4968-4981.

Xiao, X., Shao, S., Ding, Y., Huang, Z. & Chou, K. C. (2006). Using cellular automata images and pseudo amino acid composition to predict protein subcellular location. *Amino acids*, 30(1): 49-54.

Yadav, B.K.V. & Nandy, S. 2015. Mapping aboveground woody biomass using forest inventory, remote sensing and geostatistical techniques. *Environmental Monitoring and Assessment,* 187: 1-12.

Yin, T., Gastellu-Etchegorry, J. P., Grau, E., Lauret, N. & Rubio, J. (2013). Simulating satellite waveform LiDAR with DART model. In *Geoscience and Remote Sensing Symposium (IGARSS), 2013 IEEE International* (pp. 3029-3032). IEEE.

Yu, F., Price, K. P., Ellis, J. & Shi, P. (2003). Response of seasonal vegetation development to climatic variations in eastern central Asia. *Remote Sensing of Environment*, 87(1): 42-54.

Zelazowski, P., Malhi, Y., Huntingford, C., Sitch, S. & Fisher, J.B. (2011). Changes in the potential distribution of humid tropical forests on a warmer planet. *Philosophical Transactions of the Royal Society,* 369: 137-160.
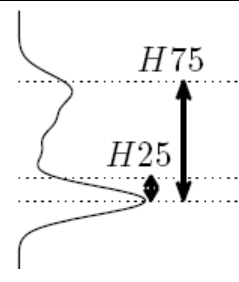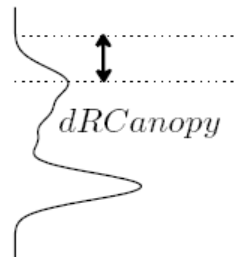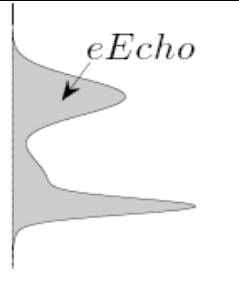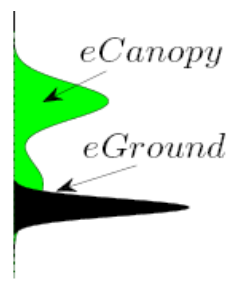
Zhang, J., Dong, W., Ye, D. & Fu, C. (2003). New evidence for effects of land cover in China on summer climate. *Chinese Science Bulletin*, 48(4): 401-405.

Zhang, X., Friedl, M. A., Schaaf, C. B. & Strahler, A. H. (2004). Climate controls on vegetation phenological patterns in northern mid-and high latitudes inferred from MODIS data. *Global Change Biology*, 10(7): 1133-1145.

Zhang, Y., Tian, Y., Myneni, R.B., Knyazikhin, Y. & Woodcock, C.E. (2002a). Assessing the information content of multiangle satellite data for mapping biomes: I. Statistical Analysis. *Remote Sensing of Environment,* 80:418-434.

Zhang, Y., Shabanov, N., Knyazikhin, Y. & Myneni, R.B. (2002b). Assessing the information content of multiangle satellite data for mapping biomes: II. Theory. *Remote Sensing of Environment,* 80:435-446.

Zhao, K. & Popescu, S. (2009). LiDAR-based mapping of leaf area index and its use for validating GLOBCARBON satellite LAI product in a temperate forest of the southern USA. *Remote Sensing of Environment*, 113:1628–1645.

Zhao, T.T. & Schwartz, M.D. (2003). Examining the onset of spring in Wisconsin. *Climate Research*, 24:59–70.

Zhou, L., Kaufmann, R. K., Tian, Y., Myneni, R. B. & Tucker, C. J. (2003). Relation between interannual variations in satellite measures of northern forest greenness and climate between 1982 and 1999. *Journal of Geophysical Research: Atmospheres* (1984–2012), 108(D1), ACL-3.

Zwally, H. J., Abdalati, W., Herring, T., Larson, K., Saba, J. & Steffen, K. (2002). Surface melt-induced acceleration of Greenland ice-sheet flow. *Science*, 297(5579): 218-222.

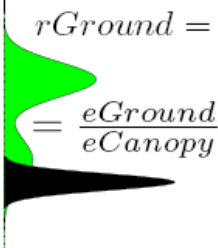Zwally, H.J. (2010). ICESat Cryosphere Sciences Branch Code 614.1. Available online at: http://icesat.gsfc.nasa.gov/icesat/(accessed 11 May 2010).
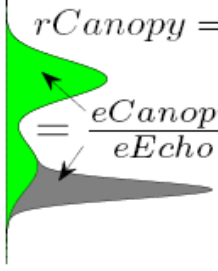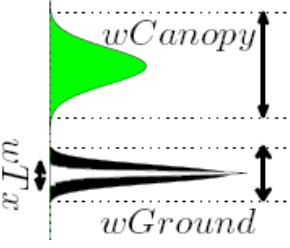
APPENDIX I

GLAS waveform Parameters for single waveform

Parameters	Definition	Physical explanation	Visualization
Waveform signal start (*pStart*) Waveform signal end (*pEnd*)	Position where the waveform first or last crosses above or below a threshold value.	*pStart:* Maximum interception point between surface and transmitted pulse. *pEnd:* Minimum elevation reflected from the earth's surface. Pertinent for surface feature height extraction like tree height.	
Waveform centroid (*wCentroid*)	Position where the return energy is divided into two equal parts.	Signifies maximum tree height and maximum canopy height.	
Waveform extent (*wExtent*)	Distance between signal start and signal end.	Signifies maximum tree height and maximum canopy height.	

Parameters	Definition	Physical Explanation	Visualization
Waveform distance (*wDistance*)	Distance from signal start to peak of the last Gaussian mode.	Signifies top tree height and top canopy height.	
Peak distance (*wpDistance*)	Distance between first and last peak.	Signifies average tree height.	
Height of median energy (*HOME*)	Distance from peak of the ground return to the waveform centroid.	Sensitive to change in vertical arrangements of tree canopy and degree of canopy openness.	
Front Slope angle (*aFSlope*)	Angle from vertical to vector from waveform begin to peak of the canopy return energy.	The variability of the upper canopy.	
Number of Gaussian fits (*wModes*)	Number of Gaussian components derived from nonlinear least squares estimation.	Represents number of height levels consistent to object and earth surface.	

Parameters	Definition	Physical Explanation	Visualization
X% Quartile height (*Hx*)[H25,H50, H75, H100]	Height at which x% of the return energy occurs.	*H50* equals to the *wCentroid.*	
Roughness of outer canopy (*d_RouCanopy*)	Distance from the waveform begins to the peak of the canopy (e.g. the first Gaussian).	Unevenness of the upmost canopy, spatial organization of plant surfaces within the canopy, and the decrease in laser energy with depth into the canopy as the pulse is interrupted by plant surfaces.	
Return waveform energy (*eEcho*)	The received energy i.e. the area below the waveform between begins and end.	Labelling the surface characteristics in absolute values.	
Ground return energy (*eGround*) and Canopy return energy (*eCanopy*)	*eGround*: is the total intensity of the last mode. *eCanopy*: is the difference between *eEcho* and *eGround*.	Return energy of the ground and canopy.	

Parameters	Definition	Physical explanation	Visualization
Ground return ratio (*rGround*)	*eGround* divided by *eCanopy*.	An estimate of the degree of the canopy closure.	$rGround =$ $= \dfrac{eGround}{eCanopy}$
Canopy return ratio (*rCanopy*)	*eCanopy* divided by *eEcho*.	Extent of canopy cover.	$rCanopy =$ $= \dfrac{eCanopy}{eEcho}$
Canopy width (*wCanopy*) and Ground width (*wGround*)	Canopy and ground extent, comparative to the transmitted pulse extent.	Extent of crown depth.	$wCanopy$ wTx $wGround$
X% Quartile height of waveform distance ratio (**Rx**) [**R25, R50, R75**]	X% Quartile height divided by waveform distance.	Regularizes the effect of different canopy heights.	